Evolution de la mort cellulaire en milieu fluctuant

Nathalie Zeballos

THÈSE POUR OBTENIR LE GRADE DE DOCTEUR DE L'UNIVERSITÉ DE MONTPELLIER

En Sciences de l'Evolution et de la Biodiversité

École doctorale GAIA - Biodiversité, Agriculture, Alimentation, Environnement, Terre, Eau

Unité de recherche CEFE

Evolution de la mort cellulaire en milieu fluctuant

Présentée par Nathalie Zeballos
Le 21 juin 2023

Sous la direction de Luis-Miguel CHEVIN
et co-encadrée par Christelle LEUNG

Devant le jury composé de

Delphine SICARD, DR INRAe, SPO Montpellier	Présidente du jury
Delphine DESTOUMIEUX-GARZON, DR CNRS, IHPE Montpellier	Membre du jury
Staffan JACOB, CR CNRS, SETE Moulis	Rapporteur
Tom VAN DOOREN, CR CNRS, iEES Paris	Rapporteur

UNIVERSITÉ DE MONTPELLIER

Résumé

Un changement environnemental rapide peut exposer les organismes vivants à un stress qui réduit les paramètres démographiques composant leur valeur sélective (survie, fécondité), suscitant ainsi un risque d'extinction. La plasticité phénotypique, soit la capacité d'un génotype donné d'exprimer différents phénotypes dans des environnements différents, peut permettre d'éviter l'extinction lorsqu'elle est adaptative, c'est-à-dire qu'elle augmente la valeur sélective moyenne à travers les environnements. A l'inverse, des diminutions de valeur sélective en réponse à l'environnement sont généralement considérées comme de la plasticité mal-adaptative, dues à des réponses passives au stress. Cependant, une mort induite par un stress environnemental et aboutissant à un fort déclin de la population pourrait-elle dans certains cas être une forme de plasticité adaptative ? Et comment la sélection agirait sur un tel trait en environnement fluctuant ? Je me suis intéressée à ces questions chez la microalgue halotolérante *Dunaliella salina*, où la mort cellulaire programmée a été précédemment démontrée. J'ai d'abord montré que lors d'une hausse de salinité, l'une des souches que nous étudions au laboratoire présente un fort déclin démographique (-69% en une heure), mais qu'il est suivi par un rebond démographique. Une autre souche génétiquement proche ne présente pas ce déclin initial, mais croît plus lentement dans la seconde phase. Etonnamment, la souche qui décline présente une corrélation positive entre déclin et rebond, d'autant plus prononcée que les conditions sont plus favorables à la croissance (plus grande intensité de lumière, moins de compétition). De plus, le déclin peut être atténué par un inhibiteur de mort programmée, indiquant qu'il ne s'agit pas d'une simple réponse passive au stress. Nous avons par la suite mis en compétition ces deux souches en alternant haute et moyenne salinités pendant 26 semaines. La souche déclinante s'est maintenue jusqu'à la fin de l'expérience avec une fréquence supérieure à 50% à chaque fin de cycle de salinité, malgré son fort déclin à chaque hausse de salinité. J'ai montré que ce maintien s'explique en partie par la compétition proche de la phase stationnaire, qui atténue l'effet des dynamiques initiales déclin-rebond. Enfin, j'ai modélisé 3 mécanismes pouvant expliquer d'une part la dynamique en déclin-rebond, et d'autre part la compétition avec la souche non déclinante : une libération altruiste par les cellules mourantes de ressources utilisables par les cellules restantes ; un compromis entre tolérance à la salinité et reproduction ; et une hétérogénéité de l'état des cellules, où l'élimination des mauvaises cellules cause une augmentation du taux de croissance moyen de la population. L'ensemble de mes résultats suggèrent que la mort cellulaire peut être favorisée par la sélection naturelle, et

potentiellement représenter une forme de plasticité adaptative en réponse à un stress environnemental.

Mots-clés : stress environnemental, mort cellulaire programmée, plasticité phénotypique, dynamiques éco-évolutives, sélection naturelle, modélisation.

Abstract

A rapid environmental change represents stressful conditions for living organisms and may reduce the demographic components of fitness (survival rate, reproduction), leading to a risk of extinction. Phenotypic plasticity, whereby a given genotype expresses different phenotypes in different environments, enables organisms to cope with fluctuating environments and avoid extinction when it is adaptive, i.e. when it increases mean fitness across environments. Conversely, fitness reduction induced by environmental changes is generally considered as maladaptive plasticity, due to passive response to stress. But can stress-induced death, leading to severe population decline, sometimes be interpreted as adaptive plasticity? And how may selection operate on such a trait in fluctuating environments? I investigated these questions with the halotolerant microalga *Dunaliella salina*, where programmed cell death has been established. We showed that after a salinity rise, one of the strains from our collection displayed a massive population decline (-69% in one hour), but that this decline was followed by a demographic rebound. Another genetically-related strain did not exhibit this initial decline, but grew more slowly in the second phase. Strikingly, the declining strain presented a positive correlation between decline and subsequent growth, which was more pronounced in conditions more favourable to growth (more light, less competition). Moreover, the decline could be diminished by a programmed cell death inhibitor, indicating that is not merely a passive response to stress. We have then grown these two strains in competition for 26 weeks, alternating intermediate and high salinity. The declining strain persisted until the end of the assay at frequencies higher than 50% at the end of each salinity cycle, despite its massive decline at each salinity rise. I showed that this co-existence may be partially explained by the competition near the stationary phase, which attenuates the effect of the initial decline-rebound dynamics. Finally, I modelled 3 mechanisms which may explain both the decline-rebound pattern and the competition with the non-declining strain: an altruistic hypothesis where dying cells release substrates usable by the remaining cells; a trade-off between salinity tolerance and reproduction; and a population heterogeneity in cell condition, where the elimination of damaged cells result in greater mean growth rate. Together, my results suggest that cell death can be advantaged by natural selection, and potentially represents a form of adaptive plasticity in response to an environmental stress.

Keywords: environmental stress, programmed cell death, phenotypic plasticity, eco-evolutionary dynamics, natural selection, modelling.

Remerciements

Je voudrais tout d'abord remercier vivement mon directeur de thèse, Luis-Miguel, pour son encadrement scientifique, ses conseils avisés et son accueil. Tu m'as assuré de bonnes conditions de travail pour effectuer ma thèse, que ça soit matériel, administratif et scientifique. J'ai beaucoup appris à tes côtés, je te remercie particulièrement pour ta disponibilité lorsque j'avais une question ou des soucis d'analyse. Merci d'avoir rendu l'expérience de doctorante aussi enrichissante avec les possibilités de congrès et d'enseignement.

Je remercie chaleureusement ma co-encadrante, Christelle, pour son appui infaillible, sa pédagogie et ses retours pertinents. Merci de m'avoir aiguillé pour la partie expérimentale et d'avoir continué ton encadrement à distance. Tes encouragements en fin de thèse ont été précieux.

Merci aux membres de mes comité de thèse - Oliver Kaltz, François Vasseur, Pierre Durand et Rutger de Wit - pour leur intérêt, leur implication et leurs encouragements. Ces réunions ont toujours été utiles, elles m'ont permis d'avancer plus clairement dans mon projet.

Je remercie vivement Staffan Jacob, Tom Van Dooren, Delphine Sicard et Delphine Destoumieux-Garzon d'avoir accepté d'évaluer mon travail, et plus particulièrement les deux rapporteurs Staffan et Tom pour le temps qu'ils consacreront à lire ma thèse.

Je remercie l'ensemble de l'équipe GEE pour son accueil durant ces 4 années, les présentations lors des réunions d'équipe m'ont toujours apporté de quoi alimenter ma réflexion. J'ai particulièrement apprécié participer et organiser nos réunions mensuelles des membres non-permanents, pour échanger des conseils pratiques et aborder des sujets entourant la vie en recherche, notamment le bien-être au travail.

Merci à Daphné, en charge du laboratoire Duna pour m'avoir enseigné les bonnes pratiques en microbiologie. Merci à Stan qui a pris le relais dans la gestion du labo Duna, après plusieurs mois sans ingénieur ton arrivée a été grandement appréciée. Merci aussi Stan de m'avoir permis de me reposer en prenant en charge l'acquisition de mes données d'évolution expérimentale pendant quelques semaines.

Je remercie aussi les deux stagiaires M1 que j'ai eu l'opportunité d'encadrer pendant ma thèse. Océane, merci pour ta rigueur, ton sérieux et pour l'application de mes consignes en microbiologie, me permettant de te faire confiance sur l'acquisition des données. Sudshena, grâce à toi j'ai enfin pu avancer concrètement dans la modélisation, souvent relégué au second

plan à cause des impératifs de l'expérimental. Ces deux expériences ont été totalement différentes de par le travail scientifique à mener (évolution expérimentale vs modélisation), mais aussi par vos personnalités, me permettant de réfléchir à mes pratiques d'encadrement.

Lorelei et Cécile, merci d'avoir répondu à toutes mes questions (surtout sur l'administratif et les possibilités en tant que doctorante) et pour votre amitié. Vos départs consécutifs ont laissé un vide dans le couloir. Méril, merci d'avoir partagé avec moi ma folie des plantes, pour nos discussions passionnantes et pour ton coaching en recherche de post-doc.

Une mention spéciale aux collègues ayant partagé pendant quelques mois mon bureau et qui ont participé à des échanges de conseils, mais aussi tout simplement à une bonne entente. Jeanne pour ta bonne humeur et ton rire contagieux, Mike pour ta gentillesse et ta conversation toujours intéressante, Pierre pour nos discussions le soir quand il n'y avait plus personne dans le couloir, Quentin pour tes précieux conseils et ton implication pour répondre à mes questions, Giacomo pour ton soutien dans les deux derniers mois de rédaction.

Je tiens à remercier la personne qui m'a accompagné tout au long de ces dix années d'études (!). Jonathan, merci pour ton amour et ton soutien moral, pour m'avoir supporté en période de stress, de démotivation ou de submersion sous le travail. Merci de m'avoir rappelé de garder un rythme de vie équilibrée (bon sauf les derniers mois…) et d'avoir participé à mon épanouissement personnel et professionnel. Je te remercie du fond du cœur pour avoir été assez fou, déterminé et réfléchi pour mener jusqu'au bout notre rêve de nature, et m'avoir permis de me ressourcer tout au long de cette dernière année dans notre petit coin de paradis.

J'aimerai remercier aussi ma famille, merci à mes parents pour leur amour et soutien émotionnel (et logistique sur les dernières semaines). Merci Estela, pour ton soutien malgré la distance à travers tes (très) nombreux messages mais aussi de répondre toujours présente pour aller danser, même si c'est à l'autre bout du pays. Christian, merci d'avoir partagé des moments privilégiés avec moi pour me changer les idées, avec la linogravure et nos trocs de plantes. Gracias a mi querida tía, Juanita banana, y mis primos Alessia y Renato por darme la energía que necesitaba para las últimas semanas. A mi abuelita Asunta, que fue durante toda su vida un ejemplo de valentía y fuerza de voluntad.

Ces (presque) quatre années de thèse ont été enrichissantes, passionnantes et intenses. Merci à tous ceux qui ont participé de près ou de loin à l'élaboration de ce travail, que ce soit par des discussions scientifiques et des conseils ou que ce soit en ayant participé à mon bien-être physique et émotionnel.

Table des matières

Abréviations

LM : Linear Model, modèle linéaire

GAM : Generalized Additive Model, modèle additif généralisé

GLM : Generalized Linear Model, modèle linéaire généralisé

PCD : Programmed Cell death, mort cellulaire programmée

Introduction

Contexte et état de l'art

Fluctuations environnementales et risques d'extinction

Les changements environnementaux représentent souvent des conditions stressantes pour les organismes vivants, exposant les populations incapables de tolérer les nouvelles conditions environnementales à un risque d'extinction. Ce risque est d'autant plus élevé lorsque la fluctuation environnementale est rapide, importante et peu prévisible. Or les effets prédits (et déjà observés) du changement climatique tendent à une multiplication des évènements climatiques extrêmes et une plus forte imprévisibilité des fluctuations environnementales pour les prochaines décennies (emballement climatique). Ces perturbations environnementales imprévisibles peuvent représenter des conditions abiotiques (température, salinité, précipitations cumulées etc) moins bien tolérées car trop décalées par rapport à la niche fondamentale de la population, ou l'altération/disparition de certaines interactions biotiques (diminution des ressources nutritives pour les consommateurs primaires ou secondaires, des mutualismes tels que la pollinisation par les insectes/animaux, etc). L'extinction survient lorsque l'impact du changement d'environnement sur les composantes démographiques de la valeur sélective (survie et reproduction) est trop important, conduisant à un déclin déterministe de la population, qui suscite à son tour d'autres facteurs de risques liés aux faibles effectifs (effet Allee, stochasticité démographique, dépression de consanguinité), donnant lieu à un vortex d'extinction (Fagan and Holmes 2006). L'adaptation des populations aux stress environnementaux est donc un enjeu majeur dans le contexte actuel, c'est pourquoi il est nécessaire d'étudier les processus affectant le potentiel évolutif des populations, et son impact sur leur dynamique démographique.

Stratégies en réponse à un stress environnemental

Il existe plusieurs stratégies permettant aux populations de faire face à un stress environnemental en évitant l'extinction : la dispersion, l'adaptation (sauvetage évolutif), et la plasticité phénotypique. La dispersion est tout mouvement d'individus ou de propagules qui a de potentielles conséquences sur le flux de gènes à travers l'espace (Ronce 2007), et peut permettre aux populations de retrouver des conditions proches de leur niches écologiques. L'adaptation, ou plus précisément évolution adaptative, est le processus par lequel les individus avec une meilleure valeur sélective sont sélectionnés et transmettent leurs allèles aux

générations suivantes jusqu'à fixation. Ce processus peut permettre la survie de la population hors de sa niche d'origine si l'adaptation cause un déplacement de la niche. La plasticité phénotypique est définie comme la capacité d'un génotype donné d'exprimer différents phénotypes en réponse aux conditions environnementales (Schlichting and Pigliucci 1998; Withman and Agrawal 2009). La variation de phénotype peut être au niveau morphologique, physiologique, comportemental ou traits d'histoire de vie. La plasticité permet de mieux supporter les changements environnementaux si elle est adaptative, c'est à dire si elle permet d'augmenter la valeur sélective de la population à travers plusieurs environnements. Nous nous sommes focalisés sur ces deux dernières stratégies, à savoir comment un trait plastique peut-être adaptatif, notamment lorsque la conséquence première du trait est de modifier la démographie (en induisant le suicide de l'individu).

Plasticité phénotypique

Mesure statistique. La variance phénotypique est usuellement exprimée comme le résultat de la somme de la variance génétique, environnementale, de l'interaction entre les deux et de l'erreur ; ici la variance de l'interaction entre génétique et environnement correspond à la plasticité phénotypique (partitionnement par analyse de variance).

Représentation graphique. La plasticité phénotypique peut être visualisée par des normes de réaction, c'est-à-dire représenter la valeur du trait exprimé en fonction de l'environnement, par génotype concerné.

Le partitionnement de la variance et les normes de réactions permettent de décrire la variabilité et la nature héritable de la plasticité phénotypique, mais n'expliquent pas l'évolution, les mécanismes sous-jacents et les conséquences sur la valeur sélective (Nijhout 2003, Frankino and Raff 2004, Withman and Agrawal 2009).

Evolution de la plasticité

Dans un environnement fluctuant aléatoirement, la plasticité permet de réduire les risques d'extinction lorsque les fluctuations sont suffisamment prévisibles (Reed et al. 2010; Ashander et al. 2016). Un changement environnemental est dit prévisible lorsque le signal environnemental responsable du développement du phénotype permet de prédire l'environnement de sélection de ce phénotype, permettant ainsi une adéquation entre la réponse plastique et les pressions de sélection. De ce fait, lorsque la plasticité varie génétiquement (et peut donc évoluer), on s'attend à ce que le degré de plasticité qui évolue à l'équilibre dans un

environnement fluctuant dépende de la prédictibilité des fluctuations environnementales (Gavrilets and Scheiner 1993; De Jong 1999; Lande 2009). Bien qu'il soit difficile de manipuler la variabilité et la prédictibilité des environnements sur des échelles de temps suffisamment longues, certaines vérifications empiriques de ces hypothèses théoriques ont été menées (Scheiner and Yampolsky 1998; Dey et al. 2016; Leung et al. 2020). Par exemple, grâce à l'utilisation de l'évolution expérimentale, Leung et al. (2020) ont démontré une diminution du degré de plasticité des lignées ayant évolués dans un environnement fluctuant de façon peu prévisible, tel qu'attendu théoriquement. Par ailleurs, la plasticité pourrait aussi évoluer vers un degré plus faible en environnement constant si la production et la maintenance de cette plasticité est associé à un coût (DeWitt et al. 1998).

Ces théories s'appliquent principalement dans le cas d'un trait fixe, c'est-à-dire que le phénotype adulte résultant de la plasticité en réponse à l'environnement lors de la phase de développement, et sur lequel la sélection agit, est constant. En opposition, Lande propose la modélisation de traits labiles, c'est-à-dire dont le changement développemental est réversible en fonction des fluctuations de l'environnement (Lande 2009, 2014). Dans ce scénario, la théorie sur l'évolution de la plasticité suppose que l'optimum du trait plastique est fluctuant, de ce fait une plus grande plasticité (sans coût associé) sera sélectionnée si elle permet d'approcher plus rapidement le nouvel optimum. Ainsi, les théories prédisant l'évolution de la plasticité peuvent s'appliquer aux cas les plus simples facilement modélisables, mais elles ne sont pas forcément suffisantes pour comprendre tous les contextes biologiques d'intérêt.

Plasticité adaptative et active vs passive

Comme indiqué plus haut, la plasticité est considérée comme adaptative lorsqu'elle permet de maintenir une valeur sélective plus élevée qu'une absence de plasticité, en moyenne entre environnements. Mais au-delà de cette simple définition, démontrer expérimentalement que la plasticité d'un caractère donné chez un organisme est adaptative peut être complexe, puisque cela requiert de pouvoir comparer des génotypes plastique et non-plastique pour un trait spécifique (sans autre différence), en compétition à travers plusieurs environnements. Les études expérimentales directes où la plasticité a été « éteinte » dans un génotype donné sont rares (voir par exemple Dudley and Schmitt (1996)). En l'absence de telles preuves directes, un argument indirect en faveur d'une plasticité adaptative est de mettre en évidence la nature active des processus impliqués. La distinction entre plasticité active et passive a historiquement été posée dès la fin du XXe siècle (bien que ces termes soient apparus bien après), par exemple

chez Schmalhausen avec la distinction entre « modifications » et « morphoses », c'est-à-dire plasticité passive, et continue à faire débat (Sultan 1995). La caractéristique active de la plasticité peut être définie lorsque que le trait plastique répond à un signal environnemental par un mécanisme spécifique et fonctionnellement bien défini (Pigliucci 1996), en opposition à une réponse passive et inévitable, découlant de contraintes physiques par exemple. Mais cette distinction n'est pas nécessairement toujours évidente, surtout lorsque les mécanismes sous-jacents ne sont pas connus. Par exemple, la croissance réduite et le développement ralenti d'une plante ou d'un animal en condition de ressources limitées peuvent être interprétés à première vue comme une réponse passive (et non adaptative), mais il pourrait aussi s'agir d'une réponse adaptative qui a évolué sous sélection naturelle, si cela permet à l'organisme de préserver ses ressources et s'éviter ainsi une mortalité accrue en environnement stressant. La classification actif/passif est donc en partie subjective, et dépend de notre capacité à identifier les voies spécifiques et à les interpréter de manière pertinente.

Cependant, il est plus difficile de comprendre comment peut évoluer une réponse plastique (et apparemment active) à l'environnement qui n'apparait pas comme immédiatement favorable, par exemple parce qu'elle résulte en la mort de l'individu. C'est le cas notamment de la mort cellulaire activement déclenchée chez les unicellulaires (Nedelcu et al. 2011), qui peut être interprétée comme de la plasticité active, puisqu'une cascade métabolique coûteuse en énergie est déclenchée à la suite d'un signal environnemental (Sathe et al. 2019).

Mort cellulaire programmée

Analogie entre pluricellulaires et unicellulaires

On a longtemps cru que la mort cellulaire programmée était exclusivement présente chez les multicellulaires, plus spécifiquement les métazoaires, avant que ne soit démontrée son occurrence chez les végétaux pluricellulaires, puis chez des unicellulaires (Ameisen 2002). De ce fait, le terme « programmé » désignait initialement un processus génétiquement régulé pour une élimination sélective des cellules en mauvaise condition pathologique ou physiologique (cellules cibles), promouvant le bon développement et fonctionnement de l'organisme pluricellulaire, par exemple lors du développement embryonnaire (Clarke 1990), ou de l'infection par une bactérie chez les plantes (Del Pozo & Lam, 1998). Les premières observations de mort active chez les unicellulaires ont donc historiquement importé la terminologie et les concepts depuis le champ disciplinaire développé pour les organismes pluricellulaires. De ce fait, il n'existe pas de définition exacte de la mort cellulaire programmée

lorsqu'elle s'applique chez les unicellulaires (Durand and Ramsey, 2019), d'autant plus que le concept même est encore sujet à débat (Deponte 2008; Jiménez et al. 2009; Nedelcu et al. 2011) et qu'il y a toute une gradation des formes de mort cellulaire (Minina et al. 2020). Il semble nécessaire de clarifier les termes pour une meilleure communication et compréhension du phénomène chez les unicellulaires (Pandey et al. 2018; Aguilera et al. 2022) comme proposé chez les multicellulaires (Kroemer et al. 2009; Cabon et al. 2013). Dans cette thèse, j'utilise le terme de mort cellulaire programmée (PCD pour *programmed cell death* en anglais) pour désigner une mort cellulaire active et génétiquement régulée, qui s'exprime sous différent morphotypes incluant l'apoptose, la paraptose et l'autophagie (Nedelcu et al. 2011), en réponse à un signal environnemental. Comme proposé dans Durand and Ramsey (2019), je considère que le terme 'programmé' fait maintenant référence à un mécanisme probabiliste (une partie d'une population clonale le déclenche), ramifié (certaines étapes dans la cascade métabolique peuvent mener à différents résultats) et non-discret (la perte de viabilité de la cellule peut être graduelle). Par ailleurs, la mort cellulaire peut être définie selon des critères morphologiques et structurels (quel morphotype est exprimé?), métaboliques (quelles enzymes ont été activées ?), ou bien par sa fonction et son rôle d'un point de vue évolutif (« true » PCD vs « ersatz » PCD, mort cellulaire active) (Kroemer et al. 2009; Nedelcu et al. 2011; Durand and Ramsey 2019; Durand 2020).

Mort cellulaire chez les unicellulaires

De nombreuses études expérimentales ont reporté ces trente dernières années l'existence de mort cellulaires actives chez les unicellulaires, chez plusieurs branches phylogénétiquement divergentes d'eucaryotes unicellulaires (Ameisen 2002) mais aussi des procaryotes (Nedelcu et al. 2011; Durand 2020), incluant des cyanobactéries (*Trichodesmium, Microcystis*), et des bactéries gram-positives (*Myxococcus, Streptococcus, Staphylococcus*) et gram-négatives (*Pseudomonas, Escherichia*). Parmi les eucaryotes, on retrouve des ciliés (*Tetrahymena, Blepharisma, Euplotes*), des parasites intracellulaires (*Leishmania, Trypanosoma*) ainsi que des amibozoaires (*Entamoeba, Dictyostelium*) et des champignons (*Candida, Saccharomyces*) (Nedelcu et al. 2011). A cela s'ajoutent plusieurs taxons de phytoplancton, que ce soit des diatomées (*Thalassiosira, Ditylum, Skeletonema*), des haptophytes (*Emiliania*) ou des chlorophytes tels que *Chlamydomonas, Chlorella, Dunaliella*. Or pendant longtemps, les déclins de populations chez les phytoplanctons, à l'origine de la moitié de la production primaire mondiale (Geider et al. 2001) et essentiels à la régulation du cycle du carbone, étaient plutôt attribués à la prédation, à leur sédimentation ou à l'infection par des agents pathogènes

Terminologie de mort cellulaire

Apoptose : Un morphotype de PCD caractérisé par des marqueurs morphologiques et métaboliques tels que l'externalisation des phosphatidylsérines sur la membrane externe, la condensation des chromatines, la réduction du volume cellulaire et le bourgeonnement de la membrane plasmique (mais maintenance de son intégrité jusqu'à un stade tardif). (Kroemer et al. 2009)

Autophagie : Un morphotype de PCD caractérisé par la vacuolisation du cytoplasme, l'accumulation de vacuoles d'autophagie et la non condensation de la chromatine. (Kroemer et al. 2009)

« Ersatz » PCD : Définition évolutive de la PCD selon laquelle le trait est intrinsèque à la cellule mais n'a pas été directement selectionné (Durand & Ramsey, 2018)

Mort cellulaire programmée (PCD – *programmed cell death*) : Une mort cellulaire active et génétiquement régulée, qui s'exprime sous différent morphotypes incluant l'apoptose et l'autophagie. (Nedelcu et al. 2011)

Mort cellulaire régulée (RCD – *regulated cell death*) : Initialement chez les métazoaires, terme incluant la PCD qui est spécifique au développement embryonnaire, pour distinguer de la mort accidentelle (ACD). Récemment proposé pour inclure l'ensemble des morts activement contrôlées et génétiquement encodées chez les organismes photosynthétiques, cad plantes, cyanobactéries et levures (Aguilera et al. 2022).

Mort cellulaire active : Tout processus de mort cellulaire génétiquement déterminé, qui requiert de l'énergie et implique une série d'étapes coordonnées. (Nedelcu et al. 2011)

Nécrose : Une forme de mort cellulaire caractérisée par la dilatation cytoplasmique et des organelles, et la rupture de la membrane plasmatique, et l'absence de marqueurs d'apoptose ou d'autophagie. (Kroemer et al. 2009)

Parapaptose : Un morphotype de PCD caractérisé par la vacuolisation du cytoplasme et la dilatation des mitochondries, mais sans autre marqueurs usuels de l'apoptose, il n'est donc pas empêché par un inhibiteur des activités de caspases. (Kroemer et al. 2009)

Senescence (*ageing*) : Un processus passif, graduel et parfois dépendant du nombre de divisions cellulaires, augmentant le risque de mort de l'individu au cours de sa vie (actuarial senescence), et existant aussi chez les unicellulaires à reproduction clonale.

« True » PCD : Définition évolutive selon laquelle la PCD est une adaptation en réponse à un stress environnemental biotique ou abiotique résultant en la mort de la cellule, en tant que cible directe de la sélection (Durand & Ramsey, 2018).

(bactéries ou virus) (Franklin et al. 2006; Kozik et al. 2019). Une des premières observations de mort active reportée chez les algues vertes a été mise en évidence par le déclin démographique en réponse à l'obscurité prolongée, *Dunaliella tertiolecta* (Berges and Falkowski 1998). Depuis, l'occurrence de PCD chez plusieurs espèces du genre *Dunaliella* (auquel nous allons nous intéresser dans cette thèse) a été confirmée par des marqueurs cellulaires, chez *D. tertiolecta* (Segovia et al. 2003), mais aussi *D. viridis* (Jiménez et al. 2009) et *D. salina* (Orellana et al. 2013). Le déclenchement d'une telle mort répond à différents

signaux environnementaux, incluant le choc thermique, les UV, la salinité, la privation de nutriments et l'obscurité prolongé (Nedelcu et al. 2011).

Marqueurs cellulaires et mécanismes de PCD chez les phytoplanctons

Les changements morphologiques et métaboliques caractérisant la mort cellulaire programmée incluent: l'externalisation précoce des phosphatidylsérines (PS) dans le feuillet externe de la membrane cellulaire associée au maintien de l'intégrité de celle-ci; l'activité de méta-caspases et autres caspases dans les mitochondries ; et la fragmentation de l'ADN (Bidle and Falkowski 2004). Le premier signal est traditionnellement détecté par l'ajout de l'Annexine V fluorescente, qui se lie au PS et peut ensuite être quantifiée par cytométrie ou spectroscopie. Le deuxième signal peut être mis en évidence par l'ajout d'un inhibiteur de caspase spécifique, qui empêche la cascade métabolique menant à la mort cellulaire. Enfin sont utilisés la microscopie électronique à transmission (TEM) pour détecter les altérations ultra structurales de l'ADN, et la coloration TUNEL (Terminal deoxynucleotidyl transferase dUTP nick end labelling) pour visualiser des marqueurs fluorescents se liant aux brins d'ADN ouverts).

Cependant, détecter rigoureusement et quantifier la mort cellulaire programmée chez les unicellulaires est particulièrement complexe (Durand 2020; Barreto Filho et al. 2022*a*), pour plusieurs raisons. Tout d'abord, plusieurs morphotypes associés à la PCD existent selon le signal environnemental et le contexte écologique (Jiménez et al. 2009). Deuxièmement, les marqueurs standards utilisés chez les pluricellulaires ne sont pas toujours appropriés pour les unicellulaires (par exemple à cause de l'absence de phosphatidylsérines dans les membranes cellulaires), ou bien leur signal peut ne pas être spécifique à la PCD. Enfin, une fois choisis les marqueurs à utiliser, il y a souvent des problèmes techniques à résoudre pour leur mise en application, par exemple concernant le moment approprié pour vérifier l'induction du signal. De plus, la nature active ou programmée de la mort cellulaire est toujours sujette à débat, car il existe une graduation de situations impliquant des signaux et des cascades métaboliques plus ou moins complexes. De ce fait, interpréter les résultats de tests requiert de la nuance (Barreto Filho et al. 2022*a*).

Barreto Filho et al. (2022*a*) ont passé en revue l'ensemble des méthodes de détection utilisés chez les phytoplanctons chlorophytes, ainsi que leur efficacité et leur significativité d'un point de vue statistique. Il en ressort qu'il n'existe pas de marqueur « référence absolu » pour tous les chlorophytes pour le moment, c'est-à-dire un marqueur spécifique à la PCD et avec une haute sensibilité. Leur recommandation est donc d'utiliser une combinaison de marqueurs

complémentaires quant à leurs spécificité et sensibilité à la PCD. Il est aussi essentiel de noter que l'utilisation de l'activité des caspases et enzymes proches chez les algues vertes comporte plusieurs controverses. Tout d'abord, l'enzyme exacte impliquée chez chaque espèce n'est pas connue, pouvant mener à des confusions (Barreto Filho et al. 2022*a*). Ensuite, les activités de caspases ne sont pas spécifiques à la mort cellulaire, mais peuvent aussi être impliquées dans d'autres mécanismes cellulaires (Abraham and Shaham 2004), et réciproquement la PCD peut se produire sans activité des caspases (Leist and Jäättelä 2001; Abraham and Shaham 2004).

Origine évolutive de la PCD

Concernant l'origine de la PCD, plusieurs hypothèses ont été proposées, impliquant une émergence initiale chez les unicellulaires car organismes plus anciens que les pluricellulaires, avant évolution dans les différentes lignées d'unicellulaires et avant d'être exapté (sensu Gould and Vrba (1982)) chez les pluricellulaires. La similitude des cascades métaboliques chez les unicellulaires et les multicellulaires argumente fortement en faveur d'une origine commune du processus.

Ameisen (1998) propose un scénario à partir de la propagation de modules génétiques égoïstes qui ont été sélectionnés sur leur capacité à manipuler leur cellules hôtes. Ces modules incluent les modules d'addiction encodés par des plasmides chez les bactéries et les ancêtres des mitochondries dans les cellules eucaryotes. Le principe de ces modules d'addiction sont leur production de toxines de longue durée et anti-toxines de courte durée (mécanisme TA présent chez les bactéries et les archées (Yamaguchi et al. 2011)). Ainsi dans les cellules perdant le module génétique encodant pour ce système TA, les toxines stables restent plus longtemps que les antitoxines et induisent la mort de la cellule. De cette manière, les modules génétiques s'assurent de leur propre survie (Durand 2020). L'idée que la PCD ait émergé à partir d'interactions hôtes-pathogènes a été avancée par plusieurs auteurs (Kroemer 1997; Frade and Michaelidis 2005; Kourtis and Tavernarakis 2009), la perspective générale s'accordant sur le fait que la PCD a évolué à partir de mécanismes impliqués dans la destruction des pathogènes qui sont activés en réponse à un changement métabolique dans la cellule hôte.

Maintien chez les unicellulaires

Chez les multicellulaires, l'effet bénéfique au niveau de l'organisme permet facilement d'expliquer le maintien d'un tel trait léthal pour la cellule. Cependant, comment justifier sa maintenance chez les lignées d'unicellulaires, où la cellule est l'individu et donc l'unité de sélection ? Un trait devient fixé et est maintenu dans une population, soit par sélection naturelle

car il est adaptatif - il augmente la valeur sélective -, soit par dérive génétique car c'est un trait neutre (non-adaptatif), soit par co-produit de la sélection car il est associé à un autre trait (pléiotropie). Un autre pré-requis pour la propagation d'un trait léthal est la conditionnalité, c'est-à-dire que le trait soit activé uniquement par une fraction de la population and non par l'ensemble des individus.

Hypothèse adaptative

L'hypothèse la plus répandue concernant la maintenance d'une forme de mort active chez les unicellulaires est qu'il s'agit d'un comportement adaptatif et altruiste, dont le coût extrême et léthal au niveau de l'individu (la cellule) est compensé par les bénéfices (directs ou indirects) au niveau de la population ou du groupe, par similarité avec les multicellulaires où la coopération entre cellules est la règle. Cette théorie fait appel à la sélection de parentèle ou la théorie de la valeur sélective inclusive (Hamilton 1964), c'est-à-dire que les individus favorisés par la sélection sont les individus proches génétiquement de ceux qui sont activement mort, et qui ont bénéficié du comportement altruiste. Cette théorie repose sur le fait que la sélection de parentèle requiert de l'apparentement, et que la reproduction asexuée est prédominante chez les unicellulaires, menant à des populations clonales ou très fortement apparentées. On s'attend donc à ce qu'un trait altruiste évolue facilement dans des populations clonales, du moins dès lors que les apparentés restent à proximité (structure spatiale).

Dans le cas de la PCD, l'effet bénéfique peut être direct comme un relargage de nutriments par les cellules mourantes (Durand et al. 2011; Orellana et al. 2013; Vostinar et al. 2019) ou le recyclage des restes cellulaires (Fröhlich and Madeo 2000; Christensen et al. 2001), promouvant la croissance des cellules restantes. D'autres mécanismes peuvent être envisagés comme la détoxification de l'environnement par les cellules mourantes (Estrela et al. 2019), ou bien des molécules signal fournissant des informations sur les conditions environnementales (Christensen et al. 1995; Durand 2020). La sélection de parentèle pourrait favoriser la PCD s'il s'agit de *biens privés* préférentiellement utilisables par les apparentés, plutôt que des *biens communs* qui peuvent aussi être utilisés par des tricheurs – un génotype n'effectuant pas lui-même le trait couteux (Estrela et al. 2016, 2019). Un effet altruiste indirect peut passer par l'excrétion de molécules néfastes pour les individus moins apparentés ou d'une autre espèce, diminuant la compétition pour les ressources (nutritives, d'espace) et favorisant ainsi les apparentés (Durand et al. 2014; Vostinar et al. 2019). La sélection de parentèle nécessite donc une forte structuration spatiale et génétique pour que les individus plus apparentés bénéficient préférentiellement du comportement coopératif (Débarre et al. 2012).

Cependant les limites à cette théorie sont que de nombreuses lignées d'unicellulaires ne font pas (exclusivement) de la reproduction asexuée et donc les populations ne sont pas toujours clonales. Par exemple, la structure génétique des phytoplanctons dans les blooms de croissance est plutôt hétérogène (Medlin et al. 2000; Thornton 2002) (Medlin et al 2000, Thornton 2002, Rynearson and Ambrust 2005 dans Nedelcu) et il peut y avoir de la diversité génétique à l'échelle locale. Un haut niveau de similarité génétique dans les populations unicellulaires n'est pas un argument suffisant pour supporter l'idée d'une origine coopérative chez les unicellulaires, l'existence de mécanismes favorisant les apparentés est nécessaire.

Hypothèses non-adaptatives

La seconde hypothèse, moins souvent évoquée, est de considérer la mort active comme non adaptative chez les unicellulaires (Nedelcu et al. 2011). Or pour qu'un trait ayant un fort effet négatif sur la valeur sélective des individus soit maintenu à travers l'évolution, il faut soit qu'il procure un effet bénéfique sous certaines conditions, soit qu'il soit associé à un autre trait sous sélection naturelle, dont il est le co-produit mal-adaptatif. Certains suggèrent que la mort programmée est un résultat inévitable de la balance métabolique (Bidle et Falkowski 2004), arguant qu'elle a moins lieu lorsque les populations sont en phase stationnaire (cad les cellules moins actives métaboliquement). Dans cette perspective, le trait est simplement mal-adaptatif, et ne procure aucun bénéfice. On oppose à ce scenario le fait que les traits mal-adaptatifs finissent par être éliminés par la sélection naturelle. Une autre proposition est que les gènes impliqués dans l'activation et la régulation de cette mort seraient aussi essentiels pour d'autre activités métaboliques de la cellule, notamment dans des mécanismes dont leur absence en conditions n'induisant pas de PCD donnerait un désavantage (Aldsworth et al. 1999; Bidle and Falkowski 2004). Réprimer la PCD pourrait donc mener au dysfonctionnement d'autres activités primordiales pour la cellule. Puisque ce type d'effet pléiotrope semble impliqué dans le maintien de la sénescence, on peut aussi imaginer que cela soit le cas pour le maintien de la PCD chez les unicellulaires.

Il est important de souligner l'importance de distinguer les forces de sélection à l'œuvre à l'origine du trait de celles impliquées dans son maintien dans les différentes lignées (Nedelcu et al. 2011). En effet les hypothèses adaptatives et non-adaptatives ne sont pas mutuellement exclusives, dans la mesure où l'on peut imaginer un scénario où l'origine est non-adaptative mais son maintien l'est, et inversement. Par exemple, un trait initialement mal-adaptatif pourrait dans certaines conditions donner un avantage à la population, et pourrait évoluer vers un trait coopératif sous la sous sélection de parentèle ou de groupe (Nedelcu et al. 2011). Ainsi, le

maintien évolutif de la PCD ne nécessite pas une explication unique pour toutes les lignées d'unicellulaires.

Dynamiques démographiques éco-évolutives

Sélection et démographie densité-indépendante

Tout scenario impliquant l'évolution d'un trait par sélection naturelle implique l'existence de variabilité génétique (ou héritable au sens large) dans les propriétés démographiques (survie, reproduction) qui déterminent les contributions à la génération suivante. Réciproquement, l'évolution peut induire un changement de ces propriétés démographiques au niveau populationnel. Il est donc instructif de partir de modèles de croissance des populations pour comprendre le fonctionnement de la sélection naturelle d'une part, et des dynamiques éco-évolutives d'autre part.

Si l'on part de la situation la plus simple où la densité dépendance peut être négligée (faible compétition), la dynamique démographique d'un génotype *i* seul est simplement

$$\frac{dN_i}{dt} = r_i N_i, \qquad \text{(Eq. 1)}$$

conduisant à une (dé)croissance exponentielle telle que $N_i(t) = N_i(0)e^{r_i t}$, où r_i est le taux de croissance intrinsèque. Si r_i est négatif, alors il y a déclin de la population. En présence de 2 génotypes croissant indépendamment l'un de l'autre, si l'on dénote $N = N_1 + N_2$ la densité de population totale, alors

$$\frac{dN}{dt} = r_1 N_1 + r_2 N_2 = (r_1 p + r_2(1-p))N = \bar{r}N \qquad \text{(Eq. 2)}$$

où p est la fréquence relative (proportion) du génotype 1, et $\bar{r}$ le taux de croissance intrinsèque moyen de la population. Ceci montre que la dynamique démographique de la population peut être modifiée si le taux de croissance moyen change sous l'effet de changements de fréquences alléliques ou génotypiques dus à la sélection naturelle. C'est le cas en particulier dans le contexte du sauvetage évolutif où un génotype dans la population est mieux adapté aux conditions environnementales et est capable d'y croître, de sorte que la sélection naturelle cause un rebond démographique lorsque le taux de croissance moyen passe de négatif à positif.

Pour pouvoir prédire le taux de croissance moyen d'une population, il est donc indispensable de suivre le changement de fréquence, qui est donné par (Crow and Kimura 1970)

$$\frac{dp}{dt} = p(1-p)\left(\frac{dN_1}{N_1 dt} - \frac{dN_2}{N_2 dt}\right). \qquad \text{(Eq. 3)}$$

Dans le cas où la sélection est densité-indépendante (soit parce que la croissance est densité-indépendante soit parce qu'elle est la même entre génotypes), le changement de fréquence devient

$$\frac{dp}{dt} = p(1-p)(r_1 - r_2), \qquad \text{(Eq. 4)}$$

Où $r_1 - r_2 = s$ est le coefficient de sélection. Cette formulation permet d'estimer la sélection sans avoir besoin de connaitre la densité totale.

Sélection et démographie densité-dépendante

Lorsque la fécondité et la mortalité dépendent de la taille de la population, par exemple du fait de ressources limitées, la dynamique démographique densité-dépendante peut être décrite par une équation logistique de Lotka-Volterra

$$\frac{dN}{dt} = (r - \alpha\, N), \qquad \text{(Eq. 5)}$$

où α est le terme de compétition, et la taille de population à l'équilibre est égale à $N_{eq} = \frac{r}{\alpha}$. Ce modèle peut être étendu à une population composée de 2 génotypes, dans laquelle la densité de chaque génotype s'écrit

$$\begin{cases} \frac{dN_1}{dt} = (r_1 - \alpha_{11}\, N_1 - \alpha_{21}\, N_2)N_1 \\ \frac{dN_2}{dt} = (r_2 - \alpha_{22}\, N_2 - \alpha_{12}\, N_1)N_2 \end{cases}, \qquad \text{(Eq. 7)}$$

où les paramètres α_{11} et α_{22} quantifient la compétition intra-génotype, tandis que α_{21} et α_{12} quantifient l'effet négatif de la présence d'une génotype sur l'autre. Le changement de fréquence (eq. 4) devra donc prendre en compte la compétition intra- et inter-souche (eq. 7), cette dernière pouvant dépendre de la niche écologique de chaque génotype (Kot 2001). Si leur niches sont similaires, on peut s'attendre à de l'exclusion compétitive (Violle et al. 2011).

Le modèle biologique *Dunaliella salina*

Pour la partie expérimentale de mes travaux de thèse, j'ai utilisé l'algue unicellulaire *Dunaliella salina (Chlorophyceae),* le principal producteur primaire des milieux hypersalins comme les salins industriels, les lagunes côtières et lacs salés (Ben-Amotz et al. 2009). Cette espèce est capable de tolérer une large gamme de salinités, depuis des valeurs inférieures à l'eau de mer jusqu'à la saturation en sel ([NaCl] ~6.2M), ce qui lui permet de se maintenir dans ces milieux où la salinité varie tout au long de l'année (précipitation, évaporation, action de l'homme). Contrairement aux autres algues, *D. salina* ne pssède pas de paroi cellulosique la contraignant dans son volume cellulaire, ce qui conduit à une flexibilité morphologique rapide en réponse à un changement de salinité. Ses mécanismes plastiques d'halotolérance sont très bien étudiés, et incluent aussi des ajustements physiologiques (Chen and Jiang 2009; Oren 2017), notamment la production de glycérol comme osmoprotecteur (Zidan et al. 1987).

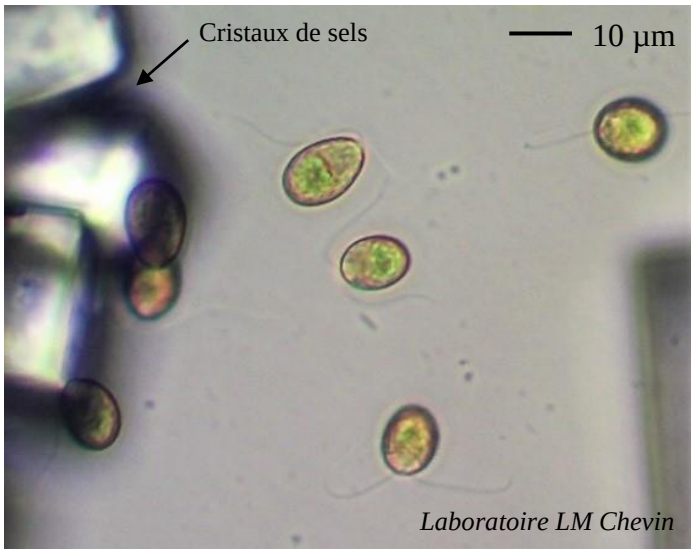

Photo au microscope électronique de *Dunaliella salina*.

Dunaliella salina est un bon modèle biologique pour étudier la mort cellulaire programmée, puisque l'existence de celle-ci a été démontrée chez cette espèce (Orellana et al. 2013). De plus, son temps de génération relativement court (~ 1.4 par jour, Ben-Amotz et al. (2009)) par reproduction asexuée nous permet de réaliser une expérience d'évolution sur des temps d'échelles raisonnables à intégrer lors d'une thèse. Elle est aussi capable de reproduction sexuée, mais dans des conditions rares et mal connues (Ben-Amotz et al. 2009), c'est pourquoi nous l'avons négligée dans ces travaux. Enfin sa niche écologique assez simple (peu d'interaction biotiques) est facile à reproduire en laboratoire, avec un contrôle facile sur les facteurs abiotiques (salinité, lumière). Précisons que cette espèce est aussi étudiée à des fins

d'applications biotechnologiques comme la production de biocarburant, en tant qu'aliment vivant en aquaculture, ou bien intégré dans cosmétiques et des suppléments alimentaires pour son contenu en carotènes (Ben-Amotz et al. 2009).

Mesure de la salinité

La salinité est la quantité de sels dissous dans l'eau. Dans la partie expérimentale de cette thèse, la salinité de notre milieu de culture est définie en moles par litre de NaCl. Ci-dessous quelques conversions avec les deux autres unités de mesures utilisées dans la littérature citée (PSU unité de salinité pratique).

0,5 M = 35 g/L de sels dissous (Eau de mer)

0,8 M = 45 g/L de NaCl

2,4 M = 140 g/L de NaCl = 141 PSU

4 M = 235 g/L de NaCl = 235 PSU

J'ai principalement utilisé deux souches de collection de l'algothèque Culture Collection of Algae and Protozoa (UK), la CCAP 19/12 (renommée souche A) et la CCAP 19/15 (renommée souche C). Ces deux souches phylogénétiquement proches (Emami et al. 2015), et fortement apparentées à la souche de référence CCAP 19/18 (Polle et al. 2017), ont été échantillonnées sur le même site naturel aux eaux saumâtres (North Sinai, Israel) en 1976 par Ginzburg. Avant mon arrivée au CEFE, une réponse démographique bien différenciée de ces deux souches face à des changements de salinité a été observée (Leung et al. 2022), avec seulement la souche A (CCAP 19/12) présentant un patron caractéristique de déclin-rebond en fonction de la salinité. Mon projet a donc été construit à partir de cette observation.

Objectifs de la thèse

Cette thèse s'attache à explorer comment la mort cellulaire, trait plastique mais létal pour l'individu, est susceptible d'évoluer chez une microalgue en milieu fluctuant. Nous avons essayé de comprendre comment la sélection peut favoriser ce trait paradoxal, et quelles seraient les conséquences d'une telle sélection sur les réponses démographiques au stress environnemental. Plus précisément, j'ai cherché à répondre à plusieurs questions de recherche :

1. Quelles sont les conséquences de la mort cellulaire sur la croissance de population et la valeur sélective chez une algue unicellulaire ?

2. Est-ce que ce caractère confère un avantage en compétition dans des environnements fluctuants ?

3. Quelles hypothèses biologiques peuvent expliquer ce motif de déclin-rebond démographique ?

Pour répondre à ces questions, j'ai tout d'abord exploré dans le chapitre 1 les facteurs écologiques pouvant influencer l'intensité de la mort cellulaire d'une part, et son impact sur la valeur sélective à plus long terme d'autre part, à travers d'une série expériences dans lesquelles j'ai suivi les dynamiques démographiques de deux souches suite à un choc osmotique. Dans le chapitre 2, j'ai étudié comment la sélection pourrait agir sur ce trait par une approche d'évolution expérimentale, en cultivant en compétition le génotype induisant de la PCD avec un génotype proche ne l'induisant pas, sous une alternance de basses et hautes salinités. Enfin dans le chapitre 3, j'ai conçu trois modèles théoriques pouvant expliquer le patron de déclin-rebond, et ses conséquences sur la sélection.

L'originalité de mes travaux repose sur une étude éco-évolutive de la mort cellulaire programmée à l'échelle intraspécifique - plutôt que par une approche comparative à grande échelle taxonomique -, à travers le prisme de l'évolution de la plasticité. Contrairement aux travaux précédents, où l'hypothèse adaptative sur la PCD n'était supportée que par des expériences écologiques (pas d'évolution, par exemple Durand et al. (2011, 2014); Orellana et al. (2013)), mon approche par l'évolution expérimentale combinée à de la modélisation me permet d'avoir une vision globale, et de comparer plusieurs hypothèses alternatives pouvant expliquer ce patron démographique de déclin-rebond.

Chapitre 1 : Conséquences d'une mort cellulaire induite par la salinité sur la valeur sélective d'une algue unicellulaire halotolérante

Entrée en matière et résumé de l'article :

L'objectif de ce chapitre est de caractériser les facteurs pouvant influencer le déclenchement et l'intensité de la mort cellulaire programmée chez *Dunaliella salina*, et de déterminer comment ce phénomène impacte la valeur sélective de la population.

Leung et al. (2022) ont récemment reporté une variabilité dans les dynamiques démographiques en réponse à la salinité chez deux souches génétiquement proches de *Dunaliella salina*. Notamment, une des deux souches présente une réponse à un choc hyper-osmotique caractérisée par un déclin majeur de la taille de la population suivi d'une forte croissance exponentielle. A l'inverse, la seconde souche présente une courbe de croissance classique, avec une phase latente (lag phase) précédant la phase exponentielle. Nous avons émis l'hypothèse que le déclin démographique observé pour la première souche est attribuable à une forme de mort active (la mort cellulaire programmée) telle que documentée chez le genre *Dunaliella* (Segovia et al. 2003; Jiménez et al. 2009) et incluant l'espèce *D. salina* (Orellana et al. 2013). Concernant l'effet de ce phénomène sur la valeur sélective de la population, nous avons émis l'hypothèse que la souche présentant un déclin démographique pourrait montrer un meilleur taux de croissance post-déclin que celui qui ne décline pas car les cellules restantes bénéficieraient du matériel relargué par les cellules mourantes (Orellana et al. 2013), comme un comportement altruiste. Cependant, nous avons aussi exploré d'autres hypothèses pouvant expliquer le déclin-rebond, comme un relâchement de la compétition, et exploré plusieurs autres déterminants possibles de ce mécanisme.

Pour tester nos hypothèses, nous avons suivi les dynamiques démographiques de ces deux souches dans diverses conditions afin d'évaluer le caractère plastique de ce phénomène en réponse à la salinité. Nous avons d'abord identifié le signal déclenchant ce déclin chez notre espèce modèle, puis caractérisé le type de mort cellulaire observé chez cette espèce. Nous avons ensuite étudié plusieurs facteurs liés aux ressources (biotiques et abiotiques) et leur impact sur l'intensité du déclin mais aussi sur le rebond démographique.

Nos résultats ont confirmé que la réponse démographique caractérisée par le patron de déclin-rebond d'une des souches est une mort active, réduite par un inhibiteur de la mort cellulaire programmée. Ce caractère plastique est déclenché par la hausse de salinité, et non pas une haute valeur de salinité, chez *D. salina*. De plus, nous avons établi une corrélation positive entre l'intensité du déclin et le taux de croissance postérieur sur l'ensemble des expériences et conditions testées, la souche qui décline montrant une croissance exponentielle plus forte que l'autre souche. De manière remarquable, le déclin est plus prononcé dans les conditions censées être plus favorable à la croissance, à savoir plus lumineuses, sans limitation de nutriments, et avec moins de compétition intraspécifique, renforçant l'idée qu'il n'est pas simplement passif.

En conclusion, ce chapitre nous a permis de montrer qu'un déclin démographique de la population peut être associé à une valeur sélective supérieure à long terme, grâce à une plus forte croissance exponentielle ultérieure. La souche réalisant de la mort cellulaire en réponse à une hausse de salinité pourrait atteindre une taille de population supérieure à celle ne déclinant pas dans certaines conditions, que le processus impliqué soit actif ou passif.

Cet article a été accepté pour publication dans le journal *The American Naturalist* en 2022 (version en ligne https://www.journals.uchicago.edu/doi/10.1086/724417) et est citée dans les chapitres suivants en tant que *Zeballos et al. (2023)*. Il sera publié dans le Volume 201, numéro 6, June 2023.

Article 1 - Acceptable loss: Fitness consequences of salinity-induced cell death in a halotolerant microalga

Running title: Fitness of cell death

Nathalie Zeballos[1], Daphné Grulois[1], Christelle Leung[1*], and Luis-Miguel Chevin[1*]

[1] CEFE, Univ Montpellier, CNRS, EPHE, IRD, Montpellier, France

* Equal contribution

Corresponding author: zeballosnathalie@gmail.com

Nathalie Zeballos: https://orcid.org/0000-0002-3828-6556; zeballosnathalie@gmail.com

Daphné Grulois: https://orcid.org/0000-0002-3054-1364; daphne.grulois83@gmail.com

Christelle Leung: https://orcid.org/0000-0002-7242-3075; leung. christelle@outlook.com

Luis-Miguel Chevin: https://orcid.org/0000-0003-4188-4618 ; luis-miguel.chevin@cefe.cnrs.fr

Keywords: programmed cell death, environmental stress, population decline, natural selection, adaptive plasticity.

Abstract:

Environmentally induced reductions in fitness components (survival, fecundity) are generally considered as passive, maladaptive responses to stress. However, there is also mounting evidence for active, programmed forms of environmentally induced cell death in unicellular organisms. While conceptual work has questioned how such programmed cell death (PCD) might be maintained by natural selection, few experimental studies have investigated how PCD influences genetic differences in longer-term fitness across environments. Here, we tracked the population dynamics of two closely related strains of the halotolerant microalga *Dunaliella salina*, following transfers across salinities. We showed that after a salinity rise, only one of these strains displayed a massive population decline (-69% in one hour), largely attenuated by exposure to a PCD inhibitor. However, this decline was followed by a rapid demographic rebound, characterized by faster growth than the non-declining strain, such that sharper decline was correlated with faster subsequent growth across experiments and conditions. Strikingly, the decline was more pronounced in conditions more favourable to growth (more light, more nutrients, less competition), further suggesting that it was not simply passive. We explored several hypotheses that could explain this decline-rebound pattern, which suggests that successive stresses could select for higher environmentally induced death in this system.

Introduction

Living organisms are pervasively exposed to stressful environments that may reduce their demographic vital rates (survival, fecundity), in turn decreasing their population size, and making them vulnerable to extinction. A widespread mechanism by which organisms can cope with such environmental stresses is phenotypic plasticity, whereby a given genotype produces different phenotypes in response to the environment (Levins 1963; Bradshaw 1965). When the expressed phenotypes increase fitness across environments, then plasticity is said to be adaptive, while plasticity that reduces fitness across environments is described as maladaptive (Ghalambor et al. 2007). Adaptive plasticity and its evolution can reduce extinction risk in fluctuating environments that are sufficiently predictable (Reed et al. 2010; Ashander et al. 2016), and may also allow tolerance of higher rates of directional environmental change (Chevin et al. 2010).

However beyond these simple definitions, demonstrating whether or not a plastic response is adaptive, and why, may be challenging in practice. This is especially true for traits whose most immediate effect is to decrease a component of fitness. For instance, increased cell death rate in response to environmental stress would seem like the archetypical maladaptive, passive trait, which the organism can neither prevent nor control. Yet many unicellular organisms can undergo forms of cell death that are genetically controlled, and involve complex cellular cascades - from caspase-like activity to nuclear DNA degradation (Jiménez et al. 2009; Kroemer et al. 2009; Bidle 2015) - that share features with programmed cell death (hereafter PCD) in multicellular organisms (Ameisen 2002; Bidle and Falkowski 2004; Deponte 2008; Kasuba et al. 2015). Because such PCD appears as an active process, it is generally considered as adaptive, in effect representing a form of adaptive plasticity triggered by a variety of environmental stimuli. However, how and why PCD may be favored by natural selection in unicellular organisms (Franklin et al. 2006; Nedelcu et al. 2011; Durand and Ramsey 2019; Vostinar et al. 2019), where it amounts to cell suicide, remains difficult to understand in most cases, except for a few well-studied examples (Durand et al. 2011; Berngruber et al. 2013). In general, the main argument for considering PCD as adaptive in unicells is that it is an active process, but this is not satisfying because (i) the line between PCD and less active forms of deaths is somewhat blurred, with a range of intermediate situations that are difficult to classify (Kroemer et al. 2009; Barreto Filho et al. 2022*a*, 2022*b*); and (ii) even plastic response that are not evidently active or programmed could still have been favoured by natural selection. Therefore, understanding the causes of selection on PCD – or any form of environmentally

induced rapid death, regardless of where it stands along the PCD continuum - requires demonstrating that this trait varies genetically, and that it is associated with differential fitness (as highlighted by e.g. Reece et al. 2011). Even though PCD is unlikely to be favoured directly, since it causes an immediate demographic decline of the corresponding genotype, it may still be selected indirectly if it is associated with higher fitness in the long run, as any other trait that is selected through its covariance with fitness (Price 1970; Durand and Ramsey 2019). Therefore, understanding selection on PCD requires establishing its covariance with longer-term fitness across genotypes, as well as experimentally testing specific hypotheses for how its fitness costs and benefits arise.

Here, we undertake such an approach with the unicellular microalga *Dunaliella salina*. This halotolerant microalga is the main primary producer of hypersaline biomes such as continental saline lakes, coastal lagoons, and industrial salt ponds, where salinity fluctuates along the year (Ben-Amotz et al. 2009). *Dunaliella salina* can tolerate a broad range of salinities, from below seawater to saturated brine ([NaCl] ~6.2M), through a number of well-characterized, phenotypically plastic mechanisms (Oren 2005; Ben-Amotz et al. 2009; Chen and Jiang 2009). These include rapid morphological flexibility in response to sudden osmotic shock - allowed by absence of a cell wall -, followed by slower physiological adjustments, most notably the production of glycerol as osmoprotectant (Zidan et al. 1987). Overall, phenotypic plasticity is thus a key adaptive feature in this species, and was also recently shown to readily evolve in the laboratory (Leung et al. 2020).

Species of the genus *Dunaliella* can undergo PCD under various environmental triggers, such as darkness (Berges and Falkowski 1998; Segovia et al. 2003; Orellana et al. 2013), UV radiation (Jiménez et al. 2009), or hyper-osmotic shock (Jiménez et al. 2009), the latter being directly relevant for adaptation to salinity. But here again, the potential benefits of PCD remains unclear. A study in *Dunaliella salina* has suggested an advantage of PCD via resource sharing, since dying cells can release large amounts of intracellular glycerol they produced for osmoregulation, which may then be remineralized by prokaryotes, or directly consumed via a heterotrophic pathway (Orellana et al. 2013). However, this study did not compare genotypes that differ in their rate of PCD, to investigate how these differences covary with fitness in the longer run. Recently, Leung et al. (2022) have identified two closely related strains of *Dunaliella salina* that vary in their rate of salinity-induced death. Interestingly, it has also been shown that strain-specific demographic response to salinity, including a rapid decline followed by rebound under hyperosmotic stress for one strain, is also related to gene expression

response involved in chloroplast functions (Leung et al. 2022). This lends support to the hypothesis of chloroplast-mediated programmed cell death, as described in plants and different unicellular organisms (Zuppini et al. 2009; Thamatrakoln et al. 2013; Murik et al. 2014; Ambastha et al. 2015; Bidle 2016). We here use these strains to explore hypotheses about what drives the intensity of cell death, and more crucially, how this decline relates to later population growth. One of our most puzzling finding is that more cell death is associated to faster subsequent population growth across treatments.

Materials & Methods

Strains

We focused on two closely related strains of *Dunaliella salina*, CCAP 19/12 (hereafter strain A) and CCAP 19/15 (strain C) (Emami et al. 2015), which were previously found to vary in their death rates in response to salinity (Leung et al. 2022). We received these strains in 2017 from the Culture Collection of Algae and Protozoa (UK) and maintained them at constant salinity ([NaCl] = 2.4M) for over 3 years prior to this experiment, transplanting them into fresh media twice a week for 5 months (as described in Rescan et al. 2020, constant treatment), and then about once per month. In all experiments described below, we used 10 (nearly) isogenic lines (five for each strain), founded from a single haploid cell isolated using cells-sorting flow cytometry (BD FACSAria™ III ; Biosciences-US) in May 2019.

Common experimental design

Culture conditions

All lines were cultured in 50 ml flasks (CELLSTAR®; VWR 392-0016) with custom-made artificial saline water (Table S1) with modified NaCl concentration (hereafter [NaCl]), and enriched with 2% of Guillard's F/2 nutritive medium (Sigma, G0154-500 ML). The target culture salinity was obtained by mixing the required volumes of hyposaline ([NaCl] = 0M) and hypersaline ([NaCl] = 4.8M) solutions, taking into account the dilution of the inoculum for a final volume of 25 ml. Cultures were maintained in a growth chamber under 12h:12h light:dark cycles, with light intensity 100 $\mu mol.m^{-2}.s^{-1}$ (unless otherwise stated, Table 1), temperature 24°C, and position randomized with respect to treatment.

All assays followed the same general experimental design: we acclimated the lines at intermediate salinity ([NaCl] = 2.4M) for several days (between 4 to 13 days, see Table 1). Then we induced either hyper-osmotic shock or iso-osmotic transfer, by inoculating a volume

of the acclimated cultures into fresh medium at the required expected initial density, and then followed demographic dynamics over 10 days. The initial densities varied between 5,000 and 50,000 cells/mL across experiments for practical reasons: we needed the minimal density (after putative population decline) to be large enough to be detectable with our flow cytometer, but still low enough for substantial exponential growth to occur following decline. More details on each experiment appear in Table 1 and the corresponding sections below.

Population density measures

Population density was assayed using a Guava® EasyCyte™ HT cytometer (Luminex Corporation, Texas, USA), with a laser emitting at 488 nm. We checked the cytometer performance before each measure with the Guava® EasyCheck™ kit. The acquisition settings were 30 seconds, or until the number of counted events reached 200,000 (never reached). Band pass filters based on forward scatter (FSC), side scatter (SSC), and fluorescence emissions in natural red (695/50nm) and yellow (583/26nm), enabled the discrimination of live *Dunaliella* cells from other particles, owing to chlorophyll *a* natural fluorescence (Rescan et al. 2020). Note that some dead (or dying) cells had reduced red fluorescence relative to live cells, and were thus not taken into account for population density (Rescan et al. 2020), but these apparently dead cells do not account for the large population decline we focus on here (Fig S1). We also isolated single cells from doublets (i.e. when 2 cells were detected as a single event) based on the area-to-height ratio of the electronic pulse induced in the flow cytometer (Wersto et al. 2001). To determine population density, we sampled 200 µL of each population to count the number of live cells, at several time points. First, at the end of the acclimation step for the calculation of initial population density before each experiment; then, 1h after the osmotic stress (day = 0); and finally, once per day from day 1 to 10.

When the cytometer was unavailable (nutrient limitation experiment below, days 0-1), we measured whole-well fluorescence (excitation at 390/80 nm -wavelength/bandwidth-, and emission at 685/40 nm) of cultures in 96 well plates, using a BMG ClarioStar spectrometer. To convert from these fluorescence measurements into population density, we fitted a linear model (LM) between cytometer count and fluorescence for days 2 to 4 of the nutrient limitation experiment (see Fig. S2), for which both measurements were available and the population had not yet reached stationarity (Fig. S6).

Experiments and treatments

We have performed a series of experiments to test different hypotheses about the drivers and population consequences of rapid cell death, as summarized in Table 1.

Experiment 1: Salinity change effect

Since *Dunaliella salina* faces salinity variation along the year in its natural habitat, resulting from precipitation and climatic variables (sun and wind) affecting evaporation (Ben-Amotz et al. 2009), we investigated how salinity change affects its demographic dynamics. We compared iso-osmotic transfers (no change from the acclimation salinity) at intermediate ([NaCl] = 2.4M) or high ([NaCl] = 4M) salinity, to hyper-osmotic shock from intermediate to high salinity (from 2.4M to 4M of NaCl), to assess whether the response depends on salinity change or salinity value (3 replicates per condition).

Experiment 2: PCD inhibitor

A plausible explanation for the observed rapid population decline (Fig. 1) is programmed cell death, known to be common in *Dunaliella salina* (Orellana et al. 2013) and related species (Berges and Falkowski 1998; Segovia et al. 2003; Jiménez et al. 2009), notably in response to salt. To investigate this, we used Z-VAD(Ome)-FMK (CellSignaling), a cell permeable irreversible caspase inhibitor that prevents caspase-3-like from adopting its active form, and which has been used to inhibit cell death in a diversity of unicellulars (Bidle et al. 2007; Zuppini et al. 2007; Bidle and Bender 2008; Segovia and Berges 2009; Yordanova et al. 2013), including in *Dunaliella tertiolecta* (Segovia et al. 2003). Following a preliminary test (Fig. S3), we compared the decline rate of cells treated with four concentrations of this inhibitor: 0, 1.6, 3, and 4 µM. Treated cells were incubated in the dark for 30min, before performing iso-osmotic and hyper-osmotic transfers for both strains, with 3 replicates per treatment. Final volume in the flask was 10mL, with an initial total number of cells being 200 000. Population densities were then assessed through cytometer measurements 1 hour and 4 hours after the transfer on day 0, then on days 1, 2, 3. (see Fig. S4 for supplementary days 6, 7, 8 and for strain C dynamics).

Table 1: Summary of experimental conditions.

Experi-ment	Acclimation [NaCl]	Osmotic conditions (n replicates)	Expected initial density, N_0 (cells/mL)	Hypothesis about decline (D) and rebound (r)	Fixed effects for GLM
Salinity change	5d at 2.4M or 4M	Hyper (n=3) Iso (=3)	50,000	D induced by salinity change	Strain × salinity transfer Time (days 1-5)
PCD inhibitor	6d at 2.4M	Hyper (n=3) Iso (n=3)	20,000	D reduced by PCD inhibitor	Inhibitor concentration
Initial density & Growth phase	4d, 13d or 41d at 2.4M	Hyper (n=4) Iso (n=1; control)	5,000 20,000 30,000	D and r modulated by metabolic state, r mediated by competition release	Strain × growth phase × initial density Time (days 4-9)
Nutrient limitation	5d at 2.4M	Hyper (n=5)	50,000	D and r affected by nutrient limitation	Strain × nutrient treatment Time (days 1-3)
Population filtrate	5d at 2.4M or 4M	Hyper (n=3) Iso (n=3)	50,000	Dying cells release molecules that affect D and r	Strain × culture media × salinity transfer Time (days 1-5)
Light intensity	7d at 2.4M	Hyper (n=5) Iso (n=10)	Unknow (spectrosco py)1/10 dilution	Light intensity as external (non-medium) resource influencing D and r	Strain × light Time (days 1-4)
Successive osmotic shocks	14d at 2.4M, then 14d at 4M or 2.4M (control), then 17d at 2.4M	Hyper (n=5)	20,000	D caused by elimination of damaged cells, resulting in faster growth in r.	Strain × acclimation treatment Time (days 3-7)

In the second column, d stands for days and M stands for molar of NaCl. All variables in the last column were treated as categorical, except the Inhibitor concentration and Time (for GLM on demographic rebound r) treated as a continuous variable.

Experiment 3: Initial density and population growth phase

The rapid cell death that we focus on strongly impacts population dynamics, which is indeed how it is detected (Fig. 1) (Berges and Falkowski 1998; Leung et al. 2022). It is thus likely to interact with population density and competition occurring in the population (Ameisen et al. 1995; Christensen et al. 1995). In particular, the initial decline may influence post-decline growth rate, because fewer live individuals means reduced competition for resources (relaxed

density dependence). These effects may also depend on the physiological state of the population prior to the transfer, which is itself influenced by competition and resource limitation in the recent past.

To test for these effects, we acclimated lines of strain A and C for 4 days (mid-exponential phase), 13 days (early-stationary phase) and 41 days (late-stationary phase), representing 3 different regimes influencing current physiological state, and then exposed them to hyper-osmotic stress, starting at 3 different initial densities (5,000; 20,000; 30,000 cells/mL, see Fig. S5). We used 4 different lines per strain as replicates, resulting in 72 flasks (2 strains x 3 Initial densities x 3 growth phases x 4 lines). For the control treatment (iso-osmotic transfer), populations were started at the acclimation salinity 2.4M, with only 1 line per strain (2 x 3 x 3 = 18 flasks). The 90 flasks were treated in 2 temporal blocs, one day apart.

Experiment 4: Nutrient limitation

It has been hypothesized that the population rebound observed following a population decline could result from a beneficial effect of nutrients released by the dying cells (Orellana et al. 2013), which may compensate for a lack of nutrients in the medium. To test this hypothesis, we compared a treatment with nutrient limitation (concentration of F/2 nutritive solution divided by 4 relative to our standard growth conditions) with a standard nutrient treatment, using 5 replicates per treatment. Population measures on day 0 and 1 were made with the spectrometer (fluorescence and optical density), while the following days were measured with the cytometer and spectrometer (Fig. S6).

Experiment 5: Cultures on population filtrates

To further investigate whether the post-decline rebound is related to substances that dying cells might release in the culture medium (nutrients or informative molecules about environmental conditions), we used population filtrates as culture medium. Indeed, it was shown in another microalgal species of the same order (*Chlamydomonas reinhardtii*) that supernatant of cells that have experienced PCD is more favourable to growth than filtrates of cells that have undergone other types of death (Durand et al. 2011), and that this effect depends on the recipient species (Durand et al. 2014). The latter is important, as it determines to what extent PCD may be favoured by kin selection (Durand et al. 2014), through so-called private goods that are preferentially used by relatives rather than public goods that may also be used by cheaters (Estrela et al. 2016, 2019). We thus tested for any strain-specific potential benefits of cell death

in terms of demographic rebound in *D. salina*, more specifically by contrasting a declining and non-declining strain.

To prepare the filtrates, cultures of strains A and C (respectively 2 and 3 lines per strain) were grown in large volume (70 mL) for 4 days at intermediate salinity ([NaCl] = 2.4M), and then transferred to high salinity ([NaCl] = 4M) at an initial cell density of 100,000 cells/mL, in V=110 mL. On the next day, when the decline was expected to be maximal for strain A (according to Fig. 1), we verified that strain A actually showed a decline (*ca.* 50% in 24 hours), while strain C did not. We centrifuged and filtered these large volumes, so as to get our 2 filtrates as culture media (filtrate A and C respectively for strain A and C). We then inoculated 3 replicate lines per strain in 3 different culture media (filtrate A, filtrate C, and standard artificial saline water as a control), mixed in a ratio 1:1 with our artificial saline water to insure the presence of nutritive solution. We applied 3 salinity transfers (Fig. S7): iso-osmotic at 2.4M and at 4M, and hyper-osmotic from 2.4M to 4M of NaCl, for a total of 54 flasks: 3 culture media x 3 salinity transfers x 2 strains x 3 replicates (minus 3 flasks because one acclimated population of strain A did not reach a sufficient density).

Experiment 6: Light intensity

Different studies have underlined the potential role of chloroplast activities in PCD phenomenon (Murik et al. 2014; Ambastha et al. 2015; Bidle 2016), and recent gene expression analysis on our focal strains revealed that strain-specific gene expression response to salinity changes involved mostly genes related to chloroplast structures and activities (Leung et al. 2022). In addition, light represents a resource that is not modified by putative elements released in their medium by dying cells (as long as transparency is not affected). We thus tested whether light intensity influences the decline and rebound induced by a salinity rise, through an effect of photosynthetic activity on the physiological state of cells. To do so, we repeated experiment 1 but at 200 $\mu mol.m^{-2}.s^{-1}$ light intensity instead of 100 $\mu mol.m^{-2}.s^{-1}$, during both acclimation and assay phases (Fig. S8). These two light levels are commonly considered in the literature as not stressful (Berges and Falkowski 1998; Sui and Harvey 2021), but 100 $\mu mol.m^{-2}.s^{-1}$ is slightly limiting compared to 200.

Experiment 7: Successive osmotic shocks

The pattern of population decline and rebound that we observed in response to osmotic stress may be explained by the elimination of cells that were initially damaged or in low condition (e.g. old); a rapid population rebound would then be the result of faster multiplication of cells

that were initially in better physiological state. This hypothesis implies a process akin to evolutionary rescue (Gomulkiewicz and Holt 1995), but where selection acts on a non-heritable phenotypic variation (as we used nearly isogenic lines). We would thus expect that the decline would be drastically reduced upon a second osmotic shock, because most cells in bad condition would already have been eliminated.

To test this hypothesis, we assessed the population decline for populations that were subjected to two successive hyper-osmotic shocks, separated by a return to intermediate salinity, which we compared to populations subjected to a single hyper-osmotic shock. We acclimated populations of strain A and C at intermediate salinity ([NaCl] = 2.4 M) for 14 days, transferred them a first time at high salinity ([NaCl] = 4 M) for 14 days. Then we transferred them back to [NaCl] = 2.4 M for 17 days (about 17 generations, assuming ~ 1 generation per day, Ben-Amotz et al. 2009), before inducing a second salinity rise at 4M, and (expected) initial density of 20,000 cells/mL (Fig. S9). In the control condition, cultures were subjected to iso-osmotic transfer first (constant salinity at 2.4M), and exposed to hyper-osmotic shock only at the second transfer. We used 5 different lines per strain as replicates for each treatment (except 4 replicates for strain C in the successive shocks treatment, because of 1 broken flask).

Statistical analysis

To investigate effects of our treatments on population dynamics, we performed generalized linear models (GLM), using cells count data as response variable (except for the nutrient limitation experiment, based on whole-well fluorescence), with a log link function and a negative binomial error structure, as this has proved more accurate than Poisson in our setting (Rescan et al. 2020). First, to test for population decline following the transfer, we applied such a GLM to population size at day 1, using the logarithm of expected initial population density (based on population size at the end of the acclimation step) as offset. The linear predictor in this model thus estimated the logarithm of the relative change in population density from day 0 to 1. For the light experiment, we compared the experiment with brighter light against all other experiments under hyper-osmotic stress (except under nutrient limitation, where cytometer counts were not available for all days, and with the PCD inhibitor). For the nutrient limitation experiment, we applied a linear model to the logarithm of population density estimated by the whole-well fluorescence values (day 1) , because fluorescence is log-normally distributed (Rescan et al. 2020). The offset was the logarithm of the initial population density estimated by

fluorescence of strain C (one hour after the transfer), as this strain does not display population decline (Fig. 1).

We then applied a second GLM for population growth in days corresponding to a phase of exponential growth (details in Table 1), visually detected as a linear trend on population dynamics on log scale (this phase is denoted as grey backgrounds on Fig. 1 and Figs. S4-S9). In this model, no offset was used for initial population size, but day was included as a continuous explanatory variable. The day effect in this model thus estimated the rate of exponential growth per day (linear trend on the log scale), and any interaction of day with other factors (treated as covariates in the regression) were effects of these factors on maximum, exponential growth. The fixed effects were experiment-dependent (Table 1). For population growth under nutrient limitation, we applied the same approach but using a LM on the logarithm of population densities based on whole-well fluorescence. For the light experiment, we applied the GLM on the subset of days corresponding to the exponential phase in each experiment (determined as specified above).

Our results suggested that across experiments, larger initial decline was associated with faster maximal growth under hyper-osmotic stress. To formally test for this effect, we estimated the decline rate (on the log scale) predicted by the GLM as:

$$D = \ln\left(N_{0,exp}\right) - e_1 \qquad \text{(Eq. 1)}$$

where e_1 is the linear predictor of the GLM (i.e. the estimator of population density on the log scale, no longer corrected by the offset) at day 1 after the shock, and $N_{0,exp}$ is the initial population density expected from the acclimation culture. A positive value of *D* means that the population has declined after the transfer. The standard error for the decline rate *D* is directly that of the linear predictor on the log scale. In the results, we also expressed the decline as proportional reduction in population size,

$$Population\ reduction\ (\%) = (1 - e^{-D}) \times 100 \qquad \text{(Eq. 2)}$$

We also estimated the maximal daily growth rate *r* in the exponential phase as

$$r = \frac{e_{x_2} - e_{x_1}}{x_2 - x_1} \qquad \text{(Eq. 3)}$$

where e_{x_1} and e_{x_2} are the linear predictors of the GLM (log population size) at days x_1 and x_2 after the shock, corresponding to the phase of exponential growth (grey backgrounds on Fig. 1 and Figs. S4-S9). We calculated the standard error of each estimated growth rate as:

$$\mathrm{SE}(r) = \frac{\sqrt{\mathrm{SE}(e_{x_2})^2 + \mathrm{SE}(e_{x_1})^2}}{x_2 - x_1} \quad \text{(Eq. 4)}$$

We then tested the significance of the relationship between the estimated decline rate and rebound growth rate using a bootstrap method. For each *D* and *r* pair (corresponding to a specific condition in a given experiment), we drew random values from a normal distribution with mean given by the estimate, and standard deviation given by the standard error of the estimate, to account for the uncertainty in each data point. A linear model was then fitted for the relationship between *D* and *r* across conditions in each of these simulations, and the corresponding regression slope and intercept were drawn from normal distributions centred on their estimates and with SD given by their SE, to account for uncertainty in each regression. We repeated this process 10000 times, from which the proportion of positive slopes was used as a p-value.

Finally, the mean slope *b* and the intercept *a* over these 10000 simulations were used to compute the predicted population density at day *t* for non-declining population as

$$\ln(N_t) = \ln(N_0) + a \times t \quad \text{(Eq.5)}$$

or for a declining population starting to rebound at day *c* (corresponding to x_1 in eqs. 3-4) as

$$\ln(N_t) = \ln(N_0) - D + (a + bD) \times (t - c) \quad \text{(Eq.6)}$$

From this, we could then estimate the day at which a declining and a non-declining population would reach equal population density, assuming exponential rebound:

$$t_{eq} = c + \frac{1}{b} + \frac{ac}{bD} \quad \text{(Eq.7)}$$

All statistical analyses were performed on Rstudio (R version 3.6) using MASS version 7.3.53 package (Venables and Ripley 2002).

Results

We wished to understand the proximal determinants and fitness consequences of programmed cell death in a unicellular organism. Our aim was to find whether, and under which conditions, such apparently detrimental phenotype may be associated with genotype-dependent benefits for population growth, and thus potentially be favoured by natural selection.

Decline in response to osmotic shock is strain-specific

As salinity is a major component of *Dunaliella salina*'s niche, we first investigated its influence on demographic dynamics in this species. We observed that an iso-osmotic transfer into fresh medium without change in salinity (either at intermediate 2.4M or high 4M NaCl concentration) did not affect demography, since population densities measured 1-hour post-transfer matched the expected initial densities, accounting for the dilution into fresh medium (Fig. 1, Table S2). In contrast, transfer from intermediate to high salinity induced a sharp demographic decline in strain A in the hours following the transfer, with population size reduced by 69% in one hour (Table S2), and reaching 77% decline at its minimum, 24 hours post-transfer. This decline was not observed for strain C (Fig. 1, Table S2), leading to a significant effect of strain identity on population density on day 1, and a significant interaction between strain and type of salinity transfer (Table 2). This indicates that the rate of rapid cell death varies among closely related strains of *D. salina* (as shown by Leung et al. 2022), and does so in a manner that depends on the type of salinity transfer, being triggered in strain A by a salinity rise rather than by high salinity *per se*. Note that the osmotic shock also led to an increase in the number of apparently dead cells (detected by their lower red fluorescence, Rescan et al 2020), but orders of magnitude lower than the observed decline of live cells, and of similar magnitude between both strains (Fig. S2).

Interestingly, the population decline of strain A was associated with a higher maximum growth rate in the following days, as compared to its growth rate without initial decline (Fig. 1, left and right panels; Table S3 $P<3e-8$ and $P< 3e-15$, respectively). In contrast, strain C, which did not decline following hyper-osmotic shock, had a weaker maximum growth rate compared to strain A in this salinity condition (Table S3, $P<2e-16$). As a result, even though strain A had a much lower population density than strain C after its initial decline under hyper-osmotic stress, it eventually compensated for its lag in population size, reaching a density similar to strain C after 6 days.

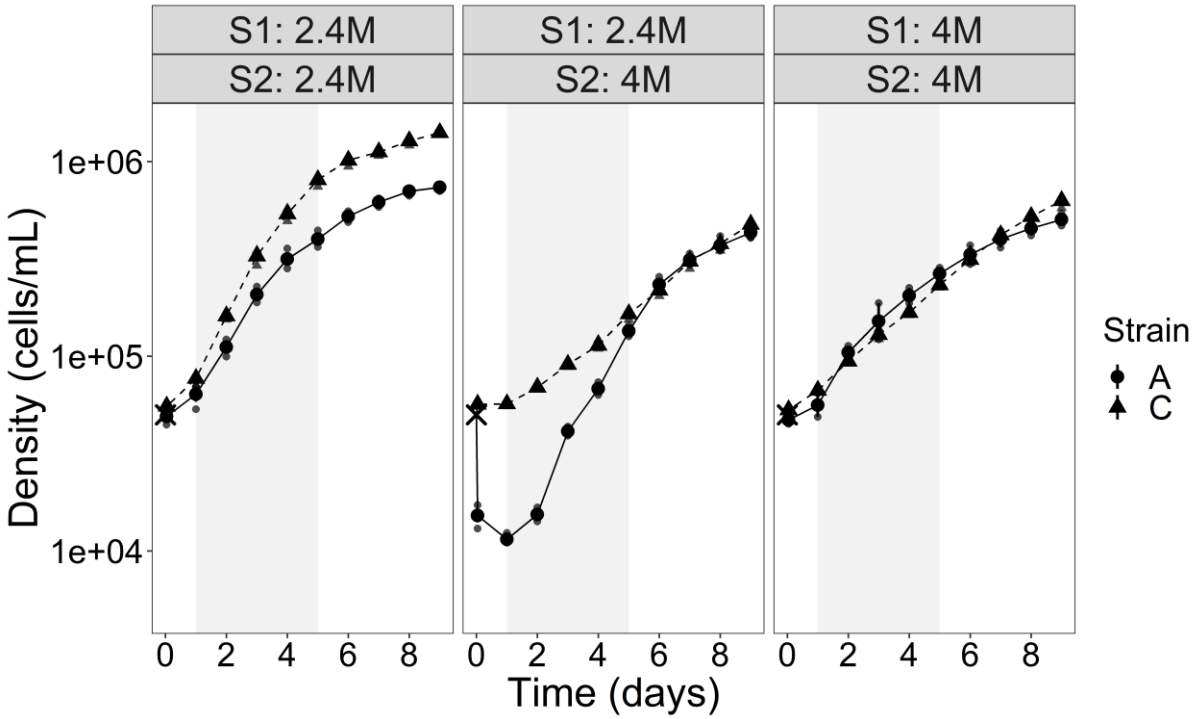

Figure 1. Demographic dynamics of *Dunaliella salina* following salinity transfers. Each panel represents a transfer condition from the acclimation salinity (S1: Salinity 1) to the assay salinity (S2: Salinity 2). Transfer occurs at day 0, and the first point is measured 1 hour after the transfer, while the cross represents the expected initial density, predicted from dilution of the acclimated population. The number of live *D. salina* cells per mL in each day is represented on log scale, for strains A (dots) and C (triangles). Symbols are averages over 3 replicates and error bars indicate the standard error, while lighter points are the raw densities.

Table 2: Analysis of deviance table for the GLM of population density on day 1.

Factors	Df	Deviance	Resid. Df	Resid. Dev	Pr(>Chi)	R^2
NULL	16	964.93				
Strain	1	154.67	15	810.26	< 2.20E-16 ***	0.16
Transfer	2	444.95	13	365.31	< 2.20E-16 ***	0.46
Strain x Transfer	2	348.31	11	17	< 2.20E-16 ***	0.36

We used a GLM with log link function and a negative binomial error structure for population density at day 1, using the expected initial (log) density as offset. Tested effects are Strain, Transfer and Strain × Transfer interaction, and *** denote p-values <0.001. R^2 was calculated as a deviance ratio (Nakagawa and Schielzeth 2013).

The decline is reduced by a programmed cell death inhibitor

To assess whether the rapid population decline may result from programmed cell death, as commonly documented in this species and genus (Berges and Falkowski 1998; Segovia et al. 2003; Jiménez et al. 2009; Orellana et al. 2013), we performed an experiment with a caspase-3-like PCD inhibitor, at four different concentrations. The PCD inhibitor had a clear quantitative effect on the intensity of the decline, with higher inhibitor concentration leading to less severe decline for strain A under hyper-osmotic shock (Fig. 2). Accordingly, the GLM treating inhibitor concentration as a continuous variable had a slighter better AIC than the one treating it as a categorical factor (AIC = 220.78 vs 223.33). We found a significantly positive relationship (Table S4A, P<1e-3) between (log) population size at day 1 (post-decline) and inhibitor concentration, with a slope of 0.150 (SD = 0.045). The model thus predicts that the population size one day after hyper-osmotic shock is reduced by 70.8% without inhibitor (consistent with our previous experiment), but is proportionally increased by ~16% with each additional µM of inhibitor. In a preliminary experiment (with only 2 replicates), we even found that strain A already started to decline 15min after the osmotic shock (43% reduction in population size), while the 3 treatments with inhibitor did not (Fig. S3). In contrast, we found no effect of the inhibitor concentration on demographic dynamics in other conditions (strain A under iso-osmotic transfer, and strain C in any salinity transfer; Fig. S4). There was no significant difference effect of inhibitor concentration on maximum growth-rate between days 1 and 6, despite the observed differences in decline intensity (Fig. 5, Table S4B, P= 0.107). These results therefore indicate that the population decline observed for strain A under hyper-osmotic shock is at least partly explained by PCD.

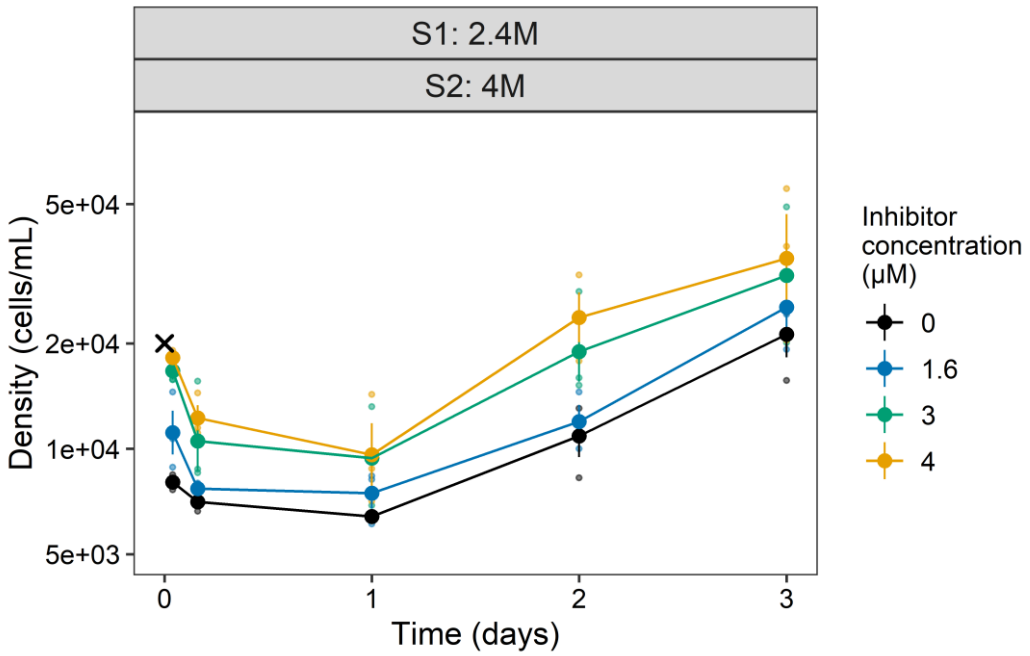

Figure 2. Influence of an inhibitor of programmed cell death. Demographic dynamics of strain A following a hyper-osmotic shock (2.4M to 4M NaCl) are shown under different concentrations (colours) of an inhibitor of caspase-3-like, a typical marker of programmed cell death. Transfers occurred at day 0, and the first measures were made 1 hour after the transfer, while the cross represents the expected initial density, predicted from dilution of the acclimated population. The number of live *D. salina* cells per mL in each day is represented on the log scale. Filled symbols are averages over 3 replicates, error bars indicate the standard error, and lighter points are the raw density measurements.

Initial decline is greater under weaker competition

To understand what benefit such salinity-induced PCD may confer, we investigated hypotheses about reduced competition. A possible explanation for the higher growth rate of strain A following its initial decline under hyper-osmotic stress may be relaxed density dependence (competition release), whereby the resources unused by dead cells become available to those cells that survived. The influence of initial decline on later growth would thus be mediated by density-dependent processes. More specifically, we may expect the post-decline population to have a similar growth rate to a population that did not decline but started at similarly low density. In addition, the rate of death (and thus the population decline) could itself be modified by the initial population density, if PCD is a plastic trait that responds to cues of the density of conspecifics, or amount of resources. However, these influences of competition-mediated resource limitation on population growth are likely to be modulated by the metabolic state of individual cells (Delong and Hanson 2009), which in turn depends not only on the immediate density of competitors, but also reflects the previous growth conditions during the acclimation phase (Rescan et al. 2020). This occurs because the influence of competition and resource

limitation on the physiological states of individual cells (and hence population growth) depends on the rates of nutrient uptake and metabolic pathways involved, and may involve some delays (Droop 1973). We thus tested for an influence of not only the initial density of the inoculum, but also of the growth phase of the populations in the acclimation phase, as an indicator of the physiological state of the population. We report results about rates of initial decline and maximal growth rate in Figure 3, while the full population dynamics appear in Figure S5.

Overall, strain A showed greater decline in conditions where population growth is expected to be more rapid, that is, when cultures were transferred during their exponential or early stationary phase, and/or starting at low initial density (Fig. 3A). When the populations experienced osmotic shock in the mid-exponential or early-stationary phases (after 4 or 13 days of acclimation, respectively), the initial density did not impact the intensity of the observed decline in Strain A (Fig. 3A & Table S5A). In contrast, populations transferred in their late stationary phase (41 days) showed no decline when starting at high density (30,000 cells/mL), but a decline comparable to that in earlier phases when starting at low density (5,000 cells/mL) (Fig. 3A). Overall, across initial densities, populations transferred in their late stationary phase declined less than when transferred in earlier phases (Table. S5B). Contrary to strain A, strain C never declined in any demographic conditions (Fig. 3A).

Following the decline, strain A displayed higher maximum growth rate than strain C for the mid-exponential and early-stationary phase populations (Fig. 3B). Furthermore, the growth phase ("age" of the cultures before the transfer) influenced the maximal growth rate for strain A, but with an effect that also depended on density. The maximum growth rate was highest for populations transferred in their early-stationary phase, when starting at N_0 = 30,000 cells/mL (Table S6, P=0.037 for the comparison with exponential phase starting at N_0 = 5,000), while when starting at N_0 = 5,000 cells/mL they did not show a significantly different rebound that those transferred in their exponential phase (Table S6, P=0.839). In particular, the rebound growth rate of strain A inoculated at N_0 =30,000 cells/mL was higher than the growth rate of the non-declining strain C that started at a density similar to A post-decline (N_0 = 5000 cells/mL; see Fig.S5 and Fig. 3). This confirmed that density-dependent effects on population growth are largely mediated by persistent responses to past conditions of competition and resource limitation (as shown for salinity by Rescan et al. 2020). The weak and inconsistent effect of initial density on the rate of population rebound further suggests that this rebound is unlikely to be due to relaxed density dependence from many cells having died. In fact, our focus on

the rate of exponential growth limits the possibility for density to have a large effect, since exponential growth is density-independent by definition.

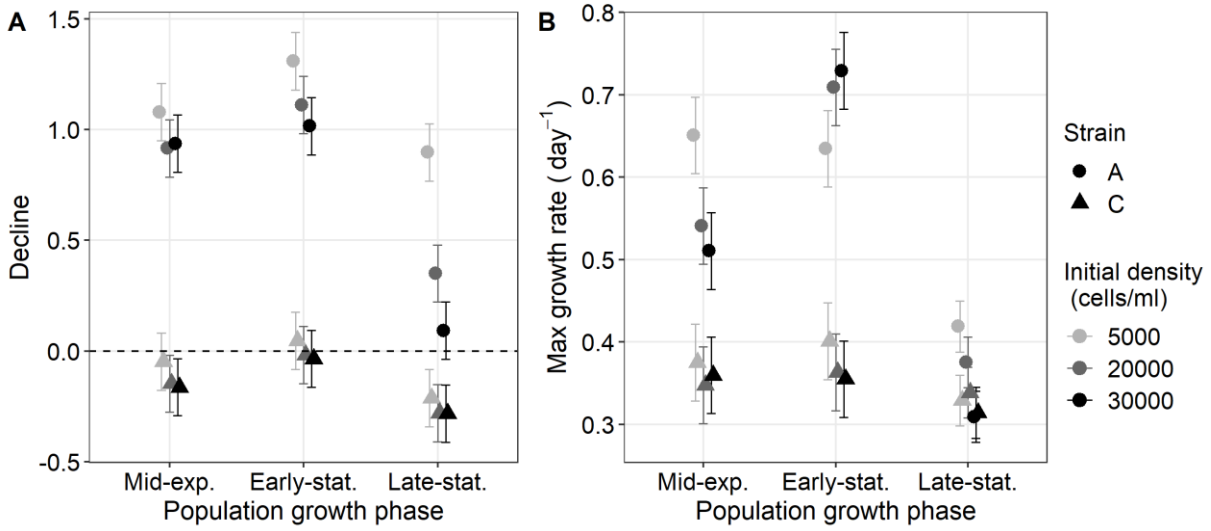

Figure 3. Impact of competitive conditions on initial decline and subsequent maximal growth following hyper-osmotic shock. Estimates and standard errors (across 4 replicates) from the negative binomial GLMs for (A) decline (days 0-1 after the osmotic shock), and (B) the maximal growth rate (corresponding to the shaded area in Fig. S5), are shown for different conditions of initial density (grey shades) and population growth phase (x-axis), for strains A (dots) and C (triangles). Population growth phase correspond to mid-exponential phase (Mid-exp: 4 days of acclimation), early-stationary phase (Early-stat: 13 days) and late-stationary phase (Late-stat: 41 days). In panel A, larger positive values indicate faster population decline, while negative values correspond to growing populations.

Decline intensity depends on resources or cues from the culture medium

To more directly assess the role of resources competition on the observed pattern of decline and rebound, we manipulated nutrient abundance. When fewer nutrients were available, strain A declined significantly less than populations in control medium (Fig. 4A, Table S7 P=1e-4). (Note that the estimated decline and maximal growth rate were predicted based on spectrometer measures (Fig. S6A) instead of flow cytometry counts for this experiment.) The estimated maximal growth rate in exponential phase (from days 1 to 3 in this experiment) was clearly lower for strain A when nutrients were missing (Fig. 4B; Table S8 P=0.003). As in the previous experiment, in standard nutrient conditions strain A displayed a higher maximal growth rate compared to strain C (Table S8, P=3e-7).

Since the medium content affects the intensity of decline for strain A, we tested the hypothesis that the dying cells causing population decline release nutrients that may be used by the remaining cells to grow faster, or informative cues about the population demographic status. We also investigated whether the ability to use this resource or information was genotype-

specific. To do so, we grew populations of each strain in medium filtered from previous cultures that had undergone a salinity rise, either from strain A (filtrate A) or strain C (filtrate C) (Fig. 4C and 4D). Populations of strain A growing on filtrate A had a slightly but significantly lesser decline than control populations A growing in standard medium (Table S9: population reduction of 73% *vs* 77 %, P=0.026). Those growing on filtrate C instead showed a greater decline than the control (Table S9: population reduction of 81% *vs* 77 %, P=0.021). In contrast, we did not detect any effect of culture medium on the rebound growth rate for strain A (control: r=0.64, strain A in filtrate A: r=0.59, P=0.129; strain A in filtrate C: r=0.68, P=0.153 in Table S10). We also did not find any effect on the population growth of strain C, either in the first day (P=0.058 & P=0.219, respectively in filtrate A and in filtrate C compared to control culture, see Table S11A), or after day 1 (in all conditions r ∈[0.26;0.28]; P=0.092 & P=0.783 see Table S11B).

Decline and rebound depend on resources outside the culture medium

We also studied the effect of light intensity, an important resource for photosynthetic organisms, which unlike the medium should not be directly affected by the dying cells. We compared the control conditions from experiments above (plus one below with successive osmotic shocks), where populations faced a salinity rise at light intensity of 100 $\mu mol.m^{-2}.s^{-1}$ photons, to populations undergoing a salinity rise at higher light intensity 200 $\mu mol.m^{-2}.s^{-1}$ (Fig. 4E and 4F). The decline rate of strain A was significantly greater under brighter light (population reduced by 82% at 200 $\mu mol.m^{-2}.s^{-1}$ *vs* 57% at 100 $\mu mol.m^{-2}.s^{-1}$; P<0.001, Table S12A). Similarly, strain A grew significantly faster in the exponential phase (shaded area on demographic dynamics) under brighter light (r=0.87 vs 0.43 for 200 *vs* 100 $\mu mol.m^{-2}.s^{-1}$, P=0.007 in Table S12B). This confirmed that resource conditions more favourable to growth led to faster decline followed by greater growth rate.

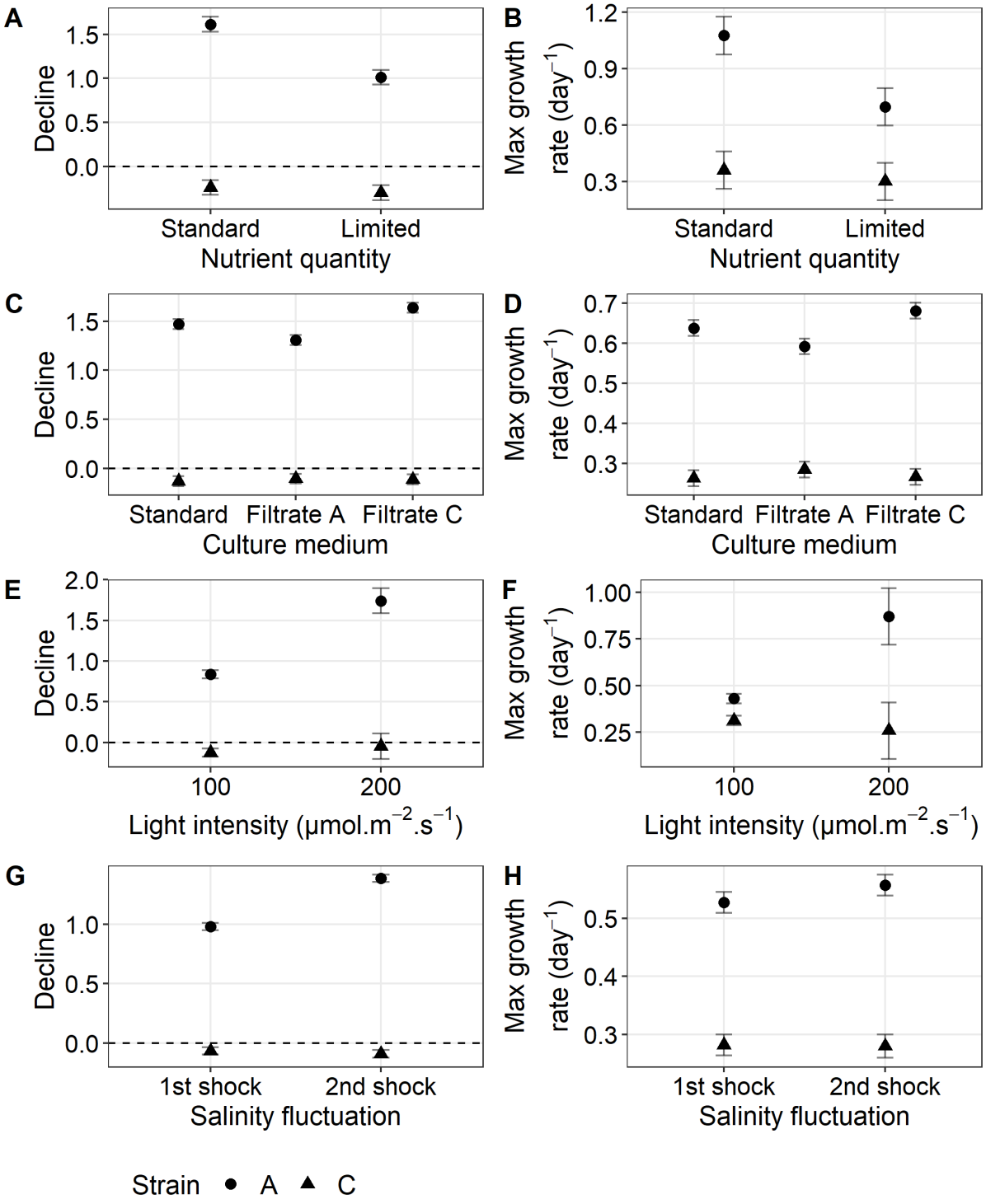

Figure 4. Influence of resources and previous stress on decline and rebound. Estimates and standard errors across 5 replicates (except for supernatant experiment: 3 replicates) from the negative binomial GLMs for decline on days 0-1 after the hyper-osmotic shock (left: A, C, E, G), and maximal growth rate on the exponential phase after the osmotic shock (right: B, D, F, H) are shown for different experimental conditions, for strains A (dots) and C (triangles). The factors investigated are the amount of nutrients in the culture medium (A-B); putative molecules released by cells that do or do not die in response to osmotic shock (C-D); light intensity, a resource type not directly modified by dying cells (E-F); and a previous salinity shock (G-H). All estimates are based on cytometer counts, except A-B on whole-well fluorescence.

A consequence of heterogeneity in cell condition?

Initial heterogeneity in the metabolic state or condition of cells could explain the decline-rebound pattern observed in response to hyper-osmotic shock (Fig. 1). Indeed, older or more damaged cells within the population may be rapidly eliminated when facing hyper-osmotic shock, while those that were originally in good condition may survive and reproduce faster.

To investigate this hypothesis, we applied successive salinity rises to the two strains, separated by a short stay of 17 days at intermediate salinity (corresponding to ~17 generations). Our prediction under the hypothesis of an effect of cell condition was that a second osmotic shock imposed shortly after the first one should lead to a more moderate decline (if any), because damaged cells have already been eliminated. Contrary to this expectation, we found that the decline of strain A was greater upon a second salinity rise than after a single salinity rise (population reduction of 75% vs 62%, Fig. 4G, Table S13A P<2e-16), while the number of salinity rises did not impact the initial growth rate of strain C (no decline, Fig. 4G). For both strains A and C, the maximum growth-rate did not differ between the two treatments (Fig. 4H, Table S13B P=0.345).

Sharper decline is associated with faster rebound across all treatments

The results of these experiments suggest that faster initial decline was generally followed by a higher maximum growth rate (e.g. Fig. 4). In order to formally test for this pattern, we gathered all estimated pairs of decline intensity D (log reduction in population size between days 0 and 1, with larger positive values denoting sharper decline) and rebound rate r (daily rate of maximum exponential growth) for strain A facing a salinity rise, across experiments (Fig. 5). We found a highly significant positive relationship ($P = 8 \times 10^{-4}$) between D and r. Decline intensity D ranged from 0.22 (19.8% reduction in population size for late stationary cultures transferred at high density) to 1.6 (79.8% reduction in population size under bright light). The slope of the regression of r against D is 0.268 (SD = 0.074). This means that relative to a putative population that would not decline, a population that initially declines by D but starts rebounding at day 1 would compensate for its initial demographic deficit by day 5 if $D = 1.47$ (77.0% initial reduction in population size), and by day 10 if $D = 0.22$, under exponential growth. In other words, a population that initially declines faster is predicted to match the size of a non-declining population more rapidly during exponential growth, and/or may reach its carrying capacity first, thus potentially exerting competitive exclusion on the non-declining strain (Kot 2001).

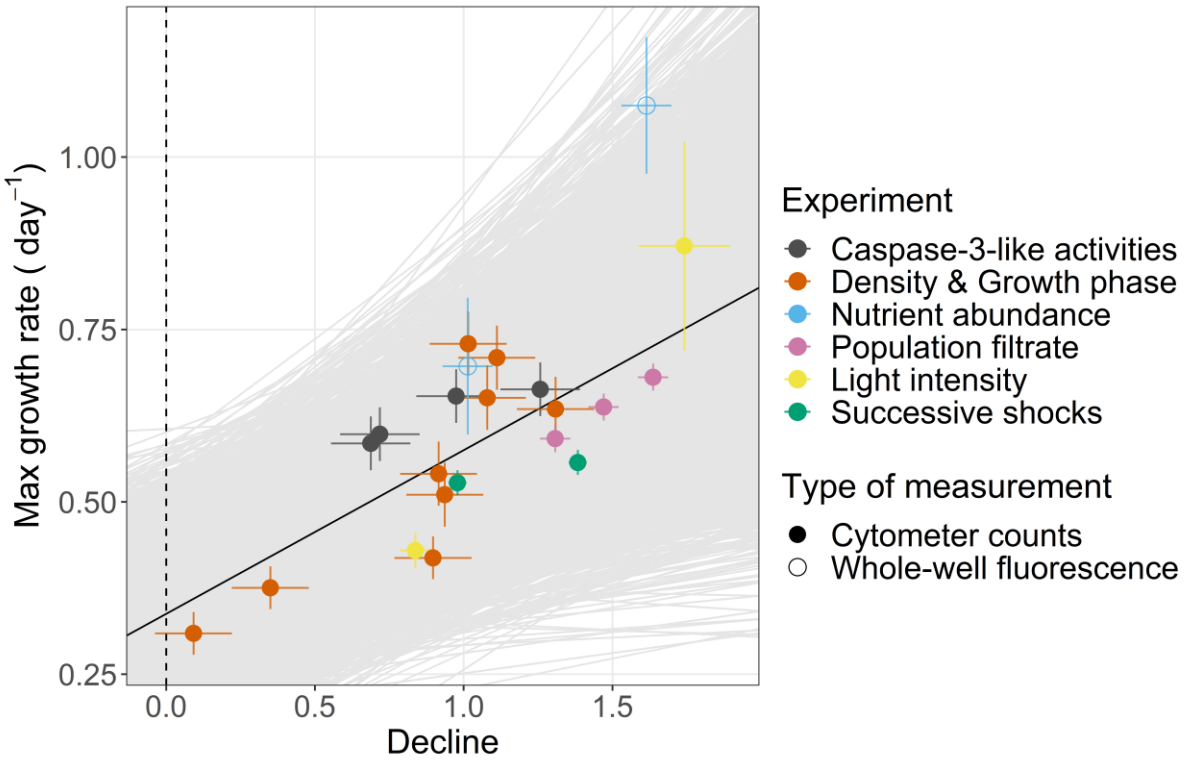

Figure 5. Faster decline is associated to faster maximal growth across experiments. All estimates and standard errors for decline and rebound rates are shown for strain A following a salinity rise. Grey lines represent 10000 linear regressions of growth rate against decline rate, based on simulated samples where each pair of values (for decline and rebound) was randomly drawn from a normal distribution with mean set to the predicted value and standard deviation set to the standard error of estimators for each condition. Height of the 10000 replicates had a negative slope ($P = 8x10^{-4}$). Estimates from the nutrient experiment (blue empty circles) are not included in the linear regression, as they were based on whole-well fluorescence instead of cytometer counts.

Discussion

We investigated the factors influencing rapid, programmed cell death (PCD) in two closely related strains of the halotolerant microalga *Dunaliella salina*, and its demographic implications beyond the initial decline it produces. Our aim was to decipher how variation among strains in these demographic responses may impact selection on a trait that seems at first like an archetype of maladaptive plasticity.

Implications of the decline-rebound pattern

We established that the demographic response to high salinity characterized by a rapid decline followed by rebound (shown by Leung et al. 2022) is induced by salinity rise, rather than high salinity *per se* (Fig. 1). This fast response (population size reduced by 69% in one hour, Table S2, and even a reduction by 43%, in 15 min Fig. S3) matched the findings for the closely related

species *D. viridis* (Jiménez et al. 2009), where about 70% of the population died one hour after a hyper-osmotic shock (from [NaCl] = 2M to [NaCl] = 5.5 M), as well as for another unicellular chlorophyte *Chlorella saccharophila* (Zuppini et al. 2010) (between 21.9% and 33.1% decline after 24 hours of hyper-osmotic stress). The decline-rebound pattern that we observed further matched the previous finding in *D. salina* that darkness (rather than salinity rise as here) causes the death of *ca.* 65% of cells, but later enhanced population growth (Orellana et al. 2013).

Interestingly, this phenotypic response varied drastically between two genetically close *Dunaliella* strains (Emami et al. 2015; Leung et al. 2022), one of which never displayed the characteristic decline-rebound pattern after a salinity rise, regardless of other experimental factors. While the specific genetic differences behind these contrasted responses to salinity are unknown, it is noteworthy that gene expression and DNA methylation responses to salinity vary between these strains (Leung et al. 2022). Orellana et al. (2013) used yet another strain (CCAP-19/18, phylogenetically close to 19/12-strain A and 19/15-strain C used here, Assunção et al. 2013; Emami et al. 2015), which did decline, suggesting that there is genetic variation for this trait within *D. salina*, unlike in other species where such demographic responses have been investigated (Nedelcu et al. 2011; Durand 2020). The putative benefits of this decline also appeared to be strain-specific, as the growth of strain C was not influenced by filtrate of declining strain A (Fig. 4D, Table S11), mirroring the lack of significant effect of induced-death filtrate on 2 strains in *Chlamydomonas reinhardtii* (Durand et al. 2011). The markedly distinct demographic responses of these closely related strains imply that natural selection can act on rapid, environmentally induced cell death, favouring it in conditions where it is associated with higher accrued fitness during the demographic rebound.

Such a positive correlation between initial decline and later demographic rebound following osmotic shock was one of our most striking results (Fig. 5). This allowed the declining genotype to compensate for its initial lag, eventually reaching a density similar to - or even higher than - the non-declining genotype (Fig. 1, Fig. S6 and S7), before attaining the stationary phase where population growth stops (commonly described as carrying capacity). Assuming that the dynamics in monocultures predict what would happen in co-cultures, i.e. neglecting genotype-by-genotype demographic interactions causing frequency-dependent selection (Chevin 2011), these results suggest that the lethal, and at first glance disadvantageous, phenotype of rapid cell death is likely to be favoured in an environment with fluctuating salinity (including hyper-osmotic shock).

Causes of selection

Which mechanism could explain the positive correlation we found between decline and rebound rates for strain A? Our main hypothesis was that the dying cells release material that is beneficial to the remaining cells, thus representing a form of cooperation (Durand et al. 2011; Orellana et al. 2013). The importance of environmental dynamics for social evolution, especially in microbes, was recently emphasized (Estrela et al. 2016, 2019), and could involve different mechanisms (Kojic and Milisavljevic 2020). For example, dying cells might provide resources by liberating nutrients (public goods) in the culture medium. This organic material may include intra-cellular glycerol (Zidan et al. 1987) that *D. salina* massively stores in its cytoplasm as osmo-protectant at high salinity, and could be used directly by the surviving cells (*D. Salina* being capable of heterotrophy (Chavoshi and Shariati 2019)), or metabolized by a halophilic archaea, as proposed by Orellana et al. 2013. However, we did not find a faster rebound for strains A growing on filtrate A, (and no "cheating" effect on the growth of strain C) and hence found no support for the altruistic nutrient-release hypothesis. Either this effect does not exist in this system, or it exists but could not be detected because death-induced molecules were too rare in the diluted filtrate, or because naturally co-occurring archaea that remineralize glycerol were absent. Another altruistic mechanisms could be the detoxification of the environment by dying cells (Estrela et al. 2019), but we are not aware of any mechanism through which *D. salina* might reduce salinity, which is the major stressful condition applied here. Signalling molecules could also be released, providing information about the environmental conditions, such as quorum-sensing molecules (Christensen et al. 1995; Durand 2020). This hypothesis cannot be discarded since strain A growing on filtrate A showed a more moderate decline (Fig. 4C), suggesting that live cells may perceive that a demographic decline already occurred, therefore modulating the proportion of cells that will die. To sum-up, our results did highlight that the declining strain is sensitive to the medium content, but we do not have clear evidence that this is an altruistic trait.

Another less adaptive hypothesis explaining the decline-rebound pattern could be a trade-off between reproduction and the rate of plastic change in a trait involved in salinity tolerance. Genotypes that invest more in salinity tolerance, by having more rapid plastic change in dedicated traits, should have higher survival probability when facing osmotic stress, but possibly at the expense of lower growth rate if salinity tolerance mechanisms are costly for reproduction. Such trade-off could involve the metabolism of glycerol, which is known to divert resources produced by photosynthesis or stored in starch (Ben-Amotz and Avron 1973), and is

thus likely to impact population growth (Jones and Galloway 1979). A related concept in ecology is the trade-off between resistance and recovery with respect to resilience, whereby a strain that is more susceptible to stress (less resistant) is able to recover faster from it (Hodgson et al. 2015). However, this hypothesis would not explain why for a given genotype (strain A), conditions that cause sharper decline also lead to faster growth during rebound.

A third hypothesis explaining the decline-rebound demography could be cell heterogeneity in the population, whereby damaged cells die when facing osmotic shock, while cells in good shape survive and have higher growth rate. However, we found that a second osmotic shock in fact induces more (rather than less) cell death than the first (Fig. 4G), so this explanation is unlikely to hold, unless a very high proportion of damaged cells is produced during the relatively short stay at intermediate salinity, which seems unlikely. These proposed hypotheses are not mutually exclusive and may partially explain the observed results depending on the ecological context.

Passive vs active plasticity and programmed cell death

A strong – albeit indirect – argument in favour of adaptive plasticity is when the plastic response can be established to involve an active mechanism (Pigliucci 1996). For the rapid decline we observed, a natural candidate of active mechanism would be programmed cell death (PCD), more commonly named cell suicide in unicellular organisms (Ameisen 2002; Durand 2020). PCD has been reported in unicellular chlorophytes under a range of environmental stresses (Bidle and Falkowski 2004; Zuppini et al. 2010; Durand et al. 2014). This includes *Dunaliella* species, such as *D. tertiolecta* (Berges and Falkowski 1998; Segovia et al. 2003), *D. viridis* (Jiménez et al. 2009), and our focal species *D. salina* (Orellana et al. 2013). Signatures of active cell suicide via PCD include the early externalisation of phosphatidylserine (PS) in the outer membrane, caspase-like activities in mitochondria, and DNA fragmentation (Barreto Filho et al. 2022*a*). Our assays with caspase-like inhibition showed a clear, quantitative reduction of the population decline with increasing inhibitor concentration (Fig. 2). Although caspase-like activity is not specific to programmed cell death (Abraham and Shaham 2004; Barreto Filho et al. 2022*a*), and PCD can occur without caspase activity (Leist and Jäättelä 2001; Abraham and Shaham 2004), our finding that a caspase inhibitor routinely used to detect PCD distinctly reduces population decline is a clear indicator that the cell death causing this decline is not an entirely passive process. Furthermore the tested inhibitor was also used in the related species

D. tertiolecta, where PCD has been firmly established using several assays and morphological criteria (Segovia et al. 2003).

In addition to this direct test for PCD, one consistent line of evidence towards an active process in our experiments was that the decline was more pronounced when the growing conditions were closer to optimal: brighter light (Fig. 4E, Table S12A), cells in better condition, and/or with less inter-individual competition (Fig. 3A, Table S5A), non-limiting nutrients (Fig. 4A, Table S7). All these effects point towards this death being an active and energy demanding process (Sathe et al. 2019).

In conclusion, our results indicate that the strain that does more PCD in response to hyper-osmotic stress eventually reaches higher population size in at least some conditions (Fig. S6 and Fig. S7). Future work should investigate whether these demographic dynamics in monoculture accurately predict what happens in competition between these strains, to better understand whether and how natural selection can favor a lethal phenotype as a form of adaptive plasticity in a stressful environment. The fact that salinity-induced death and its consequences for longer-term fitness varied drastically between closely related strains isolated in the same location suggests that PCD is a very evolvable trait, even on short evolutionary timescales.

Acknowledgements: We thank S. Fereol for help with the PCD inhibitor assay, P. Durand for discussions, and J. Lau, E. A. Ostrowski, S. Collins and an anonymous reviewer for useful feedback on a previous version of the manuscript. This work was supported by the European Research Council (Starting Grant 678140 FluctEvol) and the Agence Nationale de la Recherche (grant ANR-21-ERCC-0001-01 InterAdapt).

Statement of Authorship: NZ, CL and L-MC conceived and designed the study. NZ and DG performed the experiments and collected the data. NZ analysed the data, prepared figures and tables, and wrote the original draft, CL and L-MC reviewed and edited the draft. All the authors commented and approved the final version.

Competing interest: Authors declare no competing interests.

Data and materials availability: Data that support the findings of this study and analysis scripts are available on Dryad.

Supplementary Tables

Table S1: Artificial sea water composition.

	Hyper-saline water	Hypo-saline water
Volume H_2O (L)	1	1
NaCl (g)	280,512	-
NA_2SO_4 (g)	3,550	3,550
KCl (g)	0,599	0,599
$NAHCO_3$ (g)	0,174	0,174
KBr (g)	0,086	0,086
H_3BO_3 (g)	0,023	0,023
NaF (g)	0,003	0,003
MgCl, $6H_2O$ (g)	9,592	9,592
$CaCl_2$, $2H_2O$ (g)	1,344	1,344
$SrCl_2$, $6H_2O$ (g)	0,022	0,022

Each saline solution was subjected to autoclave sterilisation and were afterwards added with 2% of Guillard's F/2 nutritive medium.

Table S2: Initial decline (1-hour post-transfer) against type of salinity transfer (experiment 1).

	Estimate	Std. Error	z value	Pr (>|z|)	Population reduction (%)
Intercept (Strain A in Transfer 2.4 to 4M)	-1.185	0.035	-34.050	<2e-16 ***	69
Strain_C	1.309	0.049	26.690	<2e-16 ***	-13
Transfer_2.4to2.4M	1.167	0.049	23.790	<2e-16 ***	2
Transfer_4to4M	1.125	0.055	20.520	<2e-16 ***	6
Strain_C:Transfer_2.4to2.4M	-1.190	0.069	-17.180	<2e-16 ***	-13
Strain_C:Transfer_4to4M	-1.190	0.073	-16.200	<2e-16 ***	-13

GLM on population density on day 0 relative to the expected initial density. We tested the effect of the different levels of salinity transfers and strain identity on demographic decline on the logarithmic scale (from the log link function in the GLM), and also report the population size reduction (where negative values denote proportional increase). p-value: ***: <0.001 ; **: <0.01 ; : <0.05 ; .: <0.1

Table S3: Maximal population growth rate against type of salinity transfer (experiment 1).

	Estimate	Std. Error	z value	Pr (>|z|)
Intercept (Strain A in Transfer 2.4M to 4M, day 1)	8.607	0.070	123.244	< 2e-16 ***
Time	0.638	0.021	30.299	< 2e-16 ***
Strain_C	2.038	0.099	20.652	< 2e-16 ***
Transfer_2.4to2.4M	2.084	0.099	21.125	< 2e-16 ***
Transfer_4to4M	2.107	0.110	19.106	< 2e-16 ***
Time:Strain_C	-0.374	0.030	-12.591	< 2e-16 ***
Time:Transfer_2.4to2.4M	-0.166	0.030	-5.569	3e-8 ***
Time:Transfer_4to4M	-0.262	0.033	-7.884	3e-15 ***
Strain_C:Transfer2.4to2.4M	-1.950	0.139	-13.983	< 2e-16 ***
Strain_C:Transfer4to4M	-1.929	0.148	-13.040	< 2e-16 ***
Time:Strain_C:Transfer2.4to2.4M	0.494	0.042	11.748	< 2e-16 ***
Time:Strain_C:Transfer4to4M	0.306	0.045	6.859	7e-12 ***

GLM on population densities on days 1 to 5 from experiment 1, corresponding to maximal growth in this experiment (shaded area in Fig. 1). Our main interest is in the effect of Time and its interactions with other factors, which represent effects of these factors (here salinity transfer) on maximal population growth.

Table S4: Initial decline and maximal growth rate of strain A populations after a hyper-osmotic shock against PCD inhibitor concentration gradient (experiment 2).

(A)	Estimate	Std. Error	z value	Pr (>|z|)
Intercept (Strain A without inhibitor)	-1.231	0.119	-10.383	< 2e-16 ***
Inhibitor Concentration	0.150	0.045	3.321	9e-04 ***
(B)	Estimate	Std. Error	z value	Pr (>|z|)
Intercept (Strain A without inhibitor, day 1)	7.952	0.123	64.448	< 2e-16 ***
Time	0.671	0.035	19.231	< 2e-16 ***
Inhibitor concentration	0.209	0.047	4.441	9e-06 ***
Time:Inhibitor Concentration	-0.021	0.013	-1.614	0.107

(A) GLM on population density on day 1 compared to the expected initial density. We tested the effect of a PCD inhibitor concentrations. **(B)** GLM on population densities on days 1-6, corresponding to maximal growth in this experiment (shaded area in Fig. S4). Our main interest is in Time and its interactions with the factor Inhibitor Concentration, which represent effects on population growth post-decline.

Table S5: Initial decline against initial density and population growth phase (experiment 3).

(A)	Estimate	Std. Error	z value	Pr(>|z|)
Population density (day 1) for mid-exponential phase condition (4d)				
Intercept (N_0 = 5,000 cells/mL)	-1.080	0.102	-10.612	<2e-16 ***
N_0_20000	0.164	0.144	1.141	0.254
N_0_30000	0.143	0.143	0.996	0.319
Population density (day 1) for early-stationary phase condition (13d)				
Intercept (N_0 = 5,000 cells/mL)	-1.309	0.199	-6.583	5e-11 ***
N_0_20000	0.198	0.281	0.703	0.482
N_0_30000	0.294	0.281	1.045	0.296
Population density (day 1) for late-stationary phase condition (41d)				
Intercept (N_0 = 5,000 cells/mL)	-0.897	0.140	-6.409	1e-10 ***
N_0_20000	0.547	0.198	2.767	0.006 **
N_0_30000	0.805	0.198	4.073	5e-5 ***
(B)	Estimate	Std. Error	z value	Pr(>|z|)
Population density (day 1) for N_0 = 5,000 cells/mL				
Intercept (phase = 4d)	-1.080	0.113	-9.533	<2e-16 ***
Phase_13d	-0.230	0.160	-1.433	0.152
Phase_41d	0.182	0.160	1.139	0.255
Population density (day 1) for N_0 = 20,000 cells/mL				
Intercept (phase = 4d)	-0.916	0.158	-5.811	6e-09 ***
Phase_13d	-0.196	0.223	-0.879	0.380
Phase_41d	0.566	0.223	2.539	0.011 *
Population density (day 1) for N_0 = 30,000 cells/mL				
Intercept (phase = 4d)	-0.937	0.178	-5.265	1e-07 ***
Phase_13d	-0.079	0.252	-0.313	0.754
Phase_41d	0.845	0.252	3.358	8e-4 ***

(A) GLM on population density on day 1 relative to the expected initial density, testing for effects of initial density (N_0), separately for each condition of population growth phase, using only strain A. **(B)** Same GLM, but testing for the effect of population growth phase, separately for each condition of initial density (N_0), using only strain A from the experiment 3.

Table S6: Maximal growth rate against initial density and population growth phase (experiment 3).

	Estimate	Std. Error	z value	Pr (>|z|)
Intercept (Strain A N_0 = 5000 & phase = 4d on day 4)	6.39094	0.20734	30.823	< 2e-16 ***
Time	0.65079	0.0564	11.54	< 2e-16 ***
Strain_C	1.98935	0.29294	6.791	1.11e-11 ***
Phase_13d	-0.64078	0.2936	-2.182	0.029 *
Phase_41d	0.01446	0.28983	0.05	0.960
N_0_20000	1.80943	0.29292	6.177	7e-10 ***
N_0_30000	2.29943	0.2929	7.851	4e-15 ***
Time:Strain_C	-0.27583	0.0797	-3.461	0.001 ***
Time:Phase_13d	-0.01618	0.07983	-0.203	0.839
Time:Phase_41d	-0.232	0.06394	-3.629	3e-4 ***
Strain_C:Phase_13d	0.30059	0.41457	0.725	0.468
Strain_C:Phase_41d	-1.10379	0.40962	-2.695	0.007 **
Time:N_0_20000	-0.11006	0.07969	-1.381	0.167
Time:N_0_30000	-0.14041	0.07969	-1.762	0.078 .
Strain_C:N_0_20000	-0.34895	0.41402	-0.843	0.399
Strain_C:N_0_30000	-0.44318	0.41399	-1.07	0.284
Phase_13d:N_0_20000	-0.11154	0.41455	-0.269	0.788
Phase_41d:N_0_20000	0.44543	0.40953	1.088	0.277
Phase_13d:N_0_30000	-0.25146	0.4145	-0.607	0.544
Phase_41d:N_0_30000	0.86717	0.4095	2.118	0.034 *
Time:Strain_C:Phase_13d	0.04209	0.11277	0.373	0.709
Time:Strain_C:Phase_41d	0.18602	0.09037	2.059	0.040 *
Time:Strain_C:N_0_20000	0.08265	0.11266	0.734	0.463
Time:Strain_C:N_0_30000	0.12506	0.11265	1.11	0.267
Time:Phase_13d:N_0_20000	0.18438	0.11276	1.635	0.102
Time:Phase_41d:N_0_20000	0.06664	0.09035	0.738	0.461
Time:Phase_13d:N_0_30000	0.23504	0.11275	2.085	0.037 *
Time:Phase_41d:N_0_30000	0.03081	0.09035	0.341	0.733
Strain_C:Phase_13d:N_0_20000	0.17249	0.58573	0.294	0.768
Strain_C:Phase_41d:N_0_20000	-0.49085	0.57895	-0.848	0.397
Strain_C:Phase_13d:N_0_30000	0.31456	0.58569	0.537	0.591
Strain_C:Phase_41d:N_0_30000	-0.8172	0.57892	-1.412	0.158
Time:Strain_C:Phase_13d:N_0_20000	-0.19468	0.15937	-1.222	0.222
Time:Strain_C:Phase_41d:N_0_20000	-0.02966	0.12773	-0.232	0.816
Time:Strain_C:Phase_13d:N_0_30000	-0.26568	0.15936	-1.667	0.095 .

Time:Strain_C:Phase_41d:N_0_30000	-0.03044	0.12773	-0.238	0.812

GLM on population densities on days 2-5 or 4-9, corresponding to maximal growth in this experiment (shaded area in Fig. S5). Our main interest is in Time and its interactions with other factors (Strain, Initial density, Population growth phase), which represent effects of these factors on maximal population growth post-decline.

Table S7: Initial decline against nutrient abundance (experiment 4).

	Estimate	Std. Error	z value	Pr(>|z|)	Population reduction (%)
Intercept (Strain A with Nutrient standard)	-1.615	0.084	-19.260	2e-12 ***	80
Strain_C	1.854	0.119	15.637	4e-11 ***	-27
Nutrient_limitation	0.601	0.119	5.069	1e-4 ***	64
Strain_C:Nutrient_limitation	-0.542	0.168	-3.231	0.005 **	-35

LM on log population density on day 1, estimated from the log whole-well fluorescence, relative to the log expected initial density of strain C. We tested for the effect of nutrient limitation and strain identity. We also reported the population size reduction.

Table S8: Maximal growth rate against nutrient abundance (experiment 4).

	Estimate	Std. Error	z value	Pr(>|z|)
Intercept (Strain A with Nutrient standard)	8.011	0.185	43.204	< 2e-16 ***
Time	1.075	0.086	12.520	< 2e-16 ***
Strain_C	2.360	0.262	9.000	3e-12 ***
Nutrient_limitation	0.882	0.262	3.365	0.001 **
Time:Strain_C	-0.713	0.121	-5.877	3e-7 ***
Time:Nutrient_limitation	-0.378	0.121	-3.114	0.003 **
Strain_C:Nutrient_limitation	-0.774	0.371	-2.087	0.042 *
Time:Strain_C:Nutrient_limitation	0.318	0.172	1.853	0.070 .

LM on log population densities on days 1-3, corresponding to maximal growth in this experiment (shaded area in Fig. S6), estimated from the log whole-well fluorescence. Our main interest is in Time and its interactions with other factors (Strain, Nutrient abundance), which represent effects of these factors on maximal population growth post-decline.

1

Table S9: Initial decline against culture medium after a hyper-osmotic shock (experiment 5).

	Estimate	Std. Error	z value	Pr(>|z|)	Population reduction (%)
Intercept (Strain A growing in control medium)	-1.471	0.051	-28.905	<2.00e-16 ***	77
Strain C	1.600	0.072	22.290	<2.00e-16 ***	-14
Filtrate_A	0.163	0.072	2.264	0.026 *	73
Filtrate_C	-0.166	0.072	-2.308	0.021 *	81
Strain_C:Filtrate_A	-0.187	0.102	-1.845	0.065 .	6
Strain_C:Filtrate_C	0.150	0.102	1.480	0.139	-32

GLM on population density on day 1 relative to the expected initial density. We tested the effect of the different culture mediums and strain identity.

Table S10: Maximal growth rate against culture medium after a hyper-osmotic shock (experiment 5).

	Estimate	Std. Error	z value	Pr(>|z|)
Intercept (Strain A growing in control medium at day 1)	8.607	0.071	121.296	<2e-16 ***
Time	0.638	0.021	29.819	<2e-16 ***
Strain_C	2.038	0.100	20.325	<2e-16 ***
Filtrate_A	0.356	0.100	3.547	4e-4 ***
Filtrate_C	-0.127	0.100	-1.265	0.206
Time:Strain_C	-0.374	0.030	-12.391	<2e-16 ***
Time:Filtrate_A	-0.046	0.030	-1.518	0.129
Time:Filtrate_C	0.043	0.030	1.431	0.153
Strain_C:Filtrate_A	-0.373	0.142	-2.629	0.009 **
Strain_C:Filtrate_C	0.118	0.142	0.834	0.404
Time:Strain_C:Filtrate_A	0.068	0.043	1.583	0.113
Time:Strain_C:Filtrate_C	-0.040	0.043	-0.929	0.353

GLM on population densities on days 1-5, corresponding to maximal growth in this experiment (shaded area in Fig. S7). Our main interest is in Time and its interactions with other factors (Strain, Culture medium), which represent effects on population growth post-decline.

Table S11: Initial decline and maximal growth rate of strain C populations after a hyper-osmotic shock against culture medium (experiment 5).

(A)	Estimate	Std. Error	z value	Pr(>|z|)
Intercept (Strain C growing in control medium)	0.130	0.009	14.214	<2.00E-16 ***
Filtrate_A	-0.024	0.013	-1.860	0.058 .
Filtrate_C	-0.016	0.013	-1.230	0.219
(B)	Estimate	Std. Error	z value	Pr(>|z|)
Intercept (Strain C growing in control medium at day 1)	10.645	0.030	352.123	<2e-16 ***
Time	0.263	0.009	28.888	<2e-16 ***
Filtrate_A	-0.017	0.043	-0.392	0.695
Filtrate_C	-0.009	0.043	-0.203	0.839
Time:Filtrate_A	0.022	0.013	1.687	0.092 .
Time:Filtrate_C	0.004	0.013	0.276	0.783

(A) GLM on population density on day 1 compared to the expected initial density. We tested the effect of the different culture mediums. **(B)** GLM on population densities on days 1-5, corresponding to maximal growth in this experiment (shaded area in Fig. S7). Our main interest is in Time and its interactions with the factor Culture medium, which represent effects on strain C population growth post-decline.

Table S12: Initial decline and Maximal growth rate against light intensity after a hyper-osmotic shock (experiment 6).

(A)	Estimate	Std. Error	z value	Pr(>|z|)	Population reduction (%)
Intercept (Strain A growing at 100 µmol.m-2.s-1 light)	-0.838	0.052	-16.043	<2e-16 ***	57
Strain_C	0.963	0.074	13.044	<2e-16 ***	-13
Light_200	-0.905	0.163	-5.536	3e-8 ***	82
Strain_C:Light_200	0.826	0.231	3.574	4e-4 ***	-159

(B)	Estimate	Std. Error	z value	Pr(>|z|)
Intercept (Strain A growing at 100 µmol.m-2.s-1 light on first day of exponential phase)	9.722	0.110	88.262	<2e-16 ***
Time	0.429	0.029	14.855	<2e-16 ***
Strain_C	0.719	0.156	4.619	4e-6 ***
Light_200	-1.699	0.485	-3.504	5e-4 ***
Time:Strain_C	-0.118	0.041	-2.878	0.004 **
Time:Light_200	0.442	0.163	2.710	0.007 **
Strain_C:Light_200	1.940	0.686	2.829	0.005 **
Time:Strain_C:Light_200	-0.496	0.231	-2.150	0.032 *

(A) GLM on population density on day 1 compared to the expected initial density. We tested the effect of the light intensity and strain identity. **(B)** GLM on population densities on days corresponding to maximal growth for each experiment (light experiment: shaded area in Fig. S8). Our main interest is in Time and its interactions with the factor Light, which represent effects on population growth post-decline.

Table S13: Initial decline and maximal growth rate against successive shocks (experiment 7).

(A)	Estimate	Std. Error	z value	Pr(>|z|)	Population reduction (%)
Intercept (Strain A undergoing hyperosmotic shock 1)	-0.979	0.030	-32.403	<2.00E-16 ***	62
Strain_C	1.043	0.043	24.525	<2.00E-16 ***	-7
Shock_2	-0.404	0.043	-9.428	<2.00E-16 ***	75
Strain_C:Shock_2	0.430	0.062	6.920	4.52E-12 ***	-64

(B)	Estimate	Std. Error	z value	Pr(>|z|)
Intercept (Strain A undergoing hyperosmotic shock 1 at day 3)	7.501	0.115	65.501	<2e-16 ***
Time	0.528	0.022	23.947	<2e-16 ***
Strain_C	1.661	0.162	10.259	<2e-16 ***
Shock_2	-0.055	0.162	-0.339	0.735
Time:Strain_C	-0.246	0.031	-7.894	3e-15 ***
Time:Shock_2	0.029	0.031	0.944	0.345
Strain_C:Shock_2	0.031	0.236	0.133	0.894
Time:Strain_C:Shock_2	-0.032	0.045	-0.696	0.486

(A) GLM on population density on day 1 compared to the expected initial density. We tested the effect of the salinity fluctuations and strain identity. **(B)** GLM on population densities on days 3-7, corresponding to maximal growth in this experiment (shaded area in Fig. S9). Our main interest is in Time and its interactions with the factor Shock, which represent effects on population growth post-decline.

Supplementary Figures

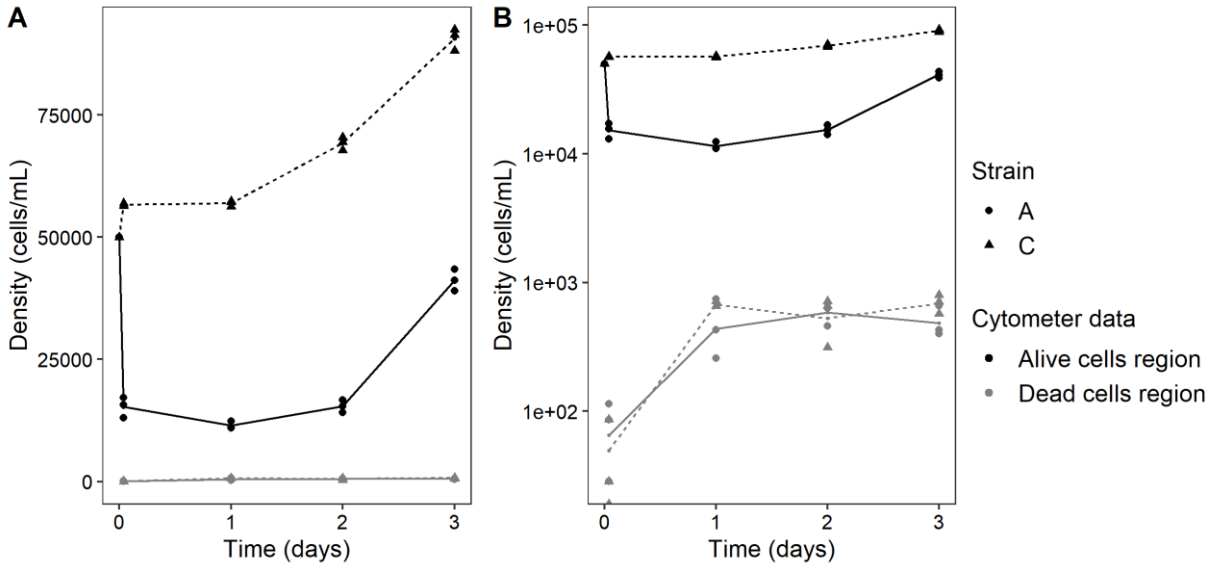

Figure S1: Cytometer estimation for live cells and apparently dead cells following a hyper-osmotic shock (experiment 1), in linear scale (A) and log scale (B). The apparently dead cells correspond to cells with much lower red fluorescence in cytometry, indicating that they are either dead or in poor condition (see Rescan et al. 2020). The number of apparently dead cells (in grey) is negligible relative to the number of disappearing live cells (in black) (A). In addition, both strains display an equivalent increase of apparently dead cells after the hyper-osmotic shock (B).

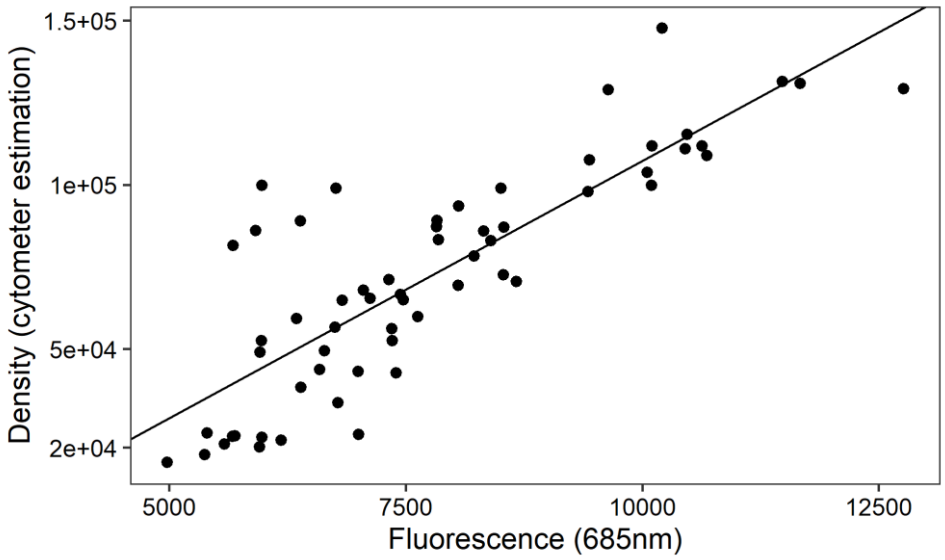

Figure S2: Linear model between the cytometer estimation for density (in cells/mL) and the 685 nm fluorescence (spectrometer). Points correspond to the measurements made on day 2 to 4 from the nutrient assay (experiment 4). This LM led to the relationship:

$$Density\ population_{Fluo} = 15.659\ (Fluo - Fluo_{blank}) - 49182.885,$$

where *Fluo* is fluorescence of the well, and $Fluo_{blank}$ is the corresponding measurement for a well that contains the culture medium but no cells.

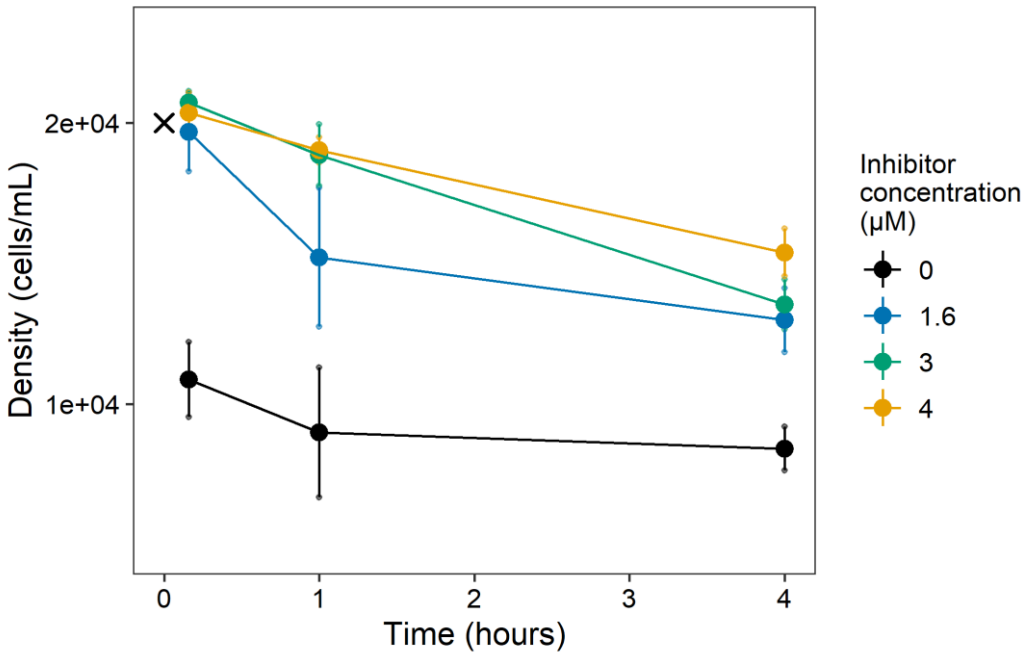

Figure S3. Preliminary test under different concentration of a PCD inhibitor for strain A under hyper-osmotic shock. Hyper-osmotic transfers occurred at time 0, and the first density measurements were made 15 minutes after the transfer, while the cross represents the expected initial density, predicted from dilution of the acclimated population. Filled symbols are averages over 2 replicates, error bars indicate the standard error, while lighter points are the raw densities.

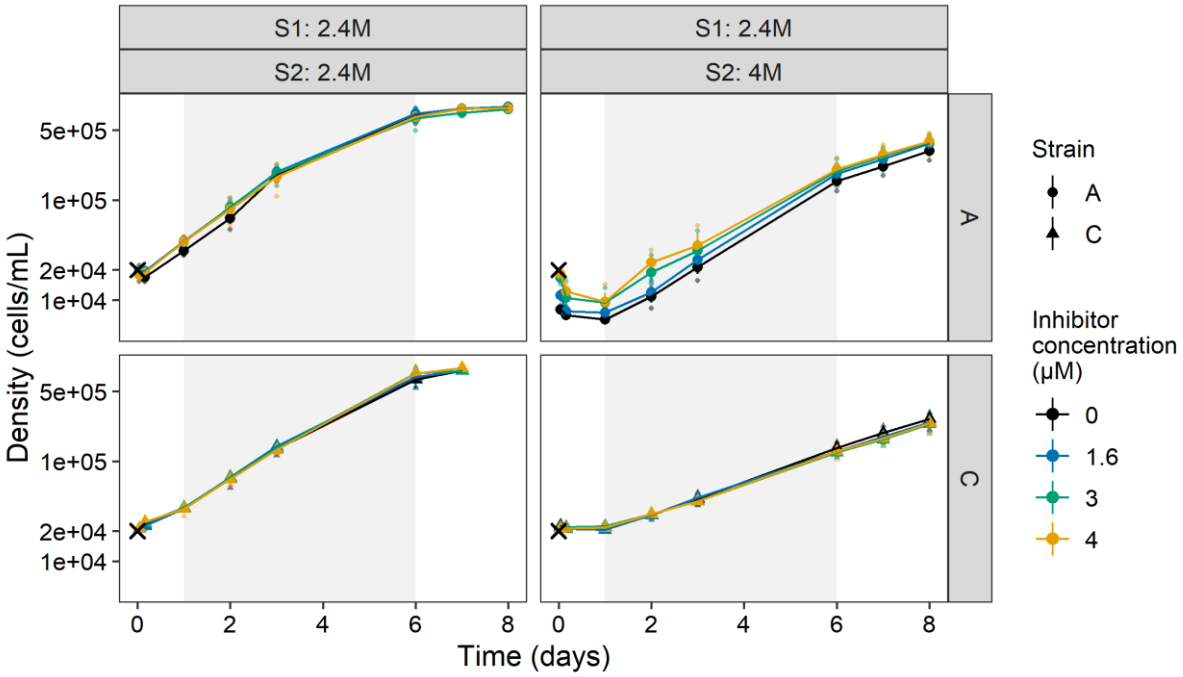

Figure S4. Demographic dynamics under different concentration of a PCD inhibitor. Iso-osmotic (left) or hyper-osmotic (right) transfers occurred at day 0, and the first measurements were made 1 hour after the transfer, while the cross represents the expected initial density, predicted from dilution of the acclimated population. The number of live *D. salina* cells per mL in each day is represented on the log scale, for strains A (dots, upper panels) and C (triangles, bottom panels). Filled symbols are averages over 3 replicates, error bars indicate the standard error, while lighter points are the raw densities. Note that the first 4 days of the upper right panel appear as Fig. 2 in the main text.

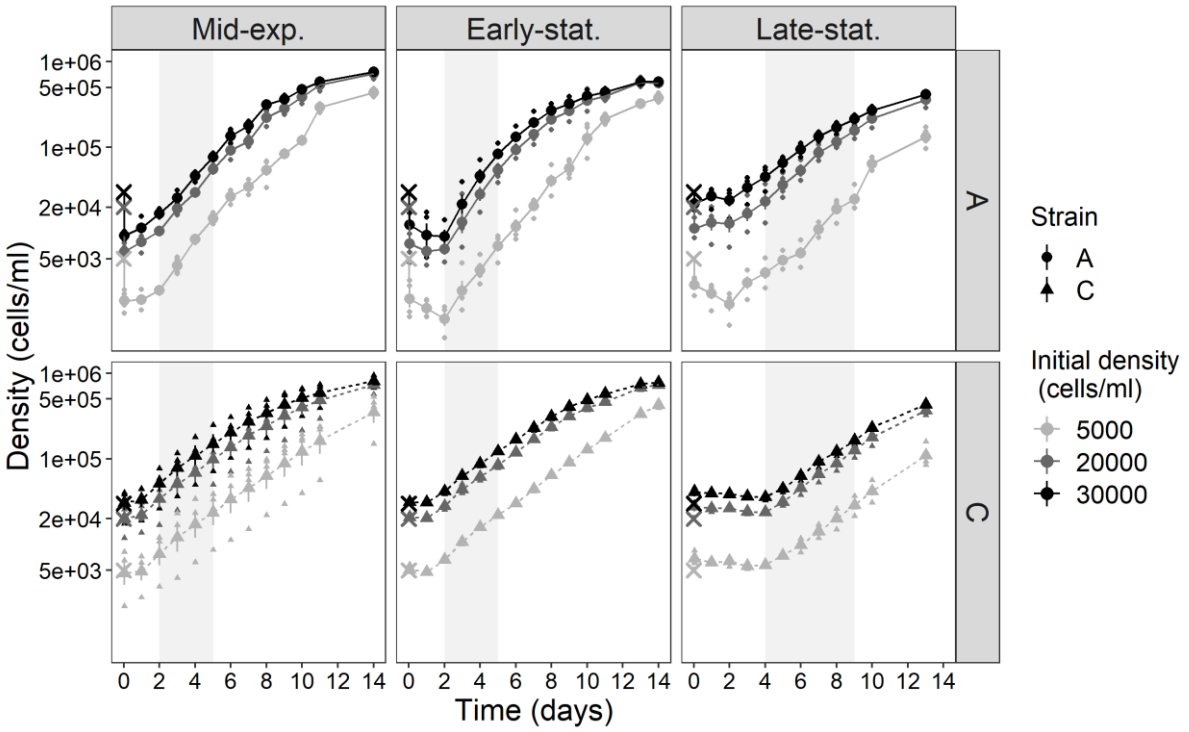

Figure S5: Influence of initial density and population growth phase on population dynamics following hyper-osmotic shock (experiment 3). Upper panels represent the demography of strain A, and lower panels the demography of strain C. Each panel from left to right represents a population growth phase: mid-exponential phase (4 days after transfer), early-stationary phase (13 days), and late stationary phase (41 days). Salinity rise occurs at time 0, and the expected initial densities are represented by crosses. The first observed point is measured 1 hour after the transfer. The y-axis is in log scale (live *D. salina* cells per mL). Filled symbols are averages over 3 replicates, with error bars representing standard error, while smaller symbols are the raw densities. The shaded areas correspond to the period of maximum exponential growth.

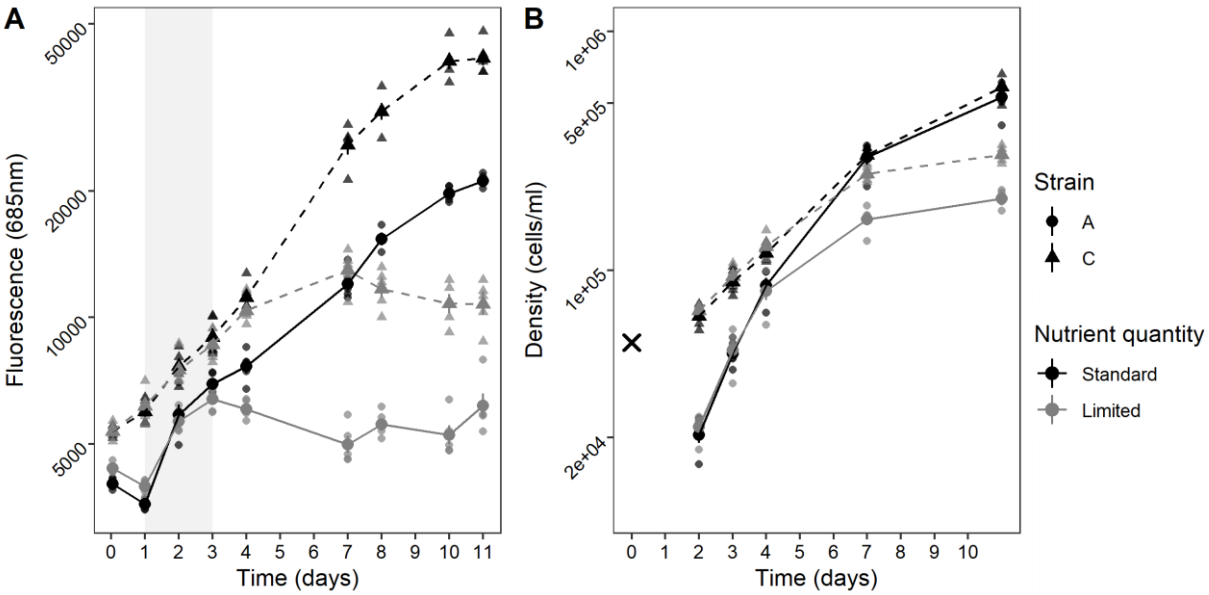

Figure S6: Influence of nutrient level on population dynamics following hyper-osmotic shock (experiment 4). Estimates of population density are based on (A) whole-well fluorescence (685nm), or (B) cytometer counts. Salinity transfer occurs at time 0, and the first observed point is measured 1 hour after the transfer, only with the spectrometer. The expected initial density is represented by a cross. Large darker symbols are mean overs 5 replicates, while small lighter symbols are the raw densities. Standard growth conditions are shown in black, and nutrients limitation in grey. In A, the shaded area corresponds to the period of maximal exponential growth.

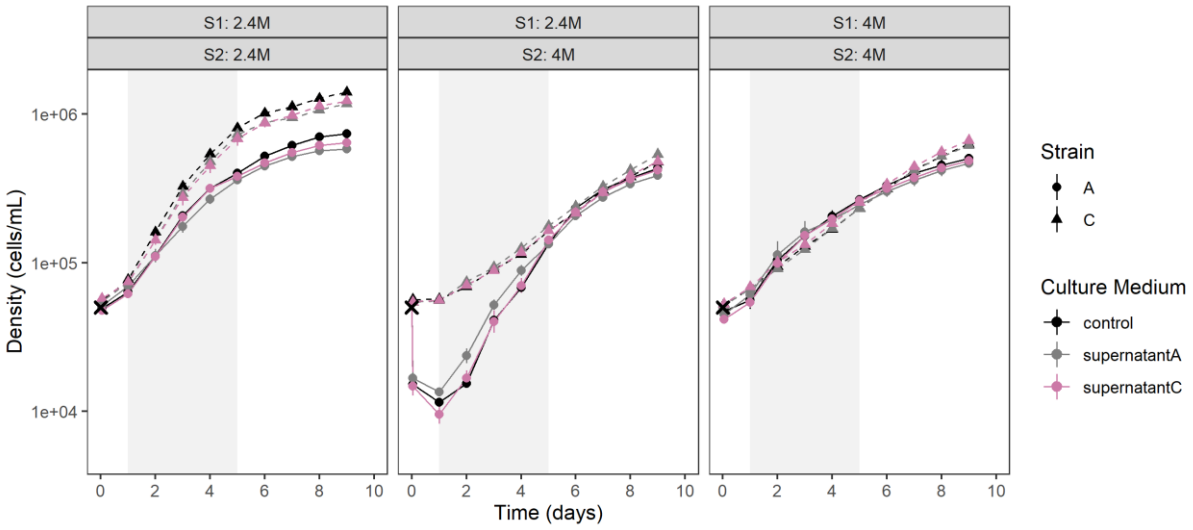

Figure S7: Demographic dynamics in population filtrates (experiment 5). Each panel from left to right represents a salinity transfer, respectively an iso-osmotic transfer at intermediate salinity, a hyper-osmotic transfer and an iso-osmotic transfer at high salinity. Salinity transfer occurs at time 0, and the predicted initial density is represented by a cross. The first observed point is measured 1 hour after the transfer. The y-axis is in log scale (live *D. salina* cells per mL). Filled symbols are averages over 3 replicates. The shaded areas correspond to the period of maximum exponential growth.

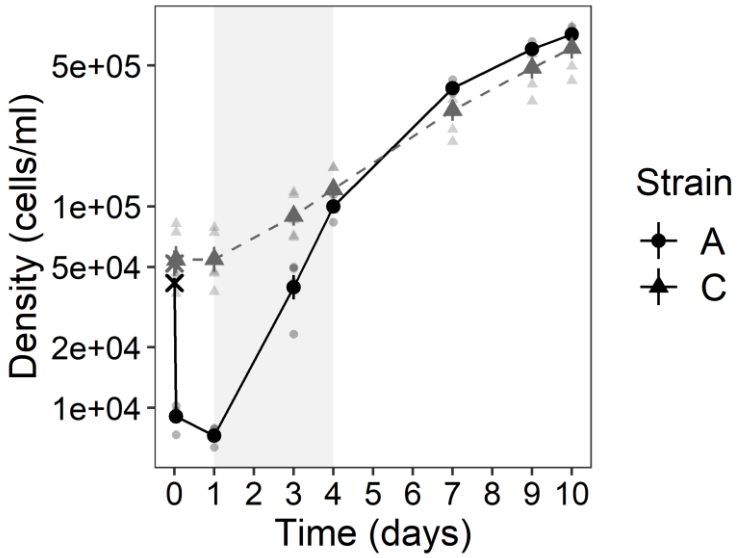

Figure S8: Demographic dynamics at higher intensity light (experiment 6). Salinity rise from 2.4M to 4M NaCl occurs at time 0, and mean expected initial densities per strain are represented by crosses. The first observed point is measured 1 hour after the transfer. The y axis is in log scale (live *D. salina* cells per mL). Black symbols are means over 5 replicates, while smaller lighter symbols are raw densities. The shaded area corresponds to the period of maximum exponential growth.

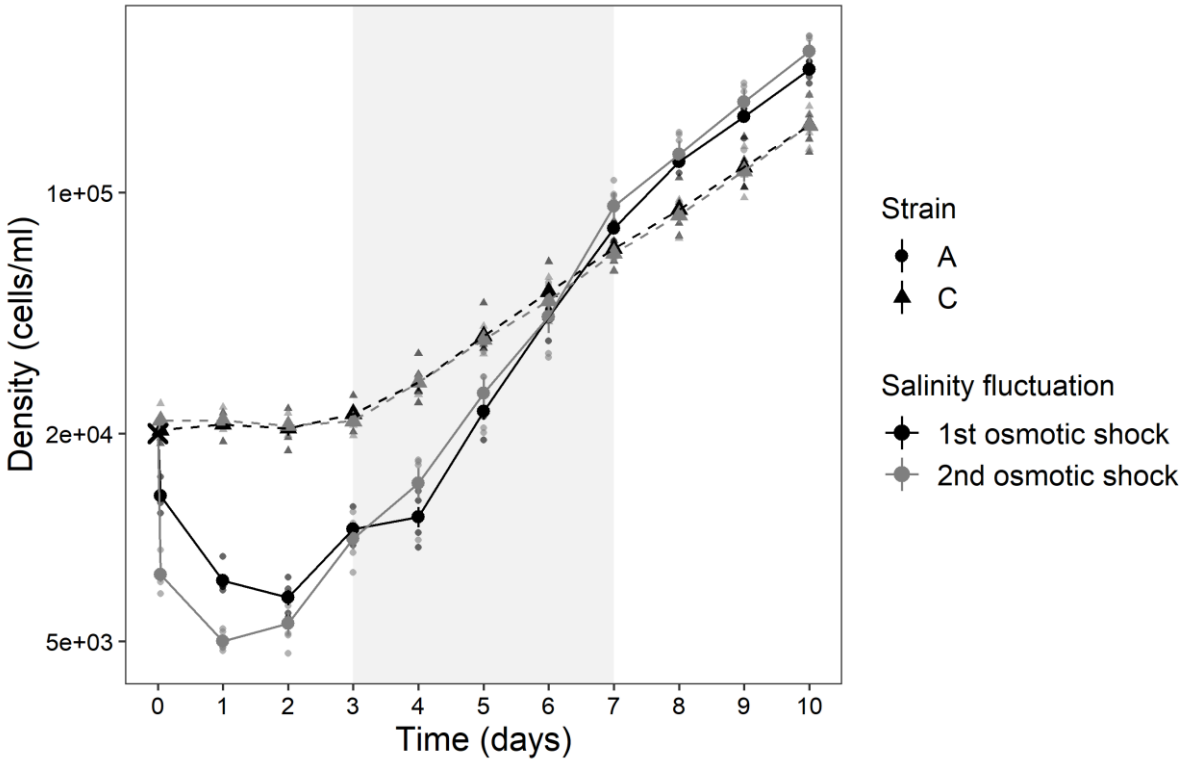

Figure S9: Demographic dynamics after one or two hyper-osmotic shocks (experiment 7). Salinity rise from 2.4M to 4M NaCl occurs at time 0, and the expected initial density is represented by a cross. The first observed point is measured 1 hour after the transfer. The y axis is in log scale (live *D. salina* cells per mL). Filled symbols are means over 5 replicates, while smaller lighter symbols are raw densities. The shaded area corresponds to the period of maximum exponential growth.

Chapitre 2 : Expérience de compétition à long-terme

Entrée en matière et résumé de l'article :

Nous avons établi dans le premier chapitre que le taux de déclin observé chez l'algue unicellulaire *Dunaliena salina* en réponse à une hausse de salinité est variable entres génotypes, et qu'il est associé à une croissance différentielle durant la phase exponentielle. L'objectif de ce 2e chapitre est d'étudier l'évolution du taux de déclin lorsque les deux génotypes sont en compétition. Plus spécifiquement, nous nous sommes demandés à quel point les dynamiques démographiques observées en monocultures peuvent prédire ce qu'il se passe en coculture. En somme, ce chapitre nous a permis de déterminer dans quelle mesure la sélection peut favoriser le génotype déclinant lorsqu'il est en compétition avec un génotype ne déclinant pas, et ce, en milieu fluctuant. Ce chapitre permet dont de s'intéresser, par une approche d'évolution expérimentale, à la problématique générale de ma thèse, c'est-à-dire comment la sélection pourrait agir sur un tel trait paradoxal. L'expérience concernée a été menée avec l'aide d'une stagiaire M1 Darwin, Océane Rieu, que j'ai co-encadrée en 2021.

En supposant que les dynamiques en monocultures sont des bons prédicteurs de celles des co-cultures, c'est-à-dire qu'il n'y a pas d'interactions fortes entre souches générant une sélection fréquence-dépendance, nous faisions l'hypothèse que la souche A (effectuant PCD) pourrait atteindre des densités similaires voire supérieurs à la souche C (sans PCD) en quelques jours après son déclin, lorsque les deux souches sont en compétition. Ainsi, si la souche A est en plus forte densité que la souche C lors du transfert à la salinité suivante, on peut s'attendre à une domination de cette souche à long terme. Suite à des augmentations successives de la salinité, la sélection favoriserait ainsi le génotype effectuant la PCD, en amenant l'exclusion de l'autre souche. Alternativement, si les souches ont de fortes interactions compétitives, par exemple parce qu'elles utilisent exactement les mêmes ressources, la souche effectuant la PCD pourrait ne pas rattraper son retard démographique car l'autre souche aurait déjà épuisé les ressources du milieu pendant qu'elle déclinait. Pour tester ces hypothèses, nous avons cultivé la souche A et C en mono- et co-cultures, alternant basse et haute salinité (cycle de salinité) sur 180 générations. Nous avons suivi les dynamiques démographiques des deux souches lors des phases de haute salinité (où les deux souches présentent des dynamiques démographiques différentielles), ainsi que leurs densités relatives lorsqu'elles sont en cocultures.

Nos résultats indiquent une coexistence stable des deux génotypes au cours des 13 cycles de salinité (26 semaines), bien que la fréquence à haute salinité varie fortement au cours de chaque cycle sous l'effet du déclin démographique répété de la souche A. Cette coexistence est expliquée par des processus densité-dépendents ayant lieu proche de la phase stationnaire de la croissance, semblant finalement peu dépendre des dynamiques complexe dues à la mort cellulaire déclenchée par la souche A.

Quoiqu'il en soit, nos résultats suggèrent que la mort cellulaire peut être maintenue par sélection à travers une série de chocs hyper-osmotiques, devenant ainsi un exemple expérimental de maintien de ce trait léthal chez les unicellulaires. En conclusion, nous avons montré dans ce chapitre que la mort cellulaire peut être un trait qui évolue même à une courte échelle de temps et que deux stratégies démographiques complétement différentes en réponse un même stress environnemental permettent la coexistence de différents génotypes dans un environnement fluctuant.

Cet article sera prochainement soumis pour publication dans le journal *Proceedings of the royal society* B ou *Ecology Letters*, et est cité dans les chapitres suivants en tant que manuscrit « compétition ».

Article 2 - Linking selection to demography in experimental evolution of active death in a unicellular organism

Running title: Selection on population decline

Nathalie Zeballos[1], Océane Rieu[1,2], Stanislas Fereol[1], Christelle Leung[1], and Luis-Miguel Chevin[1]

[1] CEFE, Université de Montpellier, CNRS, EPHE, IRD, Montpellier, France

[2] MIVEGEC, Université de Montpellier, CNRS, IRD, Montpellier, France

Abstract:

Linking selection to demography remains a major issue, especially when relating adaptive evolution to extinction risk in an eco-evolutionary framework. What matters for selection is relative fitness, the difference in relative growth rates of genotypes in competition, but measuring it experimentally may be technically challenging. Absolute fitness of genotypes in isolation is easier to access and underlies the demographic consequences of evolution, but it is unclear to what extent it can predict the outcome of competition. Nevertheless, finding similar demographic dynamics in isolation and in competition may help disentangle the ecological causes of selection, especially when demographic responses to the environment are complex. Here, we addressed this question in the context of programmed cell death (PCD) in the microalga *Dunalliela salina*. Closely related strains of this species have contrasted demographic responses to hyper-osmotic shock in monoculture, with one undergoing massive PCD-inducing population decline followed by demographic rebound, while the other grows continuously but more slowly. To understand whether and how selection may favour PCD, we exposed mixtures of these strains to 13 cycles of hyper-osmotic stress (~180 generations), together with monocultures in the first 5 cycles, and tracked demography and selection throughout. The frequency of the declining strain, despite fluctuating substantially within each cycle, reached a stable dynamic across cycles, leading to long-term coexistence. Population dynamics in mixtures were consistent with those in monocultures, suggesting that selection on PCD does not involve strong ecological interactions among strains. Competition analysis suggested that density dependence near stationary phase largely explained the stable frequency across cycles, regardless of the initial decline-rebound dynamics, such that exponential growth rates were not good predictors of selection. Further theoretical investigation could help delineate plausible underlying ecological causes for these dynamics of demography and selection.

Keywords: programmed cell death, environmental stress, population decline, natural selection, experimental evolution, competition.

Introduction

Natural selection is an intrinsically demographic process, since it arises from the differential growths of lineages with different phenotypes (Crow and Kimura 1970; Chevin 2011). However beyond this uncontroversial statement, deducing selection from demographic properties often proves a non-trivial effort, exemplified by the difficulty in finding a universally satisfying definition of fitness. One of the most common practical issues when trying to relate selection to demography involves finding out to what extent absolute fitness of genotypes measured in isolation can be used to predict selection when these genotypes are in competition. It is well understood that what matters for selection and evolution is relative fitness, the difference between the relative growth rates (absolute fitness) of different types in competition. However, many more studies have measured absolute fitness of genotypes or phenotypes in isolation rather than relative fitness in competition. First, measuring relative fitness in competition comes with technical challenges, as it requires being able to distinguish the competing genotypes. This can be achieved by using natural phenotypic variation, inserting phenotypic markers such as fluorescent proteins (accounting for potential costs of the marker or epistasis with the focal genotype, Gallet et al. 2012), or sequencing standing genetic variants (Burke et al. 2010; Rescan et al. 2021; Burny et al. 2022) or inserted 'barcode' sequences (Levy et al. 2015), but most these methods are more technically challenging than merely counting individuals. Second, deciphering the mechanisms behind selection-induced frequency change across environments and ecological contexts may require understanding how alternative demographic responses of individual genotypes leads to their differential growth. And third, in eco-evolutionary scenarios such as evolutionary rescue, the main focus is evolution of demographic properties of the population, such that only analysing relative fitness is clearly insufficient.

Relative fitnesses of competing genotypes can be predicted from their absolute fitnesses in isolation provided these genotypes do not interact ecologically in ways that lead to frequency-dependent selection (Chevin 2011). This assumption is less likely to hold whenever one of the genotypes excretes beneficial or detrimental substances in the medium, or benefits from arriving or starting to grow earlier than others (priority effect). Therefore, contexts where these or other forms of ecological interactions are strongly suspected are less likely to show consistency between fitness in isolation and in competition. Reciprocally, finding similar demographic dynamics in isolation and competition can help delineate plausible underlying ecological causes for these dynamics, especially when they markedly differ among genotypes.

We have recently shown that strains of the microalga *Dunalliela salina* have drastically different demographic strategies in response to hyper-osmotic stress (Leung et al. 2022; Zeballos et al. 2023). One strain undergoes programmed cell death (hereafter PCD), an active form of cell suicide leading to a massive and fast population decline, while a closely related strain does not (Leung et al. 2022; Zeballos et al. 2023). Strikingly, surviving cells of the declining strain later experience a rebound phase characterized by fast growth, such that their monocultures may reach similar or higher population density than those of the non-declining strain after about a week (Zeballos et al. 2023). If these dynamics in monoculture are good predictors of the outcome of competition, then this would suggest that the genotype doing PCD can be favoured over successive osmotic shocks, in turn causing evolution of faster decline in response to hyper-osmotic stress. However, these predictions would be violated if the non-declining strain exhausts resources before the declining strain has recovered from its initial decline, preventing it from rebounding, and leading to competitive exclusion. Alternatively, dying cells from the declining strain may release resources or cues in the medium that fundamentally modify the growth rate of the co-occurring non-declining strain (Durand et al. 2011; Orellana et al. 2013). Furthermore, faster growth of the declining strain during its rebound phase would need to be maintained over a long enough exponential phase to allow it to outgrow its competing strain.

To investigate these questions, and better understand the – so far largely misunderstood (Reece et al. 2011) - putative benefit of PCD, we exposed monocultures and mixture of these declining and non-declining strains of *D. salina* to 13 cycles of hyper-osmotic stress (~180 generations), and tracked demography and selection throughout. Our results indicate that stable coexistence can arise via density-dependent processes that take place near the stationary phase of growth, largely overriding the influence of complex decline-rebound dynamics caused by PCD.

Materials & Methods

Experimental evolution

We focused on two closely related strains that were previously shown to differ in their responses to a salinity rise (Leung et al. 2022; Zeballos et al. 2023). The first one, CCAP 19/12 (hereafter strain A), sharply declines following a rise to very high salinity because of programmed cell death (PCD), but this decline is followed by a rapid rebound. In contrast, CCAP 19/15 (strain C) does not exhibit this decline-rebound response to salinity rise. Our previous investigations

of monocultures of these strains suggested that strain A could reach higher density than strain C at the end of the rebound phase, so we wanted to test whether this occurs in competition, and how this affect experimental evolution of PCD. Both strains were obtained from the Culture Collection of Algae and Protozoan (CCAP) in 2017, and were isolated from the same sampling site (North Sinai, Israel). Each of the 10 biological replicates per strain used in this study was founded from a single haploid cell isolated using cells-sorting flow cytometry (BD FACSAria™ IIu; Biosciences-US) in May 2019, ensuring nearly isogenic populations per replicate.

To investigate competitive fitness among strains and the resulting experimental evolution of PCD, we exposed several mixtures of these strains to successive osmotic shocks, and tracked their population dynamics and relative frequencies through time. Cell cultures were performed in 50 ml flasks (CELLSTAR®; VWR 392-0016), using custom-made artificial saline water complemented with NaCl (Rescan et al. 2020; Zeballos et al. 2023). Growth chambers were set to 12h:12h light:dark cycles, with light intensity at 200 $\mu mol.m^{-2}.s^{-1}$, temperature at 24°C, and position randomized with respect to treatment. Mixed populations of *D. salina* were initiated with 50% of strain A and 50% of strain C, starting at a density of 50,000 cells/ml, and using a different biological replicate (i.e. isogenic population) for each mixture. They were then exposed to 13 cycles of salinity changes, leading to ~180 generations of experimental evolution. Each cycle of salinity change consisted of a step at 2.4M of NaCl (referred to as low salinity), followed by a hyper-osmotic stress where cells were subjected to a steep salinity rise to 4.0M NaCl (high salinity). Cycles lasted 14 days, and we contrasted two temporal treatments: 4 days at low salinity followed by 10 days at high salinity (hereafter 4-10d cycle), or 7 days at each salinity (hereafter 7-7d cycle). At each transfer, populations were diluted at a rate of 1/10 and target salinity was achieved by mixing the required volumes of hypo- ([NaCl] = 0 M) and hyper- ([NaCl] = 4.8 M) saline media (Rescan et al. 2020), after accounting for dilution of the pre-transfer salinity.

In addition to these mixed populations, our experiment also included control lines that were subjected the same salinity treatments for the first 5 cycles. These consisted first of monocultures with only strain A or C, with each replicate consisting of one of the isogenic lines used in the mixtures. These monocultures not only served at controls for putative variation of the decline intensity over cycles (as observed in Zeballos et al 2023), but are also necessary for estimating relative frequencies in the mixtures through the method described below. We also included mixtures similar to those in the main experiment, but newly created at each salinity

rise by mixing the monocultures at 50%-50%. This latter control allowed assessing whether the population dynamics of mixed populations differed from those of populations with equal proportions of the declining and non-declining strain, as occurred at the beginning of the experiment. Since mean generation time of *Dunaliella salina* is ~1 per day (Ben-Amotz et al. 2009), the first five cycles (with the control lines) corresponded to ~70 generations.

Population density measures

Since our interest are demographic dynamics following each hyper-osmotic transfer, we measured population density daily during the high salinity step (except days 5 and 6). In contrast at the low salinity step, we only measured population densities 1 hour after the salinity transfer, to check the dilution rate, and at the end of the step (i.e. on day 4 or day 7 depending on the temporal treatment) to estimate the initial density (if no decline occurred) and calculate the culture volumes required to start the control mixtures at 50,000 cells/mL at the next salinity transfer.

We measured population densities by passing 200 µl samples of each population through a Guava® EasyCyte™ HT cytometer (Luminex Corporation, Texas, USA), with a laser emitting at 488 nm. Cells emits natural fluorescence in red (695/50nm) and yellow (583/26nm) due to their chlorophyll α, allowing to discriminate living Dunaliella cells from other particles, as described in Rescan et al. (2020) and Zeballos et al. (2023). PCD was estimated as the rate of initial population decline during the first days following a hyper-osmotic shock.

DNA confirmation

At the end of the 13 cycles of the assay, we genetically tested for the presence of both strains within each evolved population. Specifically, we amplified one mitochondrial (333 pb fragment using the primers DsMt1-For [5'-GGTTAGTCATAGTTGGAGGT-3'] and DsMt1-Rev [5'-GAAAACCTAACATGGCTAAGC-3']) and one chloroplastic (372 bp fragment using the primers DsChl1-For [5'-TTTAGGCGAATCCATAAGAG-3'] and DsChl1-Rev [5'-CCAAGCAGGTGAATTAGCTTTG-3']) locus from Leung et al. 2020, specific to strain A and C, respectively. DNA was extracted from *c.* 1.10^6 cells using Nucleospin plant II (Macherey-Nagel) and amplicon were amplified as followed: PCR was conducted in a total volume of 20 µL, including 10 µL of MasterMix Phusion with HF Buffer 2X (ThermoScientific), 2 µL of DNA, 10 µM of forward and reverse primers and 5 µL of pure H_2O. Amplification cycle consisted in: 30 s initial denaturation at 92˚C; 45 cycles of 15 s at 92°C, 15 s at 54°C, 30 s at 68°C; and a final extension at 68°C for 5 min.

Caspase-3-like inhibitor assay

It has been shown that strain A's decline intensity can be diminished by an inhibitor of caspase-3-like (Zeballos et al. 2023), known to be a key player in the metabolic cascade leading to cell death (Slee et al. 2001; Ameisen 2002; Danial and Korsmeyer 2004; Kasuba et al. 2015). We therefore investigated how this PCD inhibitor influenced strain frequencies in mixed populations, and the subsequent growth dynamics of the mixtures. Monocultures of both strains were acclimated for 4 days at 2.4M starting at N_0 = 100 000 cells/ml. For each of the two strain, we then launched 15 populations in monoculture at two initial density (10 populations at N_0= 50,000 cells/ml, and 5 populations at N_0 = 25,000 cells/ml), and prepared 10 mixed populations of both strains started at N_0= 50,000 cells/ml (50%-50% for each strain), in total culture volume of 10mL. We applied 2 inhibitor conditions (with or without PCD inhibitor), reaching a total of 80 flasks. In the inhibitor treatment, a total number of 500,000 cells per flask were treated with 10 µM Z-VAD(Ome)-FMK (CellSignaling) caspase inhibitor, and incubated in the dark for 30min at 24°C, before being subjected to a hyper-osmotic shock at 4M of NaCl. Populations densities were measured 30min and 2 hours after the hyper-osmotic transfer, and then daily tracked over 10 days. Since the inhibitor is supplied as 1 mg of powder and has been diluted in 213.9 µl of DMSO with membrane penetration action (Jacob, S. W., & Herschler 1986), we also checked that this solvent did not prevent strain A monocultures decline (see Supplementary Material).

Demographic and competition analysis

Decline intensity

To investigate how populations decline over cycles of salinity fluctuations, we fitted generalised linear models (GLM) on population size one hour after the hyper-osmotic transfer. We used cytometer cell count at day 0 as response variable, a log link function, negative binomial error structure, and log expected initial population density (based on pre-transfer density and the dilution rate) as offset (following Rescan et al. 2020, Leung et al 2022, Zeballos et al. 2023). The fixed effects were the type of culture (monoculture or mixture), temporal treatment, and the number of cycles (treated either as factor or as continuous variable). We extracted the decline rate from those GLM as minus the linear predictor of the GLM (hence, on the log scale), such that a demographic decline is represented by a positive value (Zeballos et al. 2023), and the standard error is unchanged.

Strain frequencies in mixtures

During the assay, we noticed that we were able to distinguish the two strains by their natural yellow and red fluorescence in most mixed population. However, the distributions of strains A and C still overlapped to some extent in mixed populations (scatter plots in Figure S1), so we could not use hand-designed gates to directly count for the numbers of each strain. Instead, we estimated strain frequencies in mixtures using a custom-made maximum likelihood method. We assumed that the pair of traits (yellow and red fluorescence) follow a bivariate Gaussian distribution in each monoculture, with mean vector μ and covariance matrix Σ specific to each strain. The distribution of these same traits in each mixed population was then considered as a mixture of Gaussians from the corresponding monocultures (sampled on the same day), with frequency p for the declining strain A and 1 - p for the non-declining strain C. As all points were measured independently within each assay, we summed their log-likelihoods, and further transformed frequencies to the logit scale $u = \ln(\frac{p}{1-p})$ to facilitate maximization, leading to

$$lnLik = \sum \log\left(\frac{1}{1+e^{-u}} \times f_A(\mu_A, \Sigma_A) + \frac{e^{-u}}{1+e^{-u}} \times f_C(\mu_C, \Sigma_C)\right). \quad \text{(Eq. 1)}$$

We obtained the estimator of $\hat{u}_i$ by maximizing log-likelihood for each isogenic line i, and extracted the curvature c_i of the log-likelihood function (at its maximum) to estimate the uncertainty as $V(\hat{u}_i) = -1/c_i$ using the asymptotic normal approximation. We then computed for further analyses the 95% confidence interval endpoints on the logit scale for each estimator $\hat{u}_i$ as

$$IC_{95\%} = \left[\hat{u}_i - 1.96\sqrt{V(\hat{u}_i)}; \hat{u}_i + 1.96\sqrt{V(\hat{u}_i)}\right]. \quad \text{(Eq. 2)}$$

Isogenic lines of strains A and C used in this experiment differed in how well they could be distinguished in mixtures (Fig. S1), so the mean frequency p was estimated with variable uncertainties depending on which mixture was used. To correct for this heterogeneity, and place more weight on more precise estimates, we used the inverse-variance weighting method, which is commonly used in e.g. meta-analyses (when sample sizes differ across studies) (Borenstein et al. 2021), and more generally whenever there are known sources of variation in uncertainty across estimates (Marin-Martinez and Sánchez-Meca 2010). Accordingly, the mean $\hat{u}$ over the 10 mixtures of isogenic lines (i) (within each treatment and measurement day) was obtained as

$$\hat{u}_{mean} = \frac{\sum_i c_i \times \hat{u}_i(p)}{\sum_i c_i} \quad \text{(Eq. 3)}$$

and the error variance of $\hat{u}_{mean}$ as

$$V(\hat{u}_{mean}) = -\frac{1}{\sum_i c_i}. \quad \text{(Eq. 4)}$$

We then computed the 95% confidence interval endpoints on the logit scale for $\hat{u}_{mean}$ including eq. 3 and 4 in the Eq. 2. as

$$IC_{95\%} = \left[\hat{u}_{mean} - 1.96\sqrt{Var(\hat{u}_{mean})}; \hat{u}_{mean} + 1.96\sqrt{Var(\hat{u}_{mean})}\right]. \quad \text{(Eq. 5)}$$

For further analyses, we back-transformed the frequency of A in each replicate to the arithmetic scale using the delta method as

$$\hat{p}_i = \frac{1}{1+e^{-\hat{u}_i}} + \frac{V(\hat{u}_i)}{2} \times g''(\hat{u}_i) \quad \text{(Eq. 6)}$$

$$\text{with } g''(\hat{u}_i) = \frac{-e^{\hat{u}_i}\,(e^{\hat{u}_i}-1)}{(1+e^{\hat{u}_i})^3}.$$

We back transformed the IC end-points obtained by Eq. 2 by simply using the inverse logit function $g(IC) = \frac{1}{1+e^{-IC}}$. For the mean frequency over the 10 isogenic lines (in each condition and day), we also used the delta method including the Eq. 3 and 4 in the Eq. 6, leading to

$$\hat{p}_{mean} = \frac{1}{1+e^{-\hat{u}_{mean}}} + \frac{V(\hat{u}_{mean})}{2} \times g''(\hat{u}_{mean}) \quad \text{(Eq. 7)}$$

We can then get the 95% confidence interval endpoints on the arithmetic scale for $\hat{p}_{mean}$ using the previous Eq. 7 and replacing $\hat{u}_{mean}$ by the endpoint's values obtained with the Eq. 5.

Finally, for further analyses below, the variance for the mean frequency $\hat{p}_{mean}$ was obtained with the delta method as

$$V(\hat{p}_{mean}) = \frac{e^{2\hat{u}_{mean}}}{(1+e^{\hat{u}_{mean}})^4} \times V(\hat{u}_{mean}). \quad \text{(Eq. 8)}$$

We also applied this method to obtain strain frequencies in mixed populations from the inhibitor assay. We tested the efficiency of our estimation method compared to the use of gates on the cytogram (see Supplementary Material and Figure S2).

Models of density-dependence and competition

One of our major aims is to compare the demography of two strains in monocultures vs mixtures, to investigate how these strains interact, and to what extent the population dynamics in monocultures predict the output of competition. More specifically, we wished to understand

to what extent per-capita growth rates of each strain are dependent on their own density and that of their competitor. To that intent, we inferred the densities of each strain in the mixtures as $\hat{p} \times N_{tot}$, with $\hat{p}$ the estimated frequency of each strain - previously obtained - and N_{tot} the total population density (in cells per mL) measured in the flask. We computed the mean weighted inferred density of each strain in the long-term mixtures over the 5 cycles, using the expression

$$E(\mathrm{N}\hat{p}) = E(N) \times E(\hat{p}_{mean}), \qquad \text{(Eq. 9)}$$

thus assuming that N and $\hat{p}_{mean}$ are independent. Accordingly, the error variance of $E(\mathrm{N}\hat{p})$ over the 10 isogenic lines per condition was computed as the variance of product of two independent random variables,

$$V(N\hat{p}) = V(N) \times V(\hat{p}_{mean}) + V(N) \times E(\hat{p}_{mean})^2 + V(\hat{p}_{mean}) \times E(N)^2 \qquad \text{(Eq. 10)}$$

We then computed the confidence interval at 95% of the inferred densities over the 5 cycles using the law of the total variance, $V_{tot}(N\hat{p}) = E_{cyc}\big(V(N\hat{p})\big) + \frac{V_{cyc}(E(\mathrm{N}\hat{p}))}{nb\ cycles}$, where E_{cyc} and V_{cyc} denote expectations and variances across cycles, respectively.

Finally, we computed the *per-capita* growth rate of strain A in mixed populations as

$$r_A = \frac{\widehat{N}_{A,t} - \widehat{N}_{A,t-\tau}}{\tau\, \widehat{N}_{A,t-\tau}} \qquad \text{(Eq. 11)}$$

with τ the time interval between measurement (1, 2 or 3 days), and similarly for strain C. We restricted the analysis to t > 4 days and $\widehat{N}_t$ > 5.10^4 cells/ml for both strains, so as to focus only the phase with high competition, and not the initial phase of decline rebound, where population sizes are likely to be less well estimated, and the relationships between population growth and size are not driven by density dependence. We computed similar *per-capita* growth rates in monocultures using densities estimated directly from cytometer counts. Then, we fitted linear models (LM) with the per-capita growth rate as response variable, and the densities $\widehat{N}_{t-\tau}$ of one or both strains and the type of culture (monoculture vs mixtures) as fixed effects (see Table 1 for details). These linear models correspond to the classic Lotka-Volterra model of density-dependent competition. However, the relationship between the *per-capita* growth rate and population density need not be linear, so we also fitted semi-parametric models (cubic splines) using generalized additive models (GAM) (see Table 1 for formula).

We also applied a generalised linear model on population densities (from day 2 to 5) of strain A monocultures in the inhibitor assay, to estimate the growth rate during the exponential phase as in Zeballos et al. (2023) (Fig. S6). Time was included as a continuous explanatory variable, so the effect of time represented the rate of exponential growth per day (linear trend on the log scale), and the interaction of time with the other fixed effects (i.e. inhibitor treatment and initial density) estimated the effect of these factors on the maximal exponential growth. All statistical analyses were performed on Rstudio (R version 4.2.0.) using packages MASS (version 7.3.56) (Venables and Ripley 2002), stats (version 4.2.0), mvtnorm (version 1.1.3), mgcv (version 1.8.33).

Table 1. Linear models (LMs) and generalized additive models' (GAMs) parameters.

LMs	**Variable response: $r_{strain\ 1}$** **Fixed effects:**	**AIC** **$r_{strain\ A}$**	AIC **$r_{strain\ C}$**
Model 1	$N_{strain\ 1,t-\tau}$	204.7027	173.1958
Model 2	$N_{strain\ 1,t-\tau} + culture$	153.9641	150.3992
Model 3	$N_{strain\ 1,t-\tau} * culture$	155.0896	127.2454
Model 4	$N_{strain\ 1,t-\tau} + N_{strain\ 2,t-\tau}$	184.2437	159.2982
Model 5	$N_{strain\ 1,t-\tau} + culture + N_{strain\ 2,t-\tau}$	154.2407	152.3195
Model 6	$N_{strain\ 1,t-\tau} * culture + N_{strain\ 2,t-\tau}$	155.5339	129.2311
Model 7	$N_{Total,t-\tau}$	238.0548	164.2451
GAMs	Variable response: $r_{strain\ 1}$ Fixed effects:	AIC $r_{strain\ A}$	AIC $r_{strain\ C}$
Model 1	$s(N_{strain\ 1,t-\tau})$	127.8361	158.0672
Model 2	$s(N_{strain\ 1,t-\tau}) + culture$	116.9656	142.1332
Model 3	$s(N_{strain\ 1,t-\tau}, by = culture) + culture$	118.5395	118.633
Model 4	$s(N_{strain\ 1,t-\tau}) + s(N_{strain\ 2,t-\tau})$	1.802084	115.8518
Model 5	$s(N_{strain\ 1,t-\tau}) + s(N_{strain\ 2,t-\tau}) + culture$	2.32479	115.4148
Model 6	$s(N_{strain\ 1,t-\tau}, by = culture) + s(N_{strain\ 2,t-\tau}) + culture$	-3.609805	96.13687
Model 7	$N_{Total,t-\tau}$	195.0641	149.2998

We applied on a subset of observations: $N_{A,t-\tau}$ & $N_{C,t-\tau}$> 50,000 cells/ml, either on monocultures and mixed populations ("culture" variable). We also filtered on the confidence interval of the logit estimates to keep the more certain inferred densities. Akaike information criterion are notify, best ones are in bold.

Results

Population decline occurs repeatedly over successive hyper-osmotic shocks

The population dynamics over the first 5 cycles of salinity rise are shown in Fig. 1. At each transfer into hypersaline medium, monocultures of strain C (in black) soon started growing exponentially, while those of strain A (in red) first declined sharply, before rebounding through fast growth, eventually reaching a similar density as monocultures of strain C, consistent with results in Zeballos et al. (2023). The decline-rebound pattern of strain A was not a transient response but was instead repeatable, and the decline intensity actually increased over cycles (number of salinity cycles used as a continuous variable, Table 2, P = 0.044, red line in Fig. 1B). The same pattern was found regardless of the type of cycle (Fig. 1A & S3A), but in the 7-7d treatment the increase in decline intensity was not significant (Table 2, P = 0.914). This variation can be attributed to the plastic character of this cell death (Zeballos et al. 2023).

We analysed mixed populations of both strains to investigate whether a declining genotype could be maintained in competition with a non-declining one. Since the declining strain A can reach higher densities than the non-declining strain C in monocultures after the rebound phase (Zeballos et al. 2023), it might also be able to outcompete this strain when they are grown together. This would lead to an increasing rate of decline over cycles in the mixtures, as strain A replaces strain C. However, population dynamics may be fundamentally different in mixtures, for instance if strain C exhausts resources before A is able to rebound from its initial decline. Here in the first cycle, the initial decline of mixtures was intermediate between those of strain A and C monocultures, as expected. Mixed cultures maintained a similar initial decline rate at each hyperosmotic shock (Table 2, P = 0.913), suggesting that no strain was able to fully outcompete the other after 70 days (Fig. 1A).

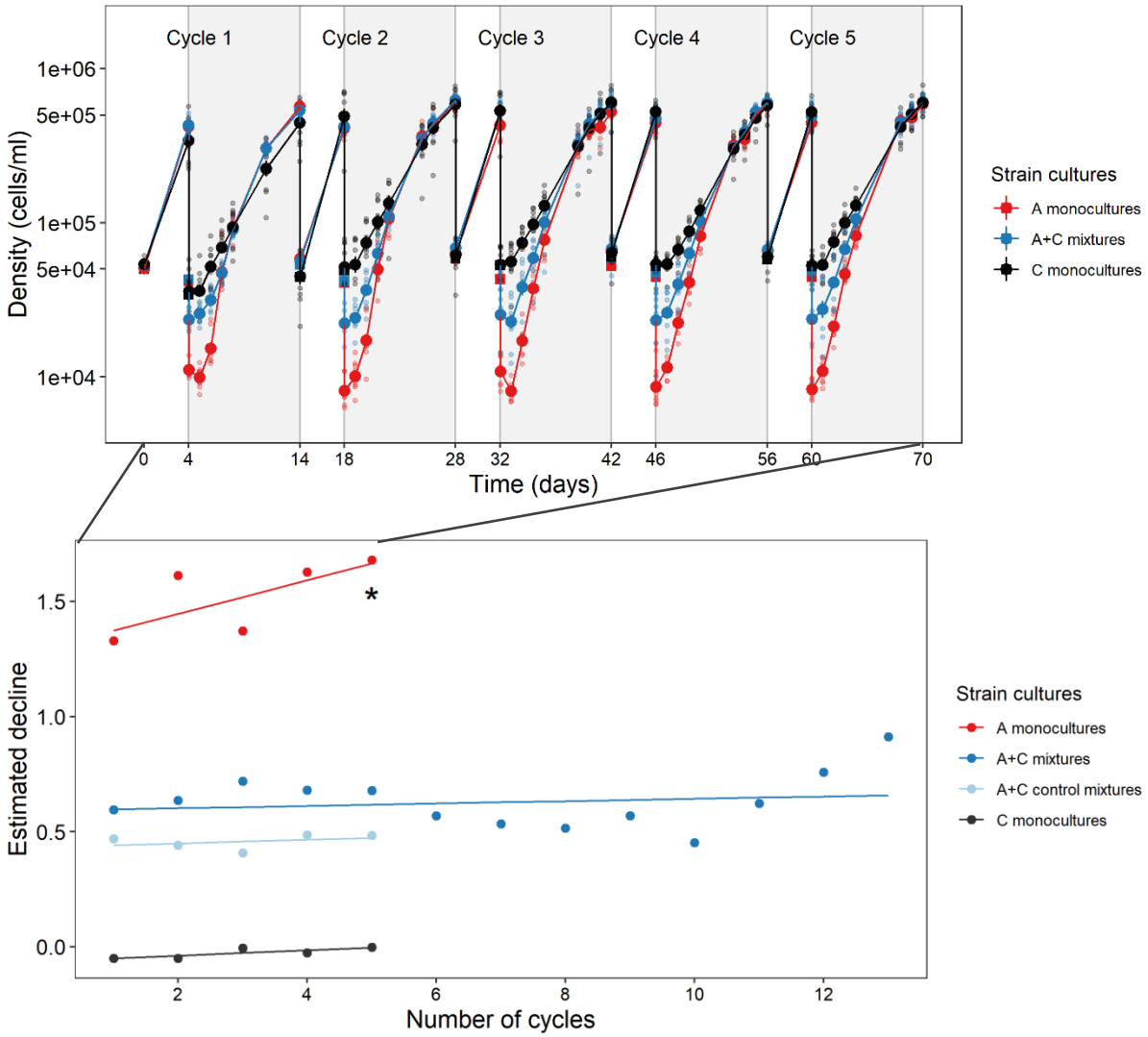

Figure 1. Demographic responses to successive salinity rises. (A) Populations densities over the first five salinity cycles are shown for monocultures of strain A (red) and strain C (black), and mixtures of A and C (blue). Small dots represent biological replicates (specific isogenic lines of each strain, or mixtures thereof), while large dots represent means over replicates (with SE not visible). Grey backgrounds correspond to the high salinity step in the cycle. (B) The rate of initial decline one hour after the hyper-osmotic shock is shown over cycles, based on GLMs where the number of cycles was treated either as factor (dots), or as a continuous variable (lines). The star denotes p-value <0.1 for the slope of decline rate against cycle number.

Table 2. Population decline rate against number of salinity cycles.

	Estimate	Std. Error	z value	Pr(>|z|)
Intercept (A+C control mixtures in cycle 1 in 4-10d fluctuations)	-0.434	0.076	-5.683	1e-08 ***
Cycle	-0.008	0.023	-0.337	0.736
Strain_Amonocultures	-0.866	0.108	-8.026	1e-15 ***
Strain_A+Cmixtures	-0.158	0.087	-1.802	0.0715
Strain_Cmonocultures	0.496	0.108	4.601	4e-6 ***
Fluct_7-7	0.102	0.108	0.949	0.343
Cycle:Strain_Amonocultures	-0.065	0.033	-2.010	0.044 *
Cycle:Strain_A+Cmixtures	0.003	0.024	0.110	0.913
Cycle:Strain_Cmonocultures	-0.004	0.033	-0.125	0.901
Cycle:fluct_7-7	0.000	0.033	-0.010	0.992
Strain_Amonocultures:fluct_7-7	0.270	0.149	1.818	0.069 .
Strain_A+Cmixtures:fluct_7-7	-0.118	0.124	-0.951	0.341
Strain_Cmonocultures:fluct_7-7	-0.089	0.153	-0.585	0.558
Cycle:Strain_Amonocultures:fluct_7-7	0.005	0.043	0.108	0.914
Cycle:Strain_A+Cmixtures:fluct_7-7	0.008	0.033	0.227	0.821
Cycle:Strain_Cmonocultures:fluct_7-7	0.005	0.046	0.117	0.907

Generalized linear model using density measured 1 hour after the salinity rise as response variable, and the logarithm of expected initial population density as offset. We tested the effect of strain cultures identity, the cycle treatment as factor and the number of cycles as a continuous variable on demographic decline. The interaction of others factors with the number of cycles represents the effects of these factors over the successive salinity rises.

Strain frequencies fluctuate within a cycle but are stable over cycles

We were able to estimate strain frequency in the mixed populations by taking advantage of their differential yellow and red natural fluorescence, and using the monocultures as references (Fig. S1). Strain A frequency strongly fluctuated in the days following hyper-osmotic shock, starting at low frequency, before increasing and becoming dominant in the mixture at the end of the high salinity step in (almost) every cycle (Fig. 2), consistent with the decline-pattern in population density observed in monocultures. In the control mixtures, in which the frequency of strain A was set to ~50% before each hyper-osmotic shock, this frequency started at lower value than in long-term mixtures when first measured in the hypersaline environment. This suggests that the proportion of strain A before the hyper-osmotic shock was greater than 50% in the long-term mixtures. We confirmed the stable coexistence of both strains in all long-term mixtures by genetically detecting both strains after 180 generations (Figs. S5).

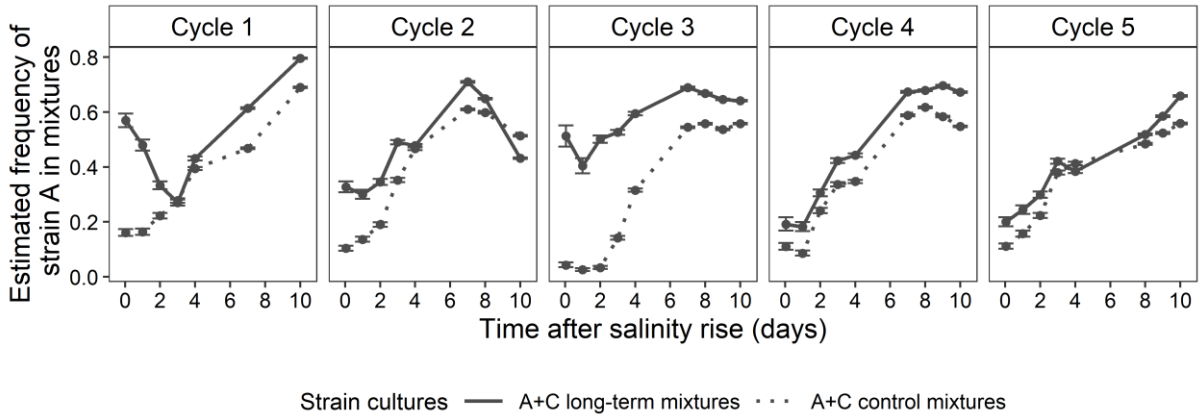

Figure 2. Frequency of strain A over 5 successive salinity rises. The proportion of strain A in mixed populations, as estimated from the cytometric traits of cells, is shown against time for long-term (solid lines) and control mixtures (dotted lines -freshly composed by mixing 50-50% of each strain before each salinity rise). Means and confidence interval at 95% were obtained on the logit scale by inverse-variance weighting over the 10 population lines, to account for the variable uncertainty of estimates among biological replicates (isogenic lines of each strain), and then combined with the delta method for the back-transformation on the arithmetic scale.

We also investigated the effect of time spent at high salinity, by comparing 4-10d and 7-7d cycles (with respectively 10 and 7 days at high salinity). Since strain A grows faster than strain C during its rebound phase (Fig. 1A; Zeballos et al. 2023), we hypothesized that longer hypersaline phases would leave more time for A to outgrow C in mixed populations, provided that they remain in near-exponential growth. However, the pattern of strain A frequency against time in the 7-7d treatment was similar to that in 4-10d, over the 5 successive cycles (Fig. S3B) and in the two last cycles (Fig. S4). This suggests that 7 days were sufficient for strain A to reach high enough frequency at the end of each hypersaline phase to not be outcompeted at the next hyperosmotic shock. This is also consistent with the fact that this frequency did not change much between days 7 and 10 under 4-10d cycles (Fig. 2), suggesting that differences in growth rates of both strains were no longer significant drivers of selection at this time.

To what extent can demography explain selection?

To investigate how these selective dynamics emerge from demography, we calculated the density of each strain in the mixed populations, by multiplying the estimated frequencies of strains A and C by the total population density. The population dynamics of each strain in mixtures (Fig. 3, dashed lines) was qualitatively consistent with that in monocultures (Fig. 3, solid lines), but starting a lower density since only half of the population was composed of each strain at the start. In the mixtures, strain A had lower density than strain C just after the hyper-osmotic shock as a consequence of PCD, but its higher exponential growth rate during rebound

allowed it to reach higher density at the end of the hypersaline phase (Fig. 3, Fig. S3C). This growth advantage during rebound was more pronounced than expected based on monocultures: in Fig. 3, the dashed red line crosses the dashed black line earlier, and their final difference is larger, than for continuous lines. This probably occurs because the density of each strain starts lower in mixtures than in monocultures, allowing growth differences to accrue during a longer exponential phase (Fig. 3, Fig. S3C). However, the outcome of this process should also depend on how density dependence acts within and between strains.

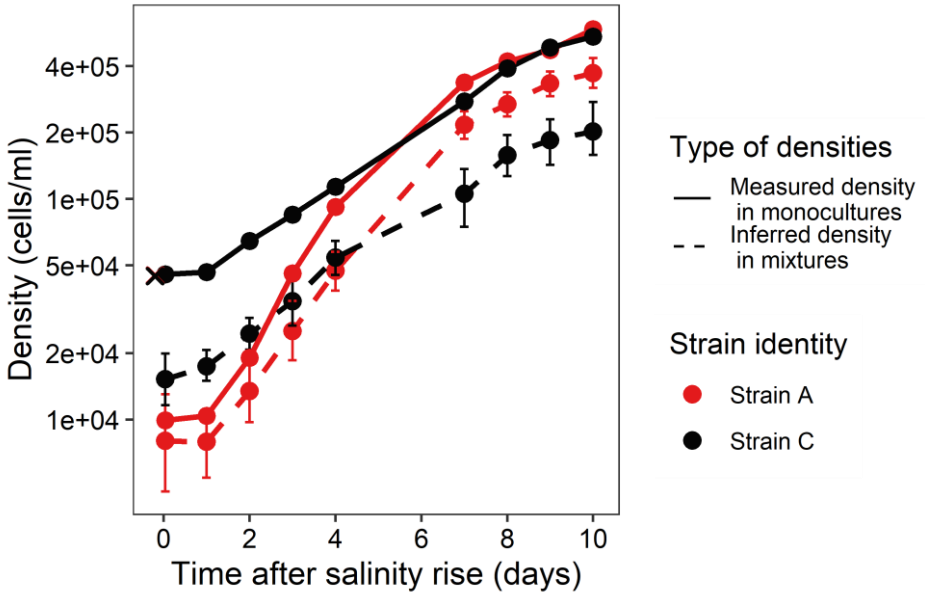

Figure 3. Growth rates in monocultures versus mixtures. Mean population densities across replicates in monocultures (solid lines; direct measurements), and long-term mixtures (dashed lines; inferred from the estimate of relative frequencies), averaged over the first 5 high salinity cycles, are shown for the 4-10d fluctuation cycle. For the monocultures, we computed the mean and standard error (not visible) over 10 isogenic lines. For the mixtures, we used inverse-variance-weighted mean and 95% confidence interval (computed with the delta method), to account for variable precision in estimation of strain A frequency among biological replicates. The overlapped crosses correspond to the mean expected initial density for each monoculture, based on the known density before the 10% dilution.

To better understand how the growth of each strain is impacted by both intra and inter-genotype competition, we calculated the sensitivity of their per-capita growth rates to population density, in both mixtures and monocultures (Fig. 4, Table 3 for LM 1, see Fig. S6 for 7-7d treatment). We observed a significant negative effect of self-density on the per-capita growth rate of each strain (analyses including mixtures and monocultures), as classically expected under negative density dependence (i.e., regulation of population growth). The strength of density dependence varied among strains, being three times weaker for strain C (6.4e-07, P = 6e-10) than for strain A (-1.92e-06, P < 2e-16). However, because the intrinsic

rate of increase (y-intercept of dashed lines in Fig. 4A,D) was more than twice higher in strain A (8.74e-01) than in strain C (4.28e-01), this difference in density dependence strength was not predicted to lead to marked differences in equilibrium population sizes (4.6e05 vs 6.7e05 cells/ml for strains A and C, respectively; x-intercept of dashed lines in Fig. 4A,D), under this simple linear model of density dependence.

Table 3. Effect of self-density on *per-capita* growth rate for both strains A and C (LM 1).

r_A	Estimate	Std. Error	z value	Pr(>|z|)
Intercept	8.74e-01	3.44e-02	25.40	<2e-16 ***
$N_{A,\, t-\tau}$	-1.92e-06	1.20e-07	-15.99	<2e-16 ***
r_C	Estimate	Std. Error	z value	Pr(>|z|)
Intercept	4.28e-01	2.60e-02	16.51	<2e-16 ***
$N_{C,\, t-\tau}$	-6.40e-07	1.01e-07	-6.34	6e-10 ***

We applied a linear model (LM 1) on the *per-capita* growth rate as response variable and their self-density as fixed effect, including growth rate computed on measured densities of monocultures and on estimated strain densities within mixtures.

To assess the effect of the competitor on the growth of each strain, we next turned to linear models that also included as predictors the type of culture (monoculture vs mixtures), and/or the density of the competitor strain. We found a greater growth rate in monocultures than in mixtures for both strains (see LM 2 in Table S1, P = 4.85e-13 for r_A and P = 7.08e-07 for r_C), in the best model based on AIC values (Table 1). The strength of density dependence did not significantly differ between monocultures and mixtures for strain A (see LM3 in Table S2, P = 0.353), while it was greater in mixtures for strain C (P= 6.08e-07). Model that included densities of self and the competitor as predictors (LM 4) showed that both strains are more sensitive to their own density than to that of their competitor, but that this is more pronounced for strain A (x2.9 for r_A vs x1.8 for r_C, Table S3). It is noteworthy that AIC was not improved when treating the density of competitor as a continuous variable, as compared to using the type of culture (monoculture vs mixture) as fixed effect (LM 4 vs LM 2 in Table 1), neither adding both fixed effect (LM 5 and 6 in Table 1), suggesting that the influence of the competitor may not be well captured by a linear influence on per-capita growth rates (see below). Surprisingly, the worst model is when the total density is used as fixed effect for strain A growth (LM 7 in Table 1). We would expect that for related close strains, population density would be density-dependent to the total number of individuals, regardless the genotype identity. In this case, declining before growing would lead to some delay in the competition and favour the non-declining strain.

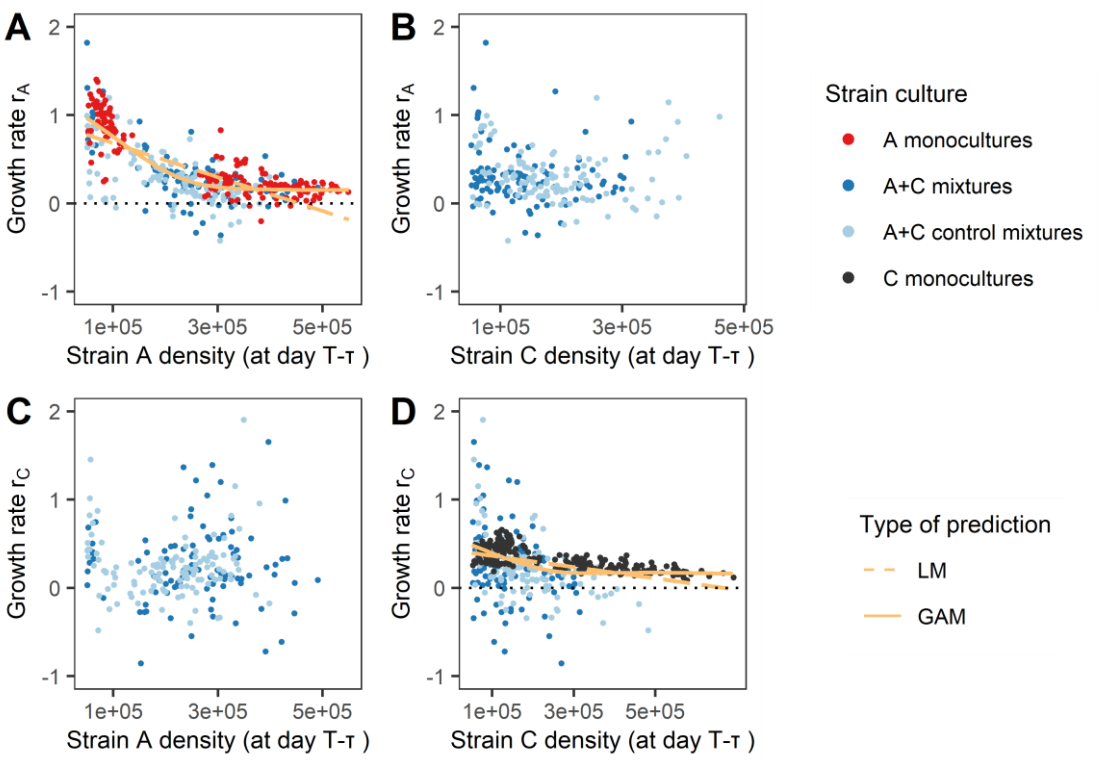

Figure 4. Intra- and inter-strain competition and population growth. The *per-capita* growth rate of strain A (A-B) or strain C (C-D) is shown against the density of strain A (A,C) or strain C (B, D), in the 4-10d fluctuation cycle. Each point corresponds to relative growth rate per day, over the interval between two subsequent measurements. Panels A and D also display (in orange) predictions from the simplest models of density dependence (LM 1 in dashed, GAM 1 in continuous). Data have been filtered on the precision of frequency estimation (CI width < 0.5 on logit scale) to remove the most uncertain values, and on population density (N >5.10^4 cells/ml). We set the y-axis maximum to 2 for the sake of graphical clarity, which led to removing 2 dots in A-B (r_A = 2.3; 3.9) and 1 in C-D (r_C =2.4).

Although the assumption of linear density dependence is convenient to get simple metrics of competition strength, and also corresponds to the classic Lotka-Volterra and logistic models from theoretical population ecology (Kot 2001), it might not be the most realistic model. Here, density dependence seemed to weaken at higher densities, such that populations maintained positive growth rates even at densities well above the equilibrium value predicted in the linear model (Fig. 4A, D). We thus also tested more flexible models that made fewer assumptions about the shape of density dependence, namely spline smoothers as implemented in generalized additive models (GAM, package mgcv in R). The predictions from the simplest GAM (GAM 1) we fitted are shown as continuous lines in Fig. 4A, D. They provide a better fit to the data than the equivalent LM, and never cross the x-axis over the range of observed densities. The best model (GAM 6, Table 1) included densities of both strains and the type of culture as fixed effect, and adding the competitor density (GAM 4 vs GAM 1, Table 1) led to

larger differences in AIC when the response variable was r_A rather than r_C. Therefore, the effect on the growth rate of the competitor as a continuous variable seems to be better captured by the GAM than the LM. The model using the total density as fixed effect (GAM 7) is the worst for strain A *per-capita* growth rate, while it is slightly better than the simplest GAM for strain C growth, consistent to the equivalent LMs. To summarise, intra-strain competition matters more than inter-strain competition for strain A.

How PCD inhibitor affect dynamics and strain frequency in mixtures?

To demonstrate the role of programmed cell death (PCD) in these eco-evolutionary dynamics, we applied a caspase-3-like inhibitor to mixed populations composed by 50-50% of each strain just before undergoing hyper-osmotic shock. We estimated strain frequencies using monocultures as references as done above (Figs. S7-S8), and then inferred the density of each strain in the mixtures (Fig. 5). While the treatment without inhibitor resulted in a sharp initial decline of this strain A as above, no population decline was observed for strain A subjected to PCD inhibitor, confirming that the initial decline was attributable to a form of programmed cell death (as also shown by Zeballos et al 2023). Interestingly, the mean growth rate of populations of strain A that underwent initial decline (without inhibitor) was higher than that of populations that did not decline (with inhibitor), over a similar range of densities (compare slopes of red vs dashed red lines between eg days 2 and 5 in Fig. 5; Table S4 P = 3.55e-11). It is noteworthy that the initial density did not affect growth rate during the exponential phase of strain A monocultures without PCD inhibitor (Table S4, P = 0.451), consolidating the idea that the demographic rebound after the decline is not just density-dependence due to released competition. Eventually, strain A in mixtures reached a similar density with and without inhibitor (Fig. 5). The population dynamics of strain C were similar under both conditions, despite its competitor having markedly different responses, supporting the idea that the growth of strain C is little sensitive to presence of the other strain.

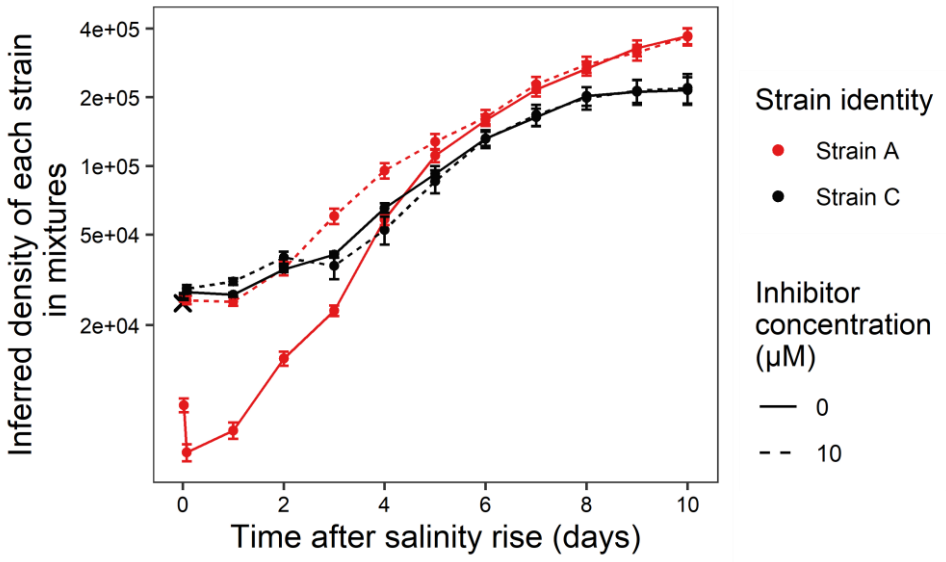

Figure 5. Impact of a programmed cell death inhibitor on growth in competition. Weighted mean inferred densities of each strain (colours) in the mixtures are shown under different PCD inhibitor doses (line type), against days following a single salinity rise. Transfers occurs at day 0, the first measures were made 30 min, and then 2 hours after the transfer. The cross corresponds to the expected initial density. Filled symbols are weighted averages over 10 replicates, error bars indicate confidence interval at 95% (with delta method).

Discussion

We investigated the outcome of competition between two strains of *Dunaliella salina*, one of which triggers PCD in response to hyper-osmotic shock, and thus undergoes a distinctive decline-rebound demographic pattern. We found a stable coexistence in the mixed populations over the 13 cyclical salinity rises, despite strong variation in strain frequencies within each cycle.

Long-term coexistence of alternative strategies

Based on the competition-relatedness relationship, also known as the limiting similarity hypothesis (Charles 1859; Gause 1934; MacArthur and Levins 1967; Violle et al. 2011), we expected that the two closely-related strains we studied would exert strong competition on each other. This could have led to exclusion of the declining strain over cycles, since it starts growing later and at much lower density following each hyperosmotic shock. Interestingly, we found that instead of responding to the total population density (Table 1, see AIC for LM 7 and GAM 7), as expected for closely related genotypes, the growth rates of strains A and C were mostly sensitive to their own density, suggesting that they have different ecological strategies (e.g. use different resources) in the same environment, as also indicated by their strikingly different demographies. This weak sensitivity to each other's presence allowed their stable coexistence

over 13 cycles of salinity changes (DNA confirmation and Fig. 1B), consistent with the fact that they have been sampled from the same brackish water site (Ginzburg and Ginzburg 1985). Previous work has shown that strain A is almost neutral with strain C at constant salinity 3.2M NaCl (Rescan et al. 2021), but strongly counter-selected at constant 2.4M NaCl (our lower salinity here). Interestingly, although the dynamics of selection is here more complex owing to the decline rebound dynamics at each salinity rise, the long-term coexistence that we find is consistent with near-neutrality overall, for a similar mean salinity of 3.2M NaCl averaged over a cycle. Hence, fluctuating and constant salinities with a mean of 3.2M here led to similar net selection, but probably for different reasons owing to their different demographic dynamics.

Relative and absolute fitness

Being able to measure relative fitness is a crucial issue in experimental evolution. This can be achieved by transforming one of the genotypes, for instance by introducing a gene for a fluorescent protein such as the Green Fluorescent Protein, to allow distinguishing it in a mixture (Gallet et al. 2012). However this may complexify analyses, as it requires taking into account the fitness effect of the fluorescent marker, and its potential epistasis with the mutation of interest (Gallet et al. 2012). Alternatively, sequencing of natural or introduced markers can be used (Rescan et al. 2021; Levy et al. 2015). Here, we instead took advantage of the natural fluorescence of pigments in our focal species to discriminate the two strains in mixtures, and thus estimate their frequencies and relative fitnesses. Our method based on analysis of mixture distributions allowed us to estimate frequencies more precisely, and at much lower cost, than using strain-specific amplicon sequencing (as done in Rescan et al. 2021). This allowed us to increase temporal resolution (daily measurements), thus yielding more insights into the non-trivial eco-evolutionary dynamics in this system. We have shown that the dynamics in monocultures were broadly consistent with those of mixtures (Fig. 3), because mixtures seem mostly driven by intra- rather than inter-strain competition. Hence, absolute fitness in monocultures partly predicted selection in mixtures. On the other hand, selection was strongly density-dependent, such that using the exponential growth rate as proxy for fitness would not have been relevant to correctly estimate the net coefficient of selection over a cycle (Chevin 2011). This was true regardless of the type of cycle (Fig. S6), and even though the transfer to the next salinity was achieved before reaching the stationary phase in the 7-7d cycle.

Selection on programmed cell death

Beyond the general goal of understanding how selection emerges from demography, the aim of our competition experiment was also to determine whether, and how, selection can favour programmed cell death (PCD). The distinctive decline-rebound pattern of strain A in response to osmotic shock was entirely removed by exposure to an inhibitor of caspase3-like activity (Fig. 5), confirming that it was a form of PCD (consistent with the results in Zeballos et al. 2023). Our results thus demonstrate that PCD can be maintained by selection against a closely related non-PCD strain over successive osmotic shocks, and yield insights into the demographic underpinnings of this selection. However, the ecological and/or physiological mechanisms behind the decline-rebound pattern observed both in monocultures and in mixtures remain to be elucidated. We proposed three potential hypothesis in Zeballos et al. (2023): an altruistic substrate release by the dying cells, cell heterogeneity in cell state, and a trade-off between halotolerance and reproduction. Further investigation of these hypotheses through modelling may help distinguish them, based on the dynamics they predict for monocultures and mixtures

In conclusion, we showed that programmed cell death could be an evolvable trait even in short evolutionary scale, and demonstrates that two drastically different strategies in response to salinity can allow coexistence in the same fluctuating environment.

Statement of Authorship: NZ, CL and L-MC conceived and designed the study. NZ, SF and OR performed the experiments and collected the data. NZ and L-MC build the estimation frequency method. NZ analysed the data, prepared figures and tables, and wrote the original draft, CL and L-MC reviewed and edited the draft.

Competing interest: Authors declare no competing interests.

Supplementary Material

Calibration and testing efficiency of frequency estimate method

We tested the efficiency of our estimation method on a calibration assay. We took 8 of the 10 monocultures per strain being at high salinity (cycle 3) and prepared the corresponding mixed populations at a range of expected frequency (from 5% to 95% in terms of volume for practical reason, the expected frequencies have been deducted from the densities of the used monocultures flasks). Cytometer measurement of these freshly prepared flasks have been achieved. We applied on the cytometer data more restrictive hand-drawn gates on strain A and strain C dots (see Figure S2A) to compare the obtained frequency in mixtures using these smaller gates and the frequency obtained through our estimation method (Figure S2B). We then simulated "numerical" mixed populations from virtually sampling cells from the strain A and strain C monocultures datasets, at different frequencies for a total number of cells of 10,000 (note that for a flask being at equilibrium stationary phase, less than 20,000 events are recorded in the 30s of flow cytometry). We then applied our estimation method on these simulated mixtures (Figure S2C).

Checking DMSO effect on PCD inhibition

The 10 replicates monocultures of strain A were acclimated for 4 days at 2.4M. The initial density was set at N_0= 50,000 cells/ml, in total culture volume of 10ml. We applied 3 conditions (standard, DMSO and inhibitor). In the inhibitor treatment, a total number of 500,000 cells per flask were treated with 10 µM Z-VAD(Ome)-FMK (CellSignaling) caspase inhibitor (diluted in DMSO) corresponding to 10 µl of the solution, while the DMSO treatment consisted in adding 10 µl of pure DMSO. Then flasks were incubated in the dark for 30min at 24°C, before being subjected to a hyper-osmotic shock at 4M of NaCl. Populations densities were measured 1 and 4 hours after the hyper-osmotic transfer, and then daily tracked over 4 days. We applied a GLM on population density 1 hour post-transfer to estimate the intensity of the decline (Table S5). We used cytometer cell concentration at day 0 as response variable, a log link function, negative binomial error structure, and log expected initial population density as offset (following Rescan et al. 2020, Leung et al 2022, Zeballos et al. 2023).

Long-term competition over successive hyper-osmotic shocks

Long-terms mixtures were maintained to their cycle treatment (4-10d or 7-7d) over a total of 13 cycles. From cycle 6 to 11 included, populations densities were measured only before and

after dilution and on the next day following the hyper-osmotic shock. For the two last cycles, we followed the usual measurement pattern, meaning that demography was daily tracked after the hyper-osmotic shock. Since we did not have any more the corresponding monocultures as needed for our frequency estimation method, we estimated the frequency in the long-term mixtures using the mean values of the monocultures over the cycle 5 after, i.e the last cycle with monocultures flasks.

Supplementary Tables

Table S1. Effect of self-density and culture type on *per-capita* growth rate (LM 2).

r_A	Estimate	Std. Error	t value	Pr(>|t|)
Intercept (A+C mixtures)	8.20E-01	3.30E-02	24.827	<2e-16 ***
NA, t- τ	-2.10E-06	1.15E-07	-18.27	<2e-16 ***
Culture_Amonocultures	2.29E-01	3.06E-02	7.486	4.85e-13 ***
r_C	Estimate	Std. Error	t value	Pr(>|t|)
Intercept (A+C mixtures)	3.95E-01	2.61E-02	15.125	<2e-16 ***
NC, t- τ	-8.19E-07	1.04E-07	-7.844	3.60e-14 ***
Culture_Cmonocultures	1.49E-01	2.96E-02	5.035	7.08e-07***

We applied a linear model (LM2) on the *per-capita* growth rate as response variable and self-density and the type of culture (monoculture or mixture) as fixed effect, including growth rate computed on measured densities of monocultures and on estimated strain densities within mixtures.

Table S2. Effect of self-density, culture type and their interaction on *per-capita* growth rate (LM 3).

r_A	Estimate	Std. Error	t value	Pr(>|t|)
Intercept (A+C mixtures)	8.55E-01	5.04E-02	16.967	<2e-16 ***
$N_{A,\, t-\tau}$	-2.25E-06	2.01E-07	-11.188	<2e-16 ***
Culture_Amonocultures	1.72E-01	6.81E-02	2.529	0.012
$N_{A,\, t-\tau}$: Culture_Amonocultures	2.28E-07	2.45E-07	0.931	0.353
r_C	Estimate	Std. Error	t value	Pr(>|t|)
Intercept (A+C mixtures)	5.56E-01	4.06E-02	13.673	<2e-16 ***
$N_{C,\, t-\tau}$	-1.78E-06	2.15E-07	-8.279	1.65e-15 ***
Culture_Cmonocultures	-8.47E-02	5.44E-02	-1.558	0.120
$N_{C,\, t-\tau}$: Culture_Cmonocultures	1.24E-06	2.44E-07	5.066	6.08E-07 ***

We applied a linear model (LM3) on the *per-capita* growth rate as response variable and fixed effects were self-density, the type of culture and the interaction, including growth rate computed on measured densities of monocultures and on estimated strain densities within mixtures.

Table S3. Effect of self- and competitor densities on *per-capita* growth rate (LM 4).

r_A	Estimate	Std. Error	t value	Pr(>|t|)
Intercept (A+C mixtures)	9.69E-01	3.89E-02	24.89	<2e-16 ***
NA, t- τ	-2.03E-06	1.19E-07	-17.06	<2e-16 ***
NC, t- τ	-7.10E-07	1.48E-07	-4.79	2.38e-6 ***
r_C	Estimate	Std. Error	t value	Pr(>|t|)
Intercept (A+C mixtures)	5.09E-01	3.24E-02	15.689	<2e-16 ***
NC, t- τ	-7.71E-07	1.04E-07	-7.379	8.5e-13 ***
NA, t- τ	-4.39E-07	1.10E-07	-4.01	7.16e-5 ***

We applied a linear model (LM4) on the *per-capita* growth rate as response variable and fixed effects were self-density and the density of the competitor, including growth rate computed on measured densities of monocultures and on estimated strain densities within mixtures.

Table S4. Effect of initial density and PCD inhibitor treatment on strain A monocultures rebound.

	Estimate	Std. Error	z value	Pr(>|z|)
Intercept (Strain A monocultures without PCD inhibitor starting at N0= 25,000 cells/ml)	7.620	0.125	61.064	<2e-16 ***
Time	0.746	0.034	21.976	<2e-16 ***
Inhibitor_10	2.087	0.176	11.830	<2e-16 ***
Initialdensity_50,000	0.871	0.153	5.699	1.20e-8 ***
Time:Inhibitor_10	-0.318	0.048	-6.622	3.55e-11 ***
Time:Initialdensity_50,000	-0.031	0.042	-0.754	0.451
Inhibitor_10:Initialdensity_50,000	0.001	0.216	0.003	0.997
Time:Inhibitor_10:Initialdensity_50,000	-0.060	0.059	-1.026	0.305

GLM on population densities on days 2 to 5 from the PCD inhibitor assay, corresponding to growth in the exponential phase (visually detected as in Zeballos et al. (2023)). Our main interest is the effect of Time and its interactions with other factors, which represent effects of these factors (here PCD inhibitor doses and initial density) on maximal population growth rate.

Table S5: Effect of DMSO on initial decline (1-hour after hyper-osmotic transfer).

Table A	Estimate	Std. Error	z value	Pr (>|z|)	Population reduction (%)
Intercept (Treatment standard)	-0.655	0.034	-19.557	3.56e-85 ***	66
Treatment_DMSO	-0.274	0.047	-5.784	7.30e-09 ***	93
Treatment_Inhibitor	0.721	0.047	15.218	2.69e-52 ***	-7

GLM on strain A population density on day 0 relative to the expected initial density from the DMSO assay. We tested the effect of the DMSO on demographic decline on the logarithmic scale (from the log link function in the GLM), and also report the population size reduction (where negative values denote proportional increase). p-value: ***: <0.001 ; **: <0.01 ; : <0.05 ; .: <0.1. This assay confirmed that the inhibition of the decline is due to the caspase activity inhibitor and not to the solvent DMSO. Actually, DMSO treatment triggered higher population reduction.

Supplementary Figures

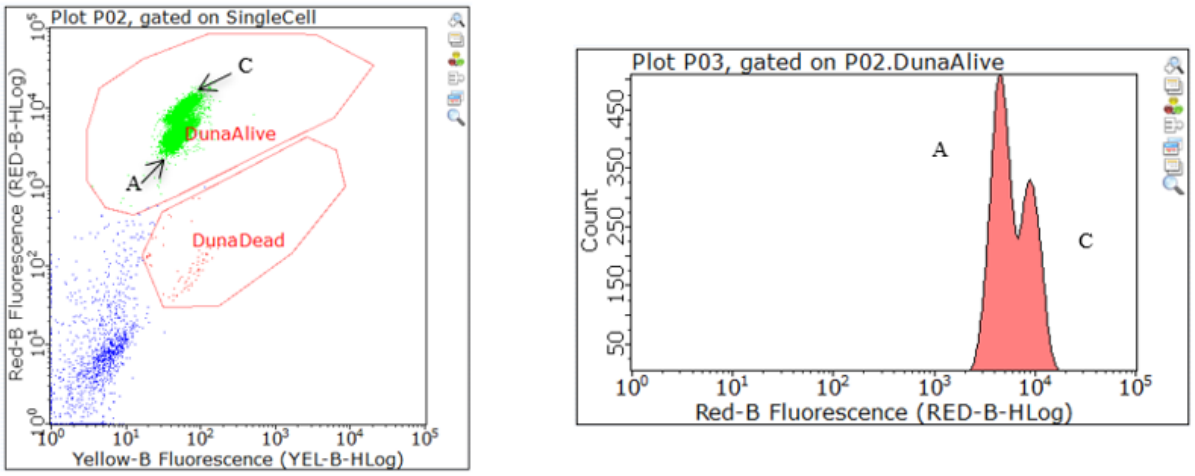

Figure S1. Example of cytogram raw data counts of a mixed strains A and C flask. (A) The two strain's dots overlap but are still noticeable. (B) Bivariate gaussian distribution of dots included in the *DunaAlive* gate for red fluorescence trait in a mixture.

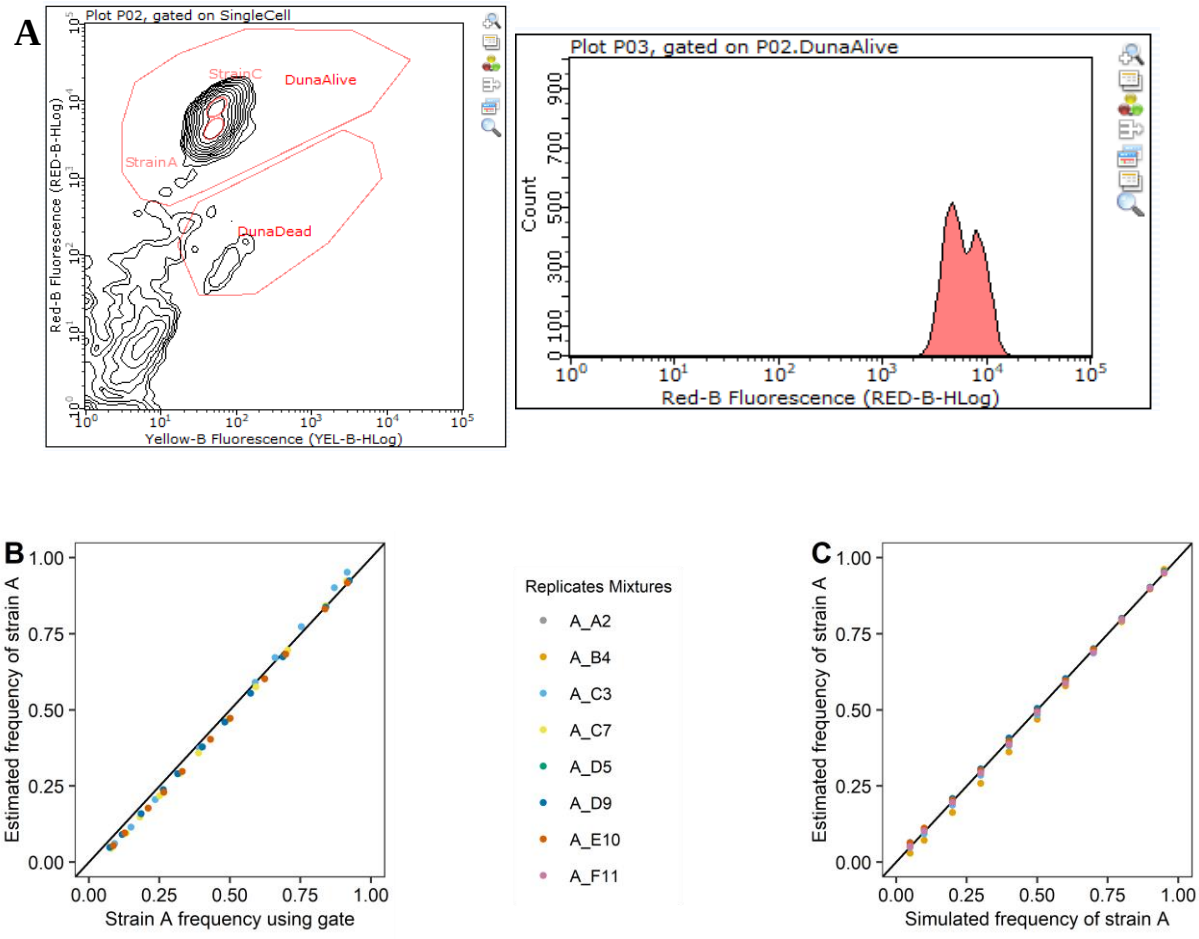

Figure S2. Calibration assay for our estimation method of frequency in mixed populations. (A) Restrictive handmade gates on the cytogram to discriminate strain A and C cells, example of a flask composed of distinguishable populations by red fluorescence. (B) Strain A frequency in well-distinguishable mixed populations obtained by our estimation method against using restrictive hand-drawn gates on the cytogram (4 replicates mixtures). (C) Estimating frequency with our method on simulated mixed populations whose proportion is chosen (8 replicates mixtures).

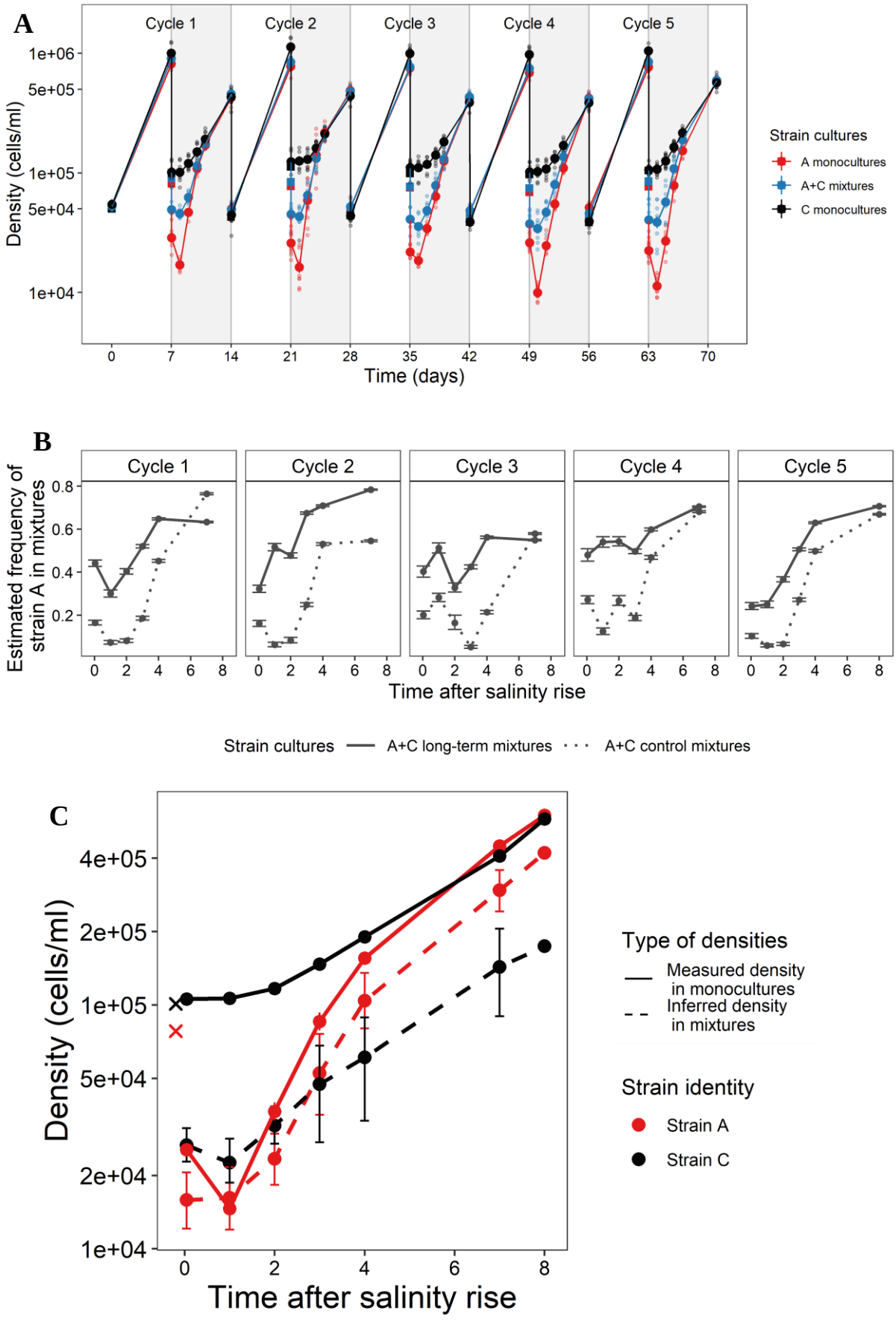
A
Cycle 1
Cycle 2
Cycle 3
Cycle 4
Cycle 5
Density (cells/ml)
1e+06
5e+05
1e+05
5e+04
1e+04
0
7
14
21
28
35
42
49
56
63
70
Time (days)
Strain cultures
A monocultures
A+C mixtures
C monocultures
B
Estimated frequency of strain A in mixtures
0.8
0.6
0.4
0.2
Time after salinity rise
Strain cultures
A+C long-term mixtures
A+C control mixtures
C
Density (cells/ml)
4e+05
2e+05
1e+05
5e+04
2e+04
1e+04
Time after salinity rise
Type of densities
Measured density in monocultures
Inferred density in mixtures
Strain identity
Strain A
Strain C

Figure S3. 7-7d cycle treatment results. (A) Demographic responses to successive salinity rises under 7-7d cycle. Populations densities over the first five salinity cycles are shown for monocultures of strain A (red) and strain C (black), and mixtures of A and C (blue). Small dots represent biological replicates (specific isogenic lines of each strain, or mixtures thereof), while large dots represent means over replicates (with SE not visible). Grey backgrounds correspond to the high salinity step in a given cycle. (B) Frequency of strain A over 5 successive salinity rises. The proportion of mixed populations composed of strain A, as estimated from the cytometric traits of cells, is shown against time for long-term mixtures (solid lines), and control mixtures (dotted lines) that were freshly composed by mixing 50-50% of each strain before each salinity rise. Means and confidence interval at 95% were obtained on the logit scale by inverse-variance weighting over the 10 population lines, to account for the variable uncertainty of estimates among biological replicates (isogenic lines of each strain), and then combined with the delta method for the back-transformation on the arithmetic scale. (C) Growth rates in monocultures versus mixtures**.** Mean population densities across replicates in monocultures (solid lines; direct measurements), and long-term mixtures (dashed lines; inferred from the estimate of relative frequencies), averaged over the first 5 high salinity steps, are shown for the 7-7d cycle. For the monocultures, we computed the mean and standard error (not visible) over 10 isogenic lines. For the mixtures, we used inverse-variance-weighted mean and 95% confidence interval (computed with the delta method), to account for variable precision in estimation of strain A frequency among biological replicates. The crosses correspond to the mean expected initial density for each monoculture, based on the known density before the 10% dilution. The dot for day 8 is because we measured the final day before transfer on day 8 instead of 7 for cycle 5.

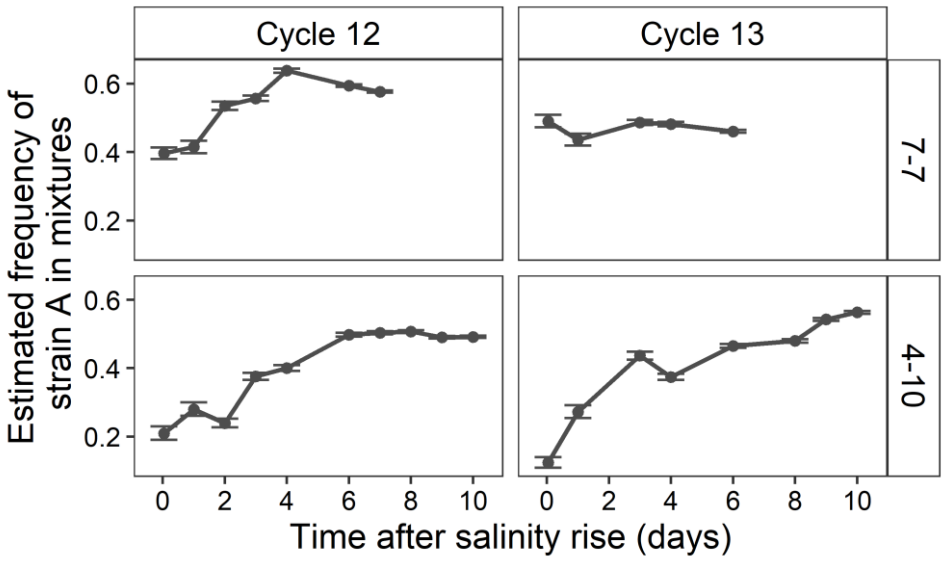

Figure S4. Frequency of strain A in the last salinity cycles in long-term mixtures. The proportion of mixed populations composed of strain A, as estimated from the cytometric traits of cells, is shown against time for long-term mixtures, using the monocultures from cycle 5 as reference. Means and confidence interval at 95% were obtained on the logit scale by inverse-variance weighting over the 10 population lines, to account for the variable uncertainty of estimates among biological replicates (isogenic lines of each strain), and then combined with the delta method for the back-transformation on the arithmetic scale.

A

Marker	Replicates mixtures + DsMt_1 (4-10d)										Control +	Control +	Control -	X	Marker
Marker 100pb	A_A2 + C_A2	A_B4 + C_B4	A_C3 + C_C3	A_C7 + C_C7	A_D5 + C_D5	A_D9 + C_D9	A_E10 + C_E10	A_F11 + C_F11	A_G3 + C_G3	A_H9 + C_H9	A_A2 (rep 1) + DsMt_1	A_A2 (rep 2) + DsMt_1	C_A2 (rep 1) + DsChl1		Marker 100pb

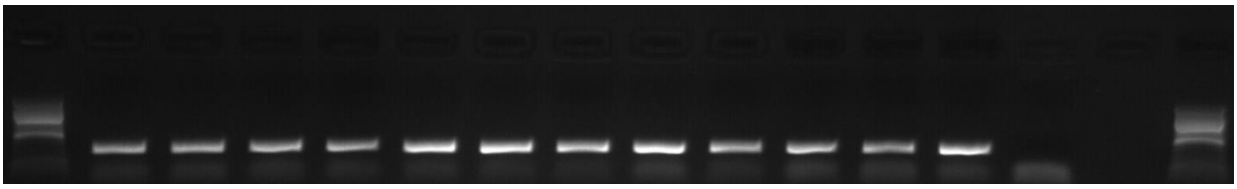

B

Marker	Replicates mixtures + DsChl_1 (4-10d)										Control +	Control +	Control -	Control +	Marker
Marker 100pb	A_A2 +C_A2	A_B4 + C_B4	A_C3 +C_C3	A_C7 +C_C7	A_D5 +C_D5	A_D9 +C_D9	A_E10 +C_E10	A_F11 +C_F11	A_G3 +C_G3	A_H9 +C_H9	C_A2 (4 months) + DsChl_1	C_H9 (4 months) + DsChl1	A_A2 (1 month) + DsMt_1	C_A2 (1 month) + DsChl1	Marker 100pb

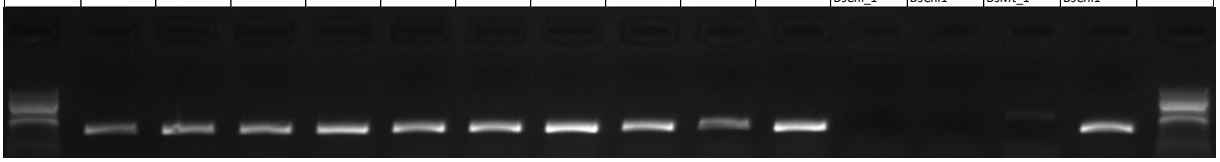

C

Marker	Replicates mixtures + DsMt_1 (7-7d)										Control +	Control -	Control -	Marker
Marker 100pb	A_A2 + C_A2	A_B4 + C_B4	A_C3 + C_C3	A_C7 + C_C7	A_D5 + C_D5	A_D9 + C_D9	A_E10 + C_E10	A_F11 + C_F11	A_G3 + C_G3	A_H9 + C_H9	A_B8 + DsMt_1	C_B8 + DsChl1	H2O + DsMt_1	Marker 100pb

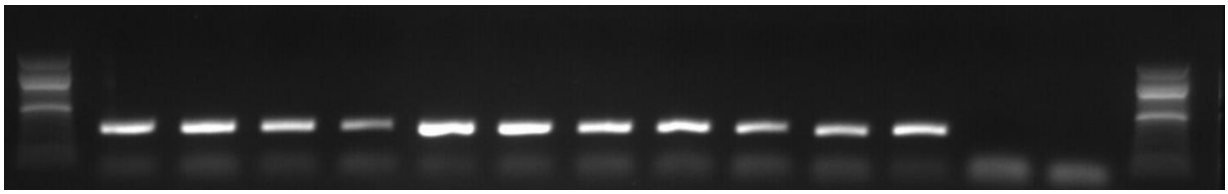

D

Marker	Replicates mixtures + DsChl_1 (7-7d)										Control +	Control -	Control -	Marker
Marker 100pb	A_A2 +C_A2	A_B4 + C_B4	A_C3 +C_C3	A_C7 +C_C7	A_D5 +C_D5	A_D9 +C_D9	A_E10 +C_E10	A_F11 +C_F11	A_G3 +C_G3	A_H9 +C_H9	C_B8 + DsChl_1	A_B8 + DsMt_1	H2O + DsChl_1	Marker 100pb

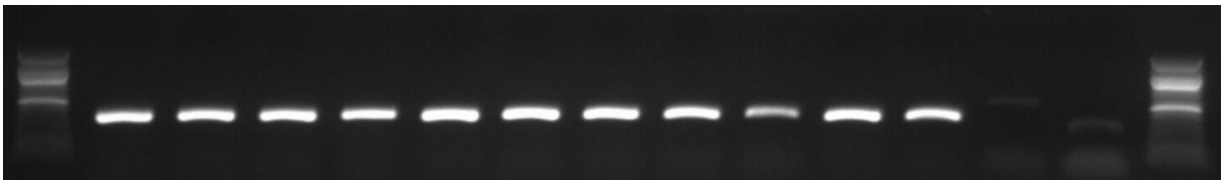

Figure S5. Genetic confirmation of the presence of both strains in long-term mixtures after 13 cycles (26 weeks). Amplicon migration on agarose gels of DsMt1 and DsChl1 locus, respectively specific to strain A and C. (A) Strain A presence (primer Ds_Mt1) on flasks under 4-10d cycle. (B) Strain C presence (primer Ds_Chl1) on flasks under 4-10d cycle. (C) Strain A presence (primer Ds_Mt1) on flasks under 7-7d cycle. (D) Strain C presence (primer Ds_Chl1) on flasks under 7-7d cycle. Positive and negative controls were also included (samples at the right position).

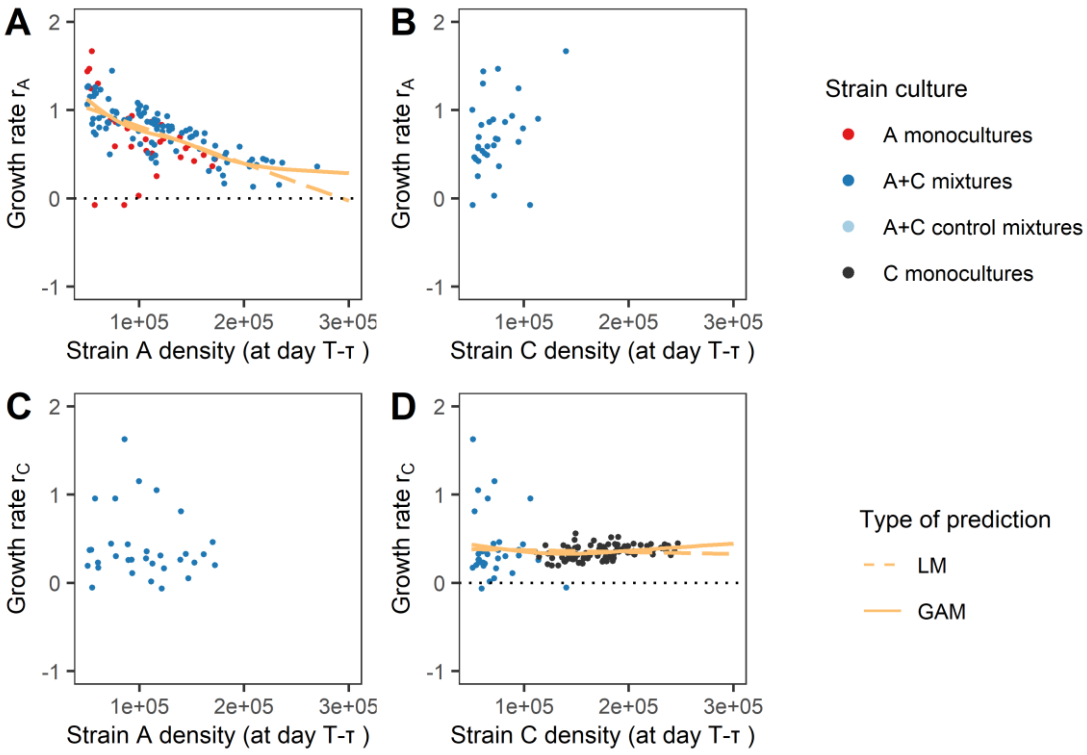

Figure S6. Intra- and inter-strain competition and population growth on 7-7d cycle. The *per-capita* growth rate of strain A (A-B) or strain C (C-D) is shown against the density of strain A (A, C) or strain C (B, D), in the 4-10d cycle. Each point corresponds to relative growth rate per day, over the interval between two subsequent measurements. Panels A and D also display (in orange) predictions from the simplest models of density dependence (LM 1 in dashed, GAM 1 in continuous). Data have been filtered on the precision of frequency estimation (CI width < 0.5 on logit scale) to remove the most uncertain values, and on population density ($N > 5.10^4$ cells/ml). Here, none control mixtures satisfied the population density condition on both strains.

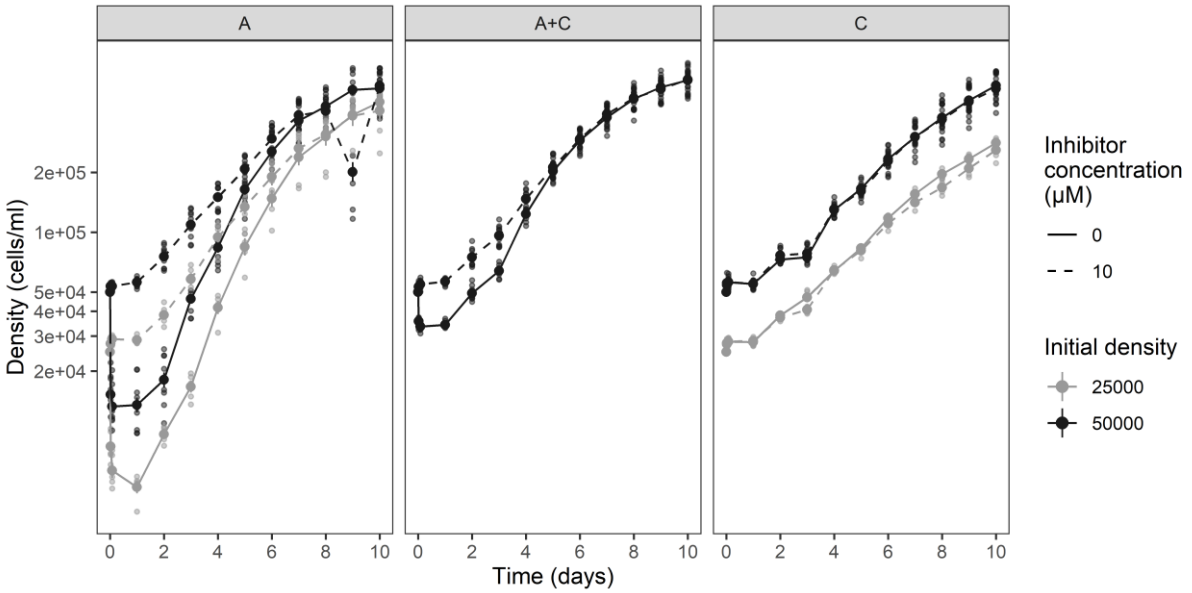

Figure S7. Effect of PCD inhibitor treatment on demographic response after one salinity rise. Populations densities of monocultures and mixtures (panels) are shown against time under inhibitor treatments (linetype), starting at initial density (colours). We computed the mean and standard error (not visible) on the cytometer counts over the isogenic lines (10 replicates for N_0= 50,000 cells/ml, 5 replicates for N_0 = 25,000 cells/ml).

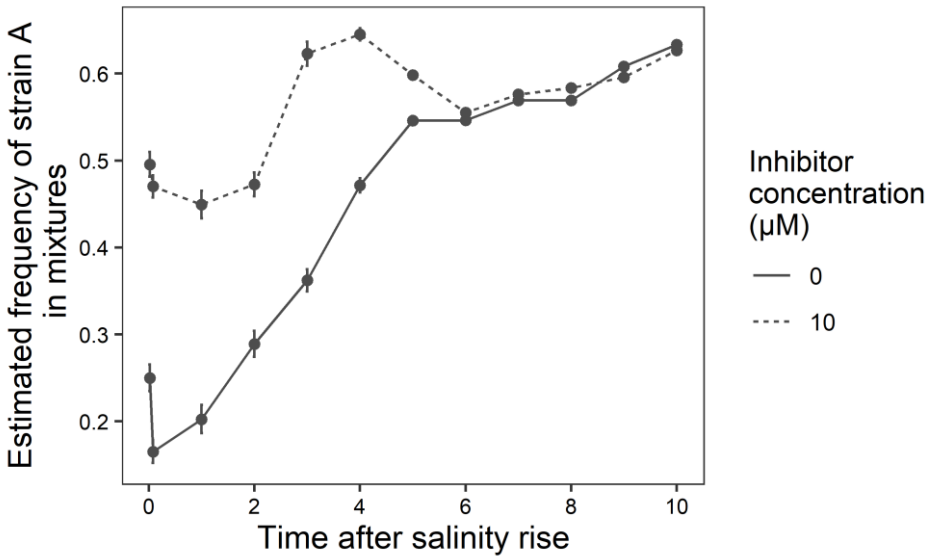

Figure S8. Effect of PCD inhibitor treatment on strain A frequency in mixtures after one salinity rise. The proportion of strain A in mixed populations, as estimated from the cytometric traits of cells, is shown against time for PCD inhibitor doses (linetype). Means and confidence interval at 95% were obtained on the logit scale by inverse-variance weighting over the 10 population lines, to account for the variable uncertainty of estimates among biological replicates (isogenic lines of each strain), and then combined with the delta method for the back-transformation on the arithmetic scale.

Chapitre 3 : Modélisation d'hypothèses adaptatives et non adaptatives

Entrée en matière et résumé de l'article :

Ce chapitre se concentre sur les hypothèses alternatives pouvant expliquer la dynamique de déclin-rebond observée dans le chapitre 1 ainsi que la coexistence à long-terme des deux souches en compétition du chapitre 2. Une partie de ce travail (modèle hétérogénéité de condition) a été réalisée avec l'aide d'une stagiaire M1 MEME, Sudeshna Chakraborty, que j'ai co-encadrée en 2022.

Par une approche de modélisation, ce 3^{e} chapitre apporte de nouveaux éléments pour répondre à la problématique générale de ma thèse, c'est-à-dire comment la sélection pourrait agir sur un tel trait paradoxal. Nous avons exploré 3 hypothèses possibles. Tout d'abord une hétérogénéité dans le statut physiologique des cellules chez la souche qui décline (hypothèse non adaptative). Ici, le déclin est dû l'élimination des cellules en mauvais état, tandis que le rebond est expliqué par un plus grand taux de croissance moyen des cellules en meilleur état. Puis, nous avons modélisé un compromis entre tolérance à la salinité et reproduction (hypothèse plasticité adaptive), selon lequel la souche qui décline investit plus dans la reproduction aux dépens de la tolérance à la salinité. Enfin, nous avons fait l'hypothèse que des molécules sont relargués par les cellules mourantes et exploités comme signal empêchant les cellules restantes de déclencher leur propre mort ou comme substrats promouvant la croissance de ces dernières.

En conclusion, les trois modèles peuvent simuler les dynamiques attendues sous certaines conditions, mais celles-ci ne sont pas toujours compatibles avec ce que l'on sait de la biologie de notre modèle *D. salina.* Pour continuer à explorer l'avantage sélectif potentiel, les modèles devront être développés dans un cadre plus général, autorisant notamment des densités dépendances variables entre génotypes, afin de mimer au mieux le comportement des populations expérimentales du chapitre 2, et de les ajuster sur les données issues de celles-ci.

Ce chapitre sera complété pour être soumis à un journal combinant théorie et expériences (American Naturalist, Ecology, Oikos …).

Article 3 - Disentangling the causes and selective advantage of population decline and rebound

Running title: Causes of population decline and rebound

Nathalie Zeballos[1], Sudeshna Chakraborty [1] and Luis-Miguel Chevin[1]

[1] CEFE, Univ. Montpellier, CNRS, EPHE, IRD, Montpellier, France

Keywords: population decline, environmental stress, programmed cell death

Abstract:

When a population recovers from a demographic decline in response to environmental change, such rebounding dynamics are generally attributed to evolutionary rescue, whereby beneficial mutations restore positive mean population growth as they sweep through the population. But what could lead to similar decline-rebound dynamics when genetic variation is limiting? We previously investigated such population dynamics in the halotolerant microalgae *Dunaliella salina*, where two closely related strains had markedly different demographic responses to a salinity rise. One of the strains underwent a rapid decline with a decrease of 70% of the population size, followed by a greater growth than the other strain that did not initially decline, and the speed of these dynamics was not consistent with evolutionary change in these isogenic populations. Using modelling can help understand and decipher the possible mechanisms underlying such experimental observations. We explored three alternative explanations for this decline-rebound pattern: heterogeneity in cell condition, a trade-off between physiological tolerance and reproduction, and an altruistic release of molecules. We showed that all hypotheses can mimic the characteristic demography dynamics under specific parameters values, but that some requirements for them to occur are not biologically plausible. We discuss our results in the light of empirical evidence that the decline is due to programmed cell death in this system, and consider their relevance for decline-rebound dynamics in other experimental systems.

Introduction

A population facing an abrupt transition towards a stressful environment is likely to experience a sharp decay in demographic vital rates (survival and fecundity), which may even lead it to decline. However, this does not necessarily mean that the population is doomed to extinction as the decline may only be transient, with a population growth rate that gradually recovers until it becomes positive again, leading to a rebound of the population. When such decline-rebound dynamics are observed, the usual interpretation is that they are caused by evolutionary rescue, whereby a population is rescued from stress-induced extinction by rapid evolution under natural selection of a positive mean population growth rate (Gomulkiewicz and Holt 1995; Bell 2017). Evolutionary rescue has become a textbook scenario of eco-evolutionary dynamics in a changing environment, and experimental evidence for its typical U-shaped dynamics have abounded in the past decade (Bell and Gonzalez 2009; Bodbyl Roels and Kelly 2011; Lindsey et al. 2013; Ramsayer et al. 2013; Rêgo et al. 2019). However, the underlying mechanism is not always demonstrated in these empirical examples, and even when beneficial mutations are identified, it is not always possible to attribute them the full demographic rebound.

Much less attention has been devoted to alternative scenarios that may lead to similar U-shaped dynamics of population decline-rebound even in the absence of genetic change, or at a pace that is not consistent with observed (or putative) genetic changes. For instance in a clonal/isogenic population, any putative rescuing mutation is either very rare or not present at the onset of stress, such that it can only affect the mean population growth rate in any appreciable way after a sufficient number of generations have elapsed, or if the decline is extremely rapid and quickly brings the population close to extinction. We would thus not expect evolutionary rescue to cause rapid decline and rebound of intermediate magnitude (i.e. not causing near extinction) in isogenic populations, and even less so repeatedly under subsequent exposures to stress. On the other hand, other mechanisms that do not involve genetic change may well be involved, and are also likely to occur even in cases where genetic change does take place. In particular, many organisms can acclimate to new environmental conditions via physiological adjustments, or any other modifications of their phenotypes that unfold over different time scales, both within and across generations (Leroi et al. 1994; Wilson et al. 2002; Beaman et al. 2016; Rescan et al. 2022). That such acclimation effects may lead to transient population dynamics is well understood, especially in microbiology where it is common practice to allow for a few cycles before populations “stabilize” in the new environment, before measuring growth rates. However, these transient dynamics are generally considered as a

nuisance, rather than as a quantitative process to investigate by itself, and contrasted to alternative explanations for decline-rebound dynamics. In particular, such dynamics may also occur when there is non-genetic heterogeneity in cell condition in the population, or under more complex ecological dynamics, whereby dying cells promote growth of surviving cells (as suggested by Zeballos et al 2023), but the requirements of these alternative hypotheses are yet unclear.

An important related question is: How do such decline-rebound dynamics evolve? If these dynamics can occur within a given genotype (rather than being caused by the selective replacement of one genotype by another), then they may also vary genetically. This implies that, depending on the magnitudes of initial decline and later rebound, and of how they are correlated among genotypes, there may be some non-trivial scenarios where a genotype that initially declines sharply under stress is favoured by selection over a non-declining genotype. In other words, natural selection may favour sharper decline under stress over repeated exposures, but whether and how this could occur may depend on the mechanism causing the decline-rebound pattern.

To exemplify our argument and parameterize our theoretical explorations below, we will rely on a case study of such puzzling demographic dynamics in the halotolerant microalgae *Dunaliella salina*. In this species, it was recently shown that two closely related strains had markedly different demographic response to a salinity rise (Leung et al. 2022; Zeballos et al. 2023). One of the strains triggered a rapid decline, losing up to 70% of its population, but then rebounded with fast growth, while the other did not decline but had lower exponential growth in exponential phase. Interestingly, conditions leading to faster decline also led to faster growth, and there was evidence that the decline was induced by programmed cell death (Zeballos et al. 2023). When growing these strains in competition, alternating between intermediate and high salinity for 13 cycles, we found that strain frequencies fluctuated substantially within each high salinity phase, but that the declining strain was maintained throughout the experiment, such that the mixed population sustained an initial decline at each salinity rise.

To understand which mechanism is more likely to explain both the decline-rebound pattern and the outcome of the competition, we explored three alternative hypotheses using mathematical models. The first model accounts for heterogeneity in cell state within the declining strain, with damaged or old cells experiencing higher stress-induced mortality and lower growth rate (Hodgson et al. 2015). The second model is based on the declining strain being specialised on reproduction, at the expense of reduced investment in the plastic

mechanisms involved in halotolerance. In the third model, the dying cells of the declining strain release molecules that are specifically usable by the related remaining cells, thus promoting their population growth (Durand et al. 2011; Berngruber et al. 2013; Orellana et al. 2013; Vostinar et al. 2019). We derived the dynamics of demography and selection produced by each of the models to find the parameter values compatible with observations, and assess their biological realism.

Models

Generic model

Generic population dynamic of monocultures

We have contrasted several mechanisms to explain the decline-rebound demographic pattern of a declining strain (hereafter denoted as A). We have then investigated what these models predict for the population dynamics of this strain in monoculture, but also for its relative frequency in competition with a non-declining strain (hereafter denoted as C).

We started from classic logistic growth modelled using a Lotka-Volterra equation,

$$\frac{dN_i}{dt} = (r_i - \alpha N_i)N_i \qquad \text{(Eq. 1)}$$

where N_i is the population density of strain i and r_i is its intrinsic growth rate (at low density). Negative density-dependence in population growth is accounted for through the competition term α. We first assumed for simplicity that both strains (and both types of cells in model 1) have similar strength of density-dependence α, quantifying their sensitivity to both within- and between-strain competition, such that their density dependence term becomes αN (with N the total density of cells). Although our experimental results suggest the opposite in the chapter 2, this simplification allows making analytical progress by making selection density independent (below). Strain C dynamics are modelled with Eq. 1 for the hypotheses of cell heterogeneity and of molecular release, and the equilibrium population density for strain C is easily obtained as $N_{C,eq} = \frac{r_C}{\alpha}$. Strain A dynamics are modified versions of Eq. 1 to consider the specific hypothesis.

Environmental conditions

We are interested in decline-rebound dynamics that occur in a stressful environment (denoted as S, e.g. high salinity in our empirical example in *Dunaliella salina*). However depending on the models, we will also need to model demography in the non-stressful phase (denoted NS),

or at least make some assumptions on the state reached by the population at the end of that phase. Since demography varies between the two salinities conditions, some of the variables are environment-dependent, such as the intrinsic growth rate *r*, and the underlying birth and death rates in the third model.

Modelling mixed populations

Since one of our interests is to simulate the outcome of competition between two types (either strains, or cell types in model 1 below), we need to track the relative frequency p of one type in co-culture. The dynamics of *p* can be shown to be (e.g. Chevin (2011))

$$\frac{dp}{dt} = p(1-p)\left(\frac{dN_1}{N_1 dt} - \frac{dN_2}{N_2 dt}\right), \qquad \text{(Eq. 2)}$$

where N_1 and N_2 are the population densities of types 1 and 2, and p and $(1-p)$ their relative frequencies. Under the assumption that both types are equally sensitive to competition (eq. 1), this leads to

$$\frac{dp}{dt} = p(1-p)\,(r_1 - r_2), \qquad \text{(Eq. 3)}$$

such that frequency change under selection is density independent, and only depends on the difference in intrinsic growth rates (Chevin 2012). Note that eq. 3 also applies more generally at low density (even with unequal competition strength), and that it can also be applied to the proportion *q* of bad cells in model 1 below.

In such mixed populations, the total number *N* of cells is

$$\frac{dN}{dt} = \frac{dN_1}{dt} + \frac{dN_2}{dt}$$

which under our assumption of equal competition strength among types becomes

$$\frac{dN}{dt} = [\bar{r} - \alpha N]N. \qquad \text{(Eq. 4)}$$

where $\bar{r} = pr_1 + (1-p)r_2$ is the mean intrinsic growth rate in the population.

Hypothesis 1: Cell heterogeneity

Modelling a declining genotype

We first investigated the scenario where cells vary in their physiological or metabolic state (hereafter condition), leading to individual heterogeneity in demographic properties. More

specifically, cells in poor condition (labelled *B* for bad) have higher stress-induced mortality and lower reproduction than those in good condition (labelled *G*), such that the elimination of bad cells and their replacement with good cells is what produces the decline-rebound pattern in the stressful environment. We further assumed that cells in good condition become damaged and turn into bad cells at a rate τ that does not depend on the environment, while the reverse transition does not occur (no recovery or rejuvenation). From Eq. 1, this leads for the differential equations for density of each type of cell in a monoculture of the declining strain A to

$$\frac{dN_G}{dt} = (r_G - \alpha N_A)N_G - \tau N_G, \qquad \text{(Eq. 5)}$$

$$\frac{dN_B}{dt} = (r_B - \alpha N_A) N_B + \tau N_G, \qquad \text{(Eq. 6)}$$

with r_G and r_B, the intrinsic growth rates of good and bad cells, respectively, and $N_A = N_G + N_B$ the overall population density of strain A. Note that we assumed that the competition term α is identical among cell types, as it is between genotypes in eq. (1). Summing eqq. (4) and (5), we obtained for the change in strain A density in monocultures

$$\frac{dN_A}{dt} = [qr_B + (1-q)r_G - \alpha N_A]N_A, \qquad \text{(Eq. 7)}$$

where q is the proportion of bad cells in strain A monocultures. Equation (7) shows that the population dynamics of strain A depend on its mean intrinsic growth rate (first two terms in square brackets), which is time-dependent since the frequency of bad cells q changes over time. Applying eq. (2) to q rather than p, the dynamics of the frequency of bad cells becomes, after some simplification,

$$\frac{dq}{dt} = q\,(1-q)\left(\delta r + \frac{\tau}{q}\right), \qquad \text{(Eq. 8)}$$

where $\delta r = r_B - r_G$ is the difference of intrinsic growth rates between good and bad cells.

Modelling mixed populations

To model the population dynamics of competition between the declining and non-declining genotypes, we adapted equation (3) with the genotype- specific dynamics (Eq. 6). Thus, the total demography in cocultures is given by

$$\frac{dN}{dt} = [p(qr_B + (1-q)r_G) + (1-p)r_C - \alpha N]N \qquad \text{(Eq. 9)}$$

and the dynamics of the frequency p of the decline strain are, after some simple algebra,

$$\frac{dp}{dt} = p(1-p)(q\,\delta r + \Delta r), \qquad \text{(Eq. 10)}$$

where $\delta r = r_B - r_G$ and $\Delta r = r_A - r_C$.

Hypothesis 2: Trade-off between physiological tolerance and reproduction

Our second hypothesis involved a trade-off between stress tolerance and reproduction. More specifically, we considered that the declining genotype specializes on reproduction and growth (during rebound) at the expense of less efficient physiological regulation, and thus reduced environmental tolerance leading to substantial death upon introduction to the new stressful environment. We modelled the mechanism of stress tolerance as a labile, dynamic plastic trait *z*, whose norm of reaction $\Phi(\varepsilon)$ in response to the environment ε (e.g. salinity in our empirical example) is genetically determined. Following Lande (2014), we implemented the developmental dynamics of the plastic trait as a linear differential equation

$$\frac{dz(t)}{dt} = -\lambda(z(t) - \Phi(\varepsilon)), \qquad \text{(Eq. 11)}$$

where λ is the developmental rate, assumed to be independent of environment but to vary with the genotype. Equation (10) means that the speed of plastic change in the physiological trait at any time depends on how much the phenotypic value for this trait deviates from the value $\Phi(\varepsilon)$ set by the reaction norm in the new environment ε. Furthermore, for a given phenotypic deviation $(z(t) - \Phi(\varepsilon))$, the speed of plastic phenotypic change is higher when the developmental rate λ is larger. To relate plastic change in the physiological trait *z* to fitness, we assumed that the intrinsic rate of increase is phenotype-dependent, such that

$$r(t) = r_{max} - \frac{[z(t) - \theta(\varepsilon)]^2}{2\omega^2}, \qquad \text{(Eq. 12)}$$

where r_{max} is the maximal growth rate (when the physiological trait is perfectly adapted), $\theta(\varepsilon)$ is the optimal value of *z* that maximizes fitness in environment ε, and ω is the width of the fitness function, where smaller ω (narrower fitness peak) lead to stronger stabilizing selection on *z*. We thus derived the dynamics of the plastic trait using eq. (11), inserted it into eq. (12) to get the dynamics of population growth rate, and then combined the latter with the logistic growth (eq. 1) to find the population dynamics in isolation. Mixtures populations dynamics and strain frequency within cocultures followed the generic equations (2) and (3), with time-dependent growth rates.

Hypothesis 3: Molecule release

Our final hypothesis to explain the decline-rebound pattern was related to the context of programmed cell death (PCD), as evidenced in numerous unicellular organisms, including our working example *Dunaliella salina* (Deponte 2008; Nedelcu et al. 2011; Orellana et al. 2013; Bidle 2016). In this case, death under stress is an active process that is triggered by environmental cues, and can be inhibited by others cues. To model this scenario, we assumed that the dying cells release molecules in the culture medium that are usable by the remaining cells. We thus analyzed coupled differential equations for the demography of strain A and the quantity of released molecule *S*. We then contrasted two sub-models that made different assumptions about the ecological function of these released molecules.

We first assumed that the released molecule acts as a signal, which informs surviving cells (as in e.g. quorum-sensing) and inhibits their own programmed death (Kaiser 1996). This conforms to the finding that in *Dunaliella salina*, a population growing in a medium where PCD already occurred triggered a diminished population decline (Zeballos et al. 2023). For this scenario, the quantity of the signal molecule fed back on the rate of cell death d, leading to

$$\begin{cases} \frac{dN_A(t)}{dt} = [b - d_{\max} \, \mathrm{e}^{-c*S(t)} - \alpha N_A(t)]N_A(t) \\ \frac{dS(t)}{dt} = v \, d_{\max} \, \mathrm{e}^{-c*S(t)} N_A(t) \end{cases} . \qquad \text{(Eq. 13)}$$

In equation (13), b is the baseline birth rate of the population, and $d = d_{\max} \, \mathrm{e}^{-c*S(t)}$ is the death rate, which decreases (from its maximal value $d_{\max}$) with increasing quantity of the signal molecules *S* presents in the medium, with a sensitivity *c* to this signal. The signal molecule *S* is in turn released at a rate *v* per unit cell that died in response environmental stress.

In a second sub-model, we assumed that these molecules are substrates that promotes population growth, as suggested by previous work on PCD (Durand et al. 2011, 2014; Orellana et al. 2013). The corresponding dynamical system was

$$\begin{cases} \frac{dN_A(t)}{dt} = [(b + wyS(t)) - d_{\max} \, \mathrm{e}^{-h*t} - \alpha N_A(t)]N_A(t) \\ \frac{dS(t)}{dt} = v d_{\max} \, \mathrm{e}^{-h*t} N_A(t) - wN_A(t)S(t) \end{cases} . \qquad \text{(Eq. 14)}$$

In equation (14), since the released molecule does not act as a cue, we assume that the death rate declines spontaneously over time at rate *h*. The influence of released substrate on reproduction is modelled as in the resource-model of Monod (Monod 1949; Sunda et al. 2009), where the parameters are the rate of consumption of substrate per capita w, the rate of

transformation of the consumed substrates (or yield) y. Hence in this model, more cell death leads to more substrate released, which may thus cause faster rebound.

Results

We modelled 3 hypotheses that may explain a repeatable pattern of decline-rebound in the face of stress, as observed in *D. salina* in response to a series of hyper-osmotic shocks (Zeballos et al. 2023). Here we present numerical and analytical solutions for the demographic dynamics, and the change in the frequency of the declining strain in mixtures.

Declining strain dynamics in monoculture

Hypothesis 1: Cell heterogeneity

We first tested the hypothesis of heterogeneity in cell condition, whereby the declining strain is composed of damaged ("bad", labelled B) cells that are more sensitive to the salinity change, and healthy ("good", labelled G) cells with higher growth rate. We numerically solved the demographic dynamics of strain A (Eq. 7) under different values of initial proportion q_0 of bad cells (Fig. 1A).

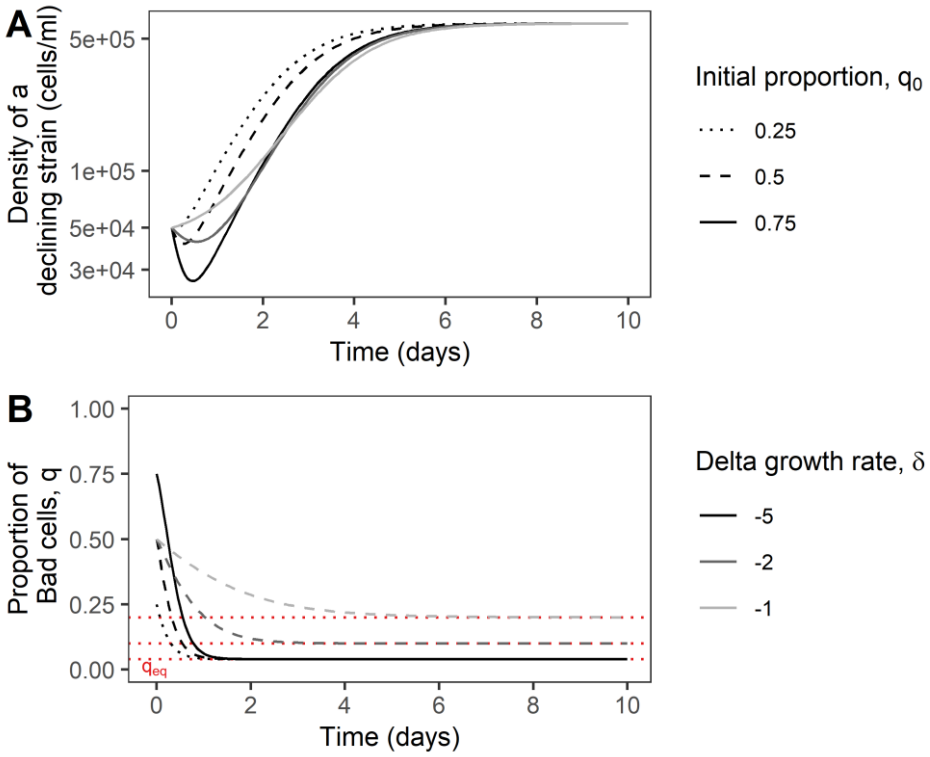

Figure 1. Cell heterogeneity. Dynamics of the population density of the declining strain (A) and of the proportion of bad cells (B) in the stressful phase, under different initial proportions q_0 of bad cells (line type), and differences in growth rates δ between good and bad cells (colours). We used numerical solution to eq. (7) in A and to eq. (8) in B, but we obtained similar

results using the analytical solution assuming simplifications (eq. S1 in Additional results). The equilibrium proportion of bad cells q_{eq}, obtained from eq. (16), is also plotted as red line of the corresponding type in B. Parameters values are: initial population size $N_{A,0} = 5.10^4$, strength of density dependent competition $\alpha = 2.10^{-6}$, decay rate of good cells $\tau = 0.2$, growth rate of good cells $r_G = 1$.

Bad cell proportion in the stressful phase

Since the proportion of bad cell is the key variable determining the population dynamics after a stressful change (Fig. 1A), we first analyzed its dynamics. We found the analytical solution for the equation (8) to be

$$q(t) = \frac{(q_0\ \delta r_S + \tau)\ e^{(\delta r_S + \tau)t} - \tau(1 - q_0)}{(q_0\ \delta r_S + \tau) e^{(\delta r_S + \tau)t} + \delta r_S (1 - q_0)} \qquad \text{(Eq. 15)}$$

where δr_S is the difference in growth rates between bad and good cells in the stressful phase, and q_0 is the initial proportion of bad cells in monoculture of the declining strain at the start of this phase. Our assumption that bad cells have poorer demographic performance under stress implies that $\delta r_S < 0$. If in addition, the transition rate τ (non-negative by definition) is low enough that $\delta r_S + \tau < 0$, then the frequency q decreases over time, faster for greater absolute values of δr_S (Figure 1B). In the long run (for $t \gg 1/|\delta r_s + \tau|$), the exponential terms in eq. (13) vanish and the frequency of bad cells reaches an asymptotic equilibrium

$$q_{eq} = -\frac{\tau}{\delta r_s}. \qquad \text{(Eq. 16)}$$

The greater the difference in growth rates between bad and good cells, the lower the equilibrium proportion q_{eq} of bad cells at the end of the stressful phase (horizontal red lines in Figure 1B). Conversely, higher degradation rate leads to greater q_{eq}, as new bad cells are constantly replenished from the degradation of good cells. Note that eq. (16) is similar to the classical equilibrium-selection balance in population genetics (Hartl and Clark 1997), except that here the degradation of cells has no genetic basis, unlike for deleterious mutations.

Bad cell proportion in the non-stressful phase

To better understand the repeated pattern of decline-rebound in subsequent cycles of stress and non-stress, we also need to model what happens in the non-stressful phase. We assumed for simplicity that the stressful phase lasts long enough that the frequency of bad cells has reached its equilibrium, such that the initial frequency in the next non-stressful phase is given by eq. (16). Then replacing q_0 by q_{eq} from eq. (16) in eq. (15), the proportion of bad cells in the non-stressful phase is, after some simplification,

$$q = \left(1 - \frac{(\delta r_{NS}+\tau)(\delta r_S+\tau)}{\tau\left(e^{(\delta r_{NS}+\tau)t}\,(\delta r_{NS}-\delta r_S)+\delta r_S+\tau\right)}\right)^{-1}. \qquad \text{(Eq. 17)}$$

where δr_{NS} is difference in growth rates between bad and good cells in the non-stressful environment. The proportion *q* of bad cells in monocultures in the non-stressful environment is shown under various parameters values in Figure S1. In order to maintain a repeated decline over successive exposures to the stressful environment, the proportion of bad cells need to be restored during the non-stressful phase. For this to be achieved, $\delta r_{NS} + \tau$ must be positive (from eq. 17), i.e $-\tau < \delta r_{NS} < 0$, assuming that bad cells also have lower demographic performance than good cells in the non-stressful environment. Further analytical progress can be made by assuming that differences in cell condition are only revealed under stress but can be neglected in non-stressful environments, such that $\delta r_{NS} + \tau \approx \tau$ and $\delta r_{NS} - \delta r_S \approx -\delta r_S$ in eq. (17), leading after some algebra to

$$q \approx 1 - \frac{\delta r_S+\tau}{\delta r_S e^{\tau t}}. \qquad \text{(Eq. 18)}$$

In this regime, the proportion of bad cells in the non-stressful phase depends only on the differential growth rate δr_S in the previous stressful phase, which determines the initial frequency in the non-stressful phase, and the degradation rate τ, which is only way through which the proportion of bad cells can increase (since we assume they grow almost as fast as good cells). Equation (18) can be further simplified by assuming that the degradation rate is negligible relative to the differential growth rate in the stressful phase ($\delta r_S \gg \tau$), leading to

$$q \approx 1 - e^{-t\tau}. \qquad \text{(Eq.19)}$$

From eq. (19), the degradation rate required to reach a given frequency q of bad cells at time T_{NS} (the duration of the non-stressful phase) is

$$\tau = -\frac{\log(1-q)}{T_{NS}}. \qquad \text{(Eq. 20)}$$

Reaching a greater proportion *q* of bad cells at the end of the non-stressful phase requires higher degradation rates (in a non-linear relationship), and the shorter this phase (low T_{NS}), the sharper the relation need to be (Fig. S2). For example, reaching 50% of bad cells requires a degradation rate τ equals to 0.10 up to 0.17 when the non-stressful phase last 7 or 4 days. Since the proportion of bad cells at the end of non-stressful phase determines the initial proportion in the stressful phase, and hence the initial decline in that phase (Fig. 1), high degradation rate is

required to obtained repeated decline - rebound dynamics when the non-stressful phase is approximately as long as the stressful phase.

Hypothesis 2: Trade-off between physiological tolerance and reproduction

We next modeled the population dynamics arising when a plastic trait involved in stress tolerance trades off with reproduction and population growth (Fig. 2A). The dynamics of the plastic trait given in eq. (11) can be simplified when the environment is constant in each phase (as assumed here), leading to an analytical solution for the dynamics of the plastic physiological trait,

$$z(t) = e^{-\lambda t}\big(z_0 - \Phi(\varepsilon)\big) + \Phi(\varepsilon), \qquad \text{(Eq. 21)}$$

where z_0 is the initial value of the plastic trait at the beginning of the phase. Recall that λ is the rate of plastic change in the trait and $\Phi(\varepsilon)$ is the genetically determined reaction norm, which represents the equilibrium value reached by the phenotype after spending time long enough ($t \gg \lambda$) in environment ε. The initial phenotype z_0 is influenced by the environment in the previous phase (though it need not have reached its equilibrium value in that previous phase), such that the trait value is initially displaced from its equilibrium value in the new environment. Combining with eq. (12) for the fitness peak with respect to the phenotype, we obtained for the growth rate

$$r(t) = r_{max} - \frac{\left[e^{-\lambda t}\left(z_0 - \Phi(\varepsilon)\right) + \Phi(\varepsilon) - \theta\right]^2}{2\omega^2}. \qquad \text{(Eq. 22)}$$

Further assuming that Φ equals the optimum value θ in each environment, i.e. that the reaction norm is well adapted from an evolutionary perspective, we obtained

$$r(t) = r_{max} - \frac{1}{2}\Delta^2 e^{-2\lambda t} \qquad \text{(Eq. 23)}$$

$$\text{with } \Delta = \frac{z_0 - \theta}{\omega}.$$

Eq. (23) shows that the population growth rate depends on the maximal growth rate r_{max} (for an optimal phenotype), the developmental rate λ, and the scaled initial maladaptation Δ (Fig. 2A). Note that what matters for Δ is how far is the initial trait value from the optimum compared to the width of the norm of reaction. Initially (when time =0), the growth rate is equals to $r(t) = r_{max} - \frac{1}{2}\Delta^2$, which is the rate of decline under large stress. The decline thus requires that the

initial mal-adaptation $\Delta > \sqrt{2r_{max}}$. When time is large, the growth rate equals the maximal growth rate r_{max}, which determines the rebound rate.

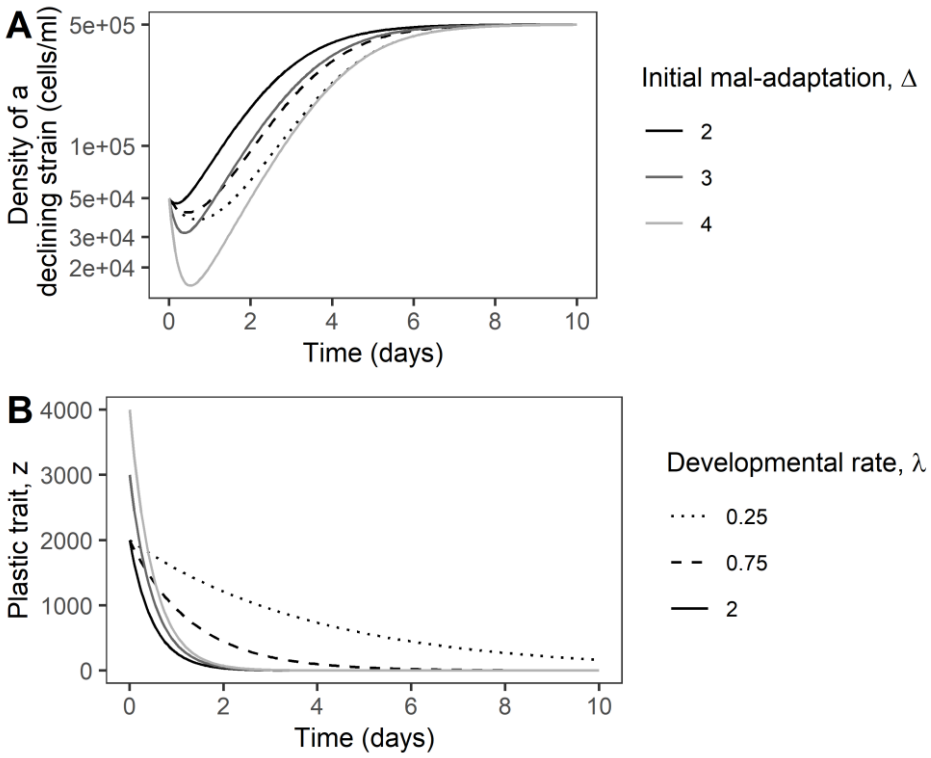

Figure 2. Trade-off between plastic tolerance and reproduction. Dynamics of the population density of a declining strain (A) and of the plastic trait *z* (B) are shown in the stressful phase, under different developmental rates λ (line type) and initial maladaptations Δ. We used the numerical solutions to eq. (11-12) combined with eq. (1) in A, and the analytical solution (eq. 21) in B. The maximum growth rate when the phenotype is at the optimum is $r_{max} = 1$ and other parameters values are as in Figure 1.

We then obtained the analytical solution for the demographic dynamics by inserting the growth rate in eq. (23) into eq. (1). The complete solution is provided below as

$$N(t) = \frac{e^{r_{\max} t + \frac{e^{-2\lambda t_\Delta^2}}{4\lambda}} N_0}{\alpha N_0 e^{r_{\max} t + \frac{e^{-2\lambda t_\Delta^2}}{4\lambda}} + e^{\frac{\Delta^2}{4\lambda}}(1 - \alpha N_0)}. \quad \text{(Eq. 24)}$$

We could then use this expression to simulate a declining and non-declining genotype, where genotype 1 invest more on reproduction at the expense of the plastic tolerance mechanisms (Fig. S3) while the genotype 2 is the opposite, and therefore we obtained similar contrasted demographic response as observed in our experimental model.

To make further analytical progress, we simplified it by focusing on the density-independent phase, for populations starting well below their carrying capacity. This is a good

approximation to what happens in the first days following environmental stress, in microbial batch cultures that are substantially diluted upon transfer to fresh medium (e.g. in our empirical example $N_0 = 5\ 10^4$, with $\alpha \leq 1.10^{-6}$). This led to

$$N(t) = N_0 e^{r_{\max} t - \frac{\Delta^2\left(1-e^{-2\lambda t}\right)}{4\lambda}}. \quad \text{(Eq. 25)}$$

This simplified expression is a good approximation to the complete expression for the first five days in our examples (Fig. S4).

From the equation (23), we can estimate when the population size stops decreasing and starts rebounding (i.e. when the growth rate $r(T) = 0$) as

$$T = \frac{2\log\Delta - \log(2r_{\max})}{2\lambda}. \quad \text{(Eq. 26)}$$

Combining eqq. (25) and (26), we can then estimate the required values for the max growth rate r_{max} and the developmental rate λ in order to obtain a given total population decline $\frac{N_{min}}{N_0}$ at time T as

$$r_{max} = -\frac{2\lambda \mathrm{Log}[\frac{N_{min}}{N_0}]}{-1+e^{2T\lambda}+\mathrm{Log}[e^{-2T\lambda}]}. \quad \text{(Eq. 27)}$$

For instance, the required values for r_{max} and λ for losing a maximum of 70% of the population at day T = 1, as in our case study, are shown in Figure S5A. When we set λ to 1, it leads to $r_{max} = 0.549$ and $\Delta = 2.847$ and to the simulated demographic density shown in figure S5B, which mimics well enough the observed decline-rebound.

Hypothesis 3: Molecule release

Finally, we modelled population dynamics influenced by the release of molecules by the dying cells, which could then act as signals preventing more cells to trigger their own death or substrates promoting population growth. We did not find analytical solution for these models, so we relied on numerical analysis. In the signal model, to be able to mimic the specific decline-rebound pattern (Fig. 3A) the maximal death rate d_{max} had to be higher than the birth rate b (but not too much otherwise extinction population occurred), and the signal sensitivity c had to be of similar order of magnitude to the inverse of number of cells. Lower sensitivity to the signal led to a delay in the onset of the rebound. This feedback between signal quantity S and cell death d lead the latter to diminish over time (Fig. 3B). However, note that cell death should

never equals to 0 because less cells dying implied that less signal released which in turns lead to slower decrease of cell death.

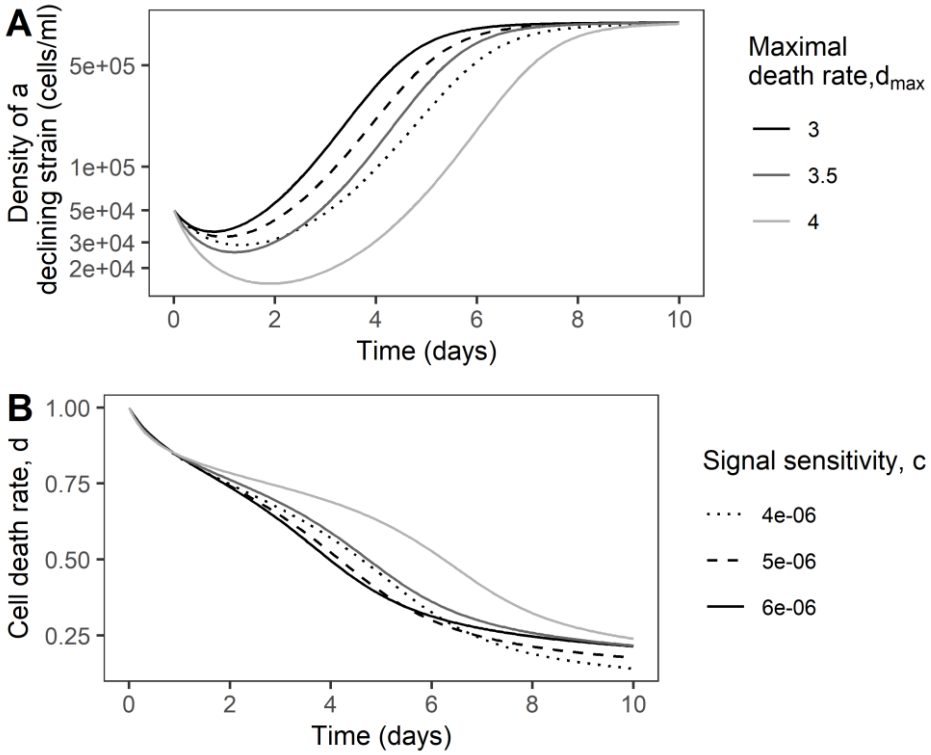

Figure 3. Signal release. Dynamics of the population density of the declining strain (A) and of the cell death rate d (B) in the stressful phase, under different sensitivities c to the signal released by dead cells. We used the numerical solution to eq. 13. The rate of nutrient release is $v = 1$, the birth rate is $b = 2$, and other parameters are as in Figure 1.

In order to mimic the specific decline-rebound pattern for the substrates model, the overall death rate d must be greater than all the components implied in the growth for the firsts days, meaning $d_{\max} \, e^{-h*t} > (b + wyS(t))$. However, we were not able to reproduce the decline-rebound dynamics for realistic parameter values for this scenario.

Dynamics of strain frequency in cocultures

We further investigated the behavior of co-cultures that combine the declining and the non-declining genotypes. Under the hypothesis of cell heterogeneity, we obtained the analytical solution for the frequency p of the declining strain over time in mixed populations by plugging the solution for the frequency of bad cells in the declining strain (eq. 18) into eq. (10), and solving the differential equation, leading to

$$p = \left(1 + \frac{1-p_0}{p_0} \frac{e^{(\tau-\Delta r)t}\,(\delta r_S+\tau)}{\delta r - q_0 + (q_0\,\delta r_S+\tau)\,e^{(\tau+\delta r_S)t}}\right)^{-1} \qquad \text{(Eq. 28)}$$

where $\delta r_S = r_B - r_G$ and $\Delta r = r_G - r_C$ in the stressful phase. Equation (28) shows that the frequency p of the declining strain depends on the initial odds ratio between both strains, the difference between the growth rates of good and bad cells of the declining strain, and that between the non-declining strain and good cells of the declining strain. As expected, the proportion of the declining strain in a mixed population initially decreased in the first days before increasing, leading to the declining strain to become dominant in the coculture in some specific conditions (Fig. S6).

We also obtained the analytical solution for p under the hypothesis of trade-off, by plugging the time-dependent growth rate for each genotype (eq. 23) into the generic equation (3), leading to

$$p = \left(1 + \frac{1-p_0}{p_0} e^{-\left(r_{max,A} - r_{max,C}\right) t + \frac{\Delta^2}{4}\left(\frac{1-e^{-2\lambda_A t}}{\lambda_A} - \frac{1-e^{-2\lambda_C t}}{\lambda_C}\right)}\right)^{-1}. \qquad \text{(Eq. 29)}$$

The frequency p of the declining strain depends on the trade-off between the difference in maximal growth rates between the two genotypes, $r_{max,A} - r_{max,C}$, and the difference in their cumulative effect of maladaptation (ratios with exponentials in eq. 29, see Fig. 4). The latter represents the cumulative effect on population growth of all maladaptation in the plastic trait, throughout the time when it has not yet reached the optimum phenotype. The slower the developmental rate, the larger the cumulative effect of maladaptation on population dynamics. For long enough times (when the trait has reached its final value for both genotypes), we can simplify eq. (29) as

$$p = \left(1 + \frac{1-p_0}{p_0} e^{-\left(r_{max,A} - r_{max,C}\right) t + \frac{\Delta^2}{4}\left(\frac{1}{\lambda_A} - \frac{1}{\lambda_C}\right)}\right)^{-1}, \qquad \text{(Eq. 30)}$$

which highlights that the maximum cumulative effect of maladaptation is inversely proportional to the rate of plasticity. Therefore, a trade-off exists when genotype A has larger maximum growth rate during the rebound, $r_{max,A} > r_{max,C}$, but slower plasticity, $\frac{1}{\lambda_A} > \frac{1}{\lambda_C}$. In this case, the term in the exponential in eqs. (29) and (30) changes sign over time, leading to a change in the direction of frequency change, as seen in Fig. 4.

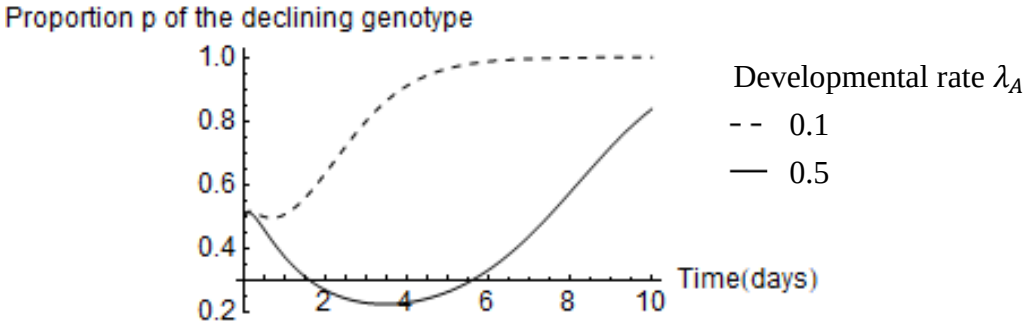

Figure 4. Frequency p of the declining genotype in mixed population in the stressful phase, under hypothesis of trade-off between tolerance and reproduction, (using eq. (29)), with different developmental rate for the declining genotype λ_A. Parameters values: $\Delta = 2$, $p_0 = 0.5$, $r_{max,A} = 1.5$, $\lambda_C = 3.5$, $r_{max,C} = 0.5$.

For the models of molecules release, such analytical solution for p were not found as the differential equation systems were more complex.

Discussion

Parameter values for decline-rebound pattern

We proposed three alternative hypotheses to explain population decline in response to an environmental stress, follow by a demographic rebound. We explored the conditions for the three models to obtain a decline-rebound demography for one genotype.

For the hypothesis of cell heterogeneity, the degradation rate from good to bad cells can represent some mechanisms such as ageing, physical damage or accumulation of free radicals, leading to poorer metabolic status. We found that observing substantial decline in this scenario requires the initial proportion of bad cells to be large enough (Fig. 1), which in turn depended on what happened during the non-stressful (NS) phase. The requirement to produce a high number of bad cells (>50% of the declining strain) is to have a degradation rate high enough, especially if the duration of the non-stressful phase is short (Fig. S2). To be compatible with the experimental data of population decline of 70% in *D. salina*, the proportion of bad cells reached in seven days (and approximately as many generations) in the NS phase needs to be higher than 0.75, which requires a degradation rate of 0.20, which seems inconsistent with the biology of this model system (and probably many other organisms). As noted above, the equation for the equilibrium proportion of bad cells (Eq. 16) is similar to the result of mutation-selection balance in classic population genetics (Hartl and Clark 1997), the degradation rate being analogous to mutation rate and the differential growth rate determining the magnitude of selection (between two genotypes). However, the degradation rates considered here (on the

order of 10%) are way too high to be compared to mutations rates (even in unicells). Note also that this model is comparable in form to models of evolutionary rescue through a bi-allelic locus (Gomulkiewicz & Holt 1995).

For the hypothesis of trade-off between halotolerance and reproduction, we assumed that a genotype displaying higher reproduction at the expense of tolerance for salinity rise (as simulated in Fig. 3) led to a growth rate that is dynamic and depends on maximal growth rate r_{max} and the initial maladaptation of the plastic trait (Fig. 2). To be able to simulate successive patterns of decline-rebound at each transfer in the stressful phase, the initial maladaptation needs to be large enough ($\Delta > \sqrt{2r_{max}}$), and the rate of plastic change needs to be fast enough for the plastic trait z to approach the required value before extinction. However, in this model the plastic trait returns to another value during the non-stressful phase, at the same rate as in the stressful phase since we assumed reversible and symmetric labile plasticity, as in Lande (2009). Therefore, in order to simulate a genotype which declines only in the stressful phase, the maximal growth rate r_{max} in the non-stressful phase needs to be higher, or the strength of stabilizing selection weaker (larger ω), such that the same phenotypic maladaptation has weaker demographic impact ($r_{max} > \frac{\Delta^2}{2}$).

Our last hypothesis relies on our experimental observation in the chapter 1 of this thesis, where the declining strain grown in a filtrate where programmed cell death has already occurred showed lower decline. We proposed a biological explanation whereby the cells which die first releases molecules used as a signal, which prevents the remaining cells from triggering PCD themselves (Kaiser 1996). We found that greater maximal death rate leads to lower minimal population size and later in time, therefore the population reach its carrying capacity later (Fig. 4). The signal sensitivity acted as expected by diminishing the population decline and allowing the population to rebound earlier. A study predict that the evolution of altruism may slow adaptation to environmental change through the reduction of population density if the cost of the altruistic trait is on viability, leading to evolutionary suicide on evolutionary scale (Henriques and Osmond 2020).

Density-dependence

We modelled density dependence using a Lotka-Volterra equation where a competition term of strength α is added to the intrinsic growth rate, rather than the latter being multiplied by a term with a carrying capacity *K*. This formulation allowed the equilibrium population size

to depend on the growth rate (and thus possibly on the environment) rather than being fixed to an arbitrary carrying capacity that is independent from the population growth rate (Mallet 2012). We further assumed in all models that the two strains had the same competition term α, such that intra and inter-genotype competition are fully equivalent. This assumption allowed us to make more analytical progress, by making relative strain frequency an autonomous variable that does not depend on population density, such that selection became density-independent in our models. Further investigation is needed to explore how selection could favour a genotype that initially decline over a non-declining genotype in larger contexts of density dependence. However, we highlight that our models are still valid in the range of population size where density-dependence can be neglected (in the exponential phase), that allowed us depict what happens during the phase of decline.

In conclusion, we were able to mimic a decline-rebound pattern of demography in the three alternative models under specific parameters requirement, but some of which are not biologically plausible.

Statement of Authorship: NZ and L-MC conceived of the theory and models. NZ, SC and L-MC performed the cell heterogeneity analysis, NZ and L-MC analysed the others models. NZ prepared figures and tables, and wrote the original draft, L-MC reviewed and edited the draft.

Competing interest: Authors declare no competing interests.

Supplementary Figures

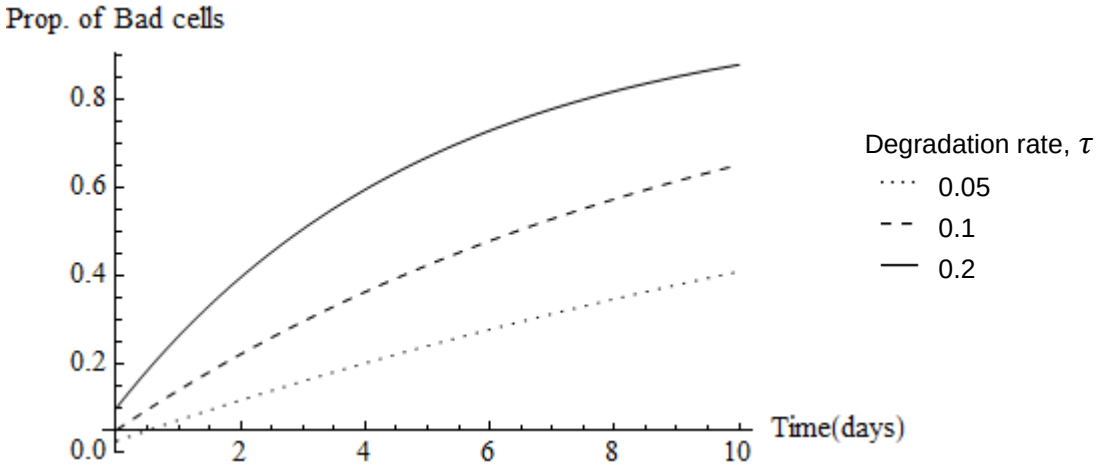

Figure S1. Proportion q of bad cells in a declining population in the non-stressful environment under different higher degradation rate τ, using eq. (17). Parameters values are the differences in growth rates between good and bad cells in the stressful phase $\delta r_S = -2$ and non-stressful phase δr_{NS}= 0.001.

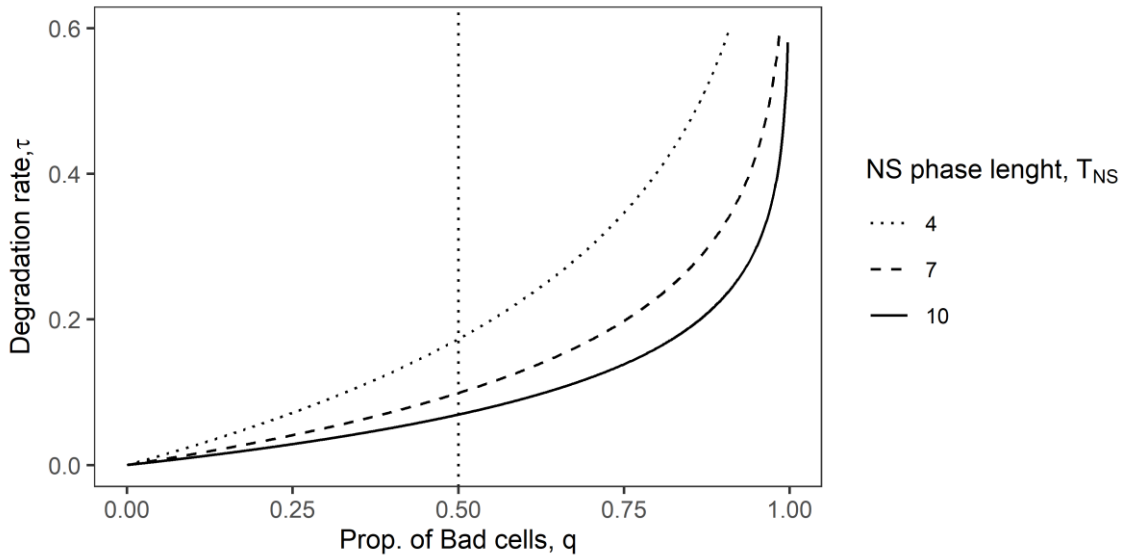

Figure S2. Degradation rate required to reach proportion q of bad cells in a declining population at the end of the non-stressful phase, under different duration of this phase (in days), using eq. (20).

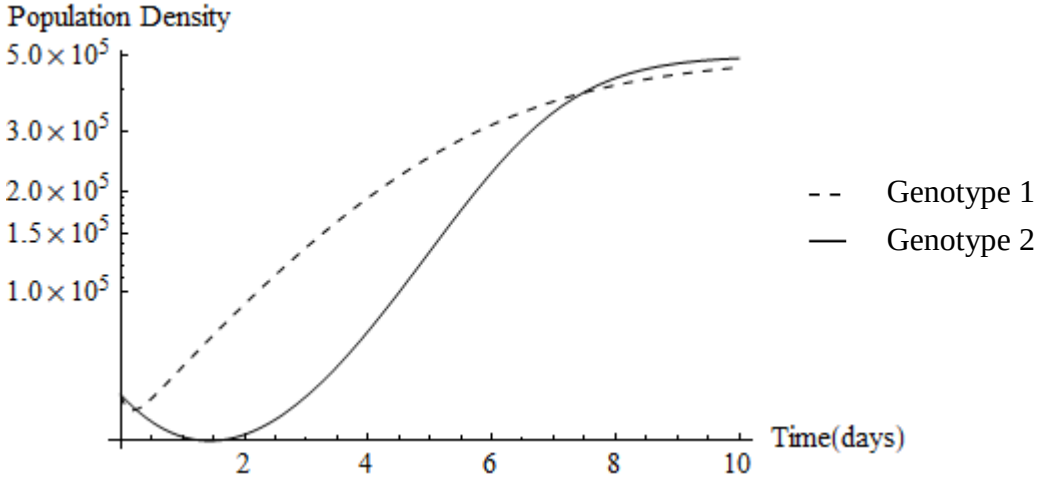

Figure S3. Trade-off between plastic tolerance and reproduction. We used the analytical solution (eq. 24) to contrast two genotypes that sit in different positions along the trade-off. Genotype 1 is characterised by a high max growth rate $r_{max} = 1.5$ at the expense of low environmental tolerance (slower change in plasticity $\lambda = 0.1$) than genotype 2 ($r_{max} = 0.5$; $\lambda = 3.5$) under the same initial maladaptation $\Delta = 2$. Other parameters values are as in Figure 2.

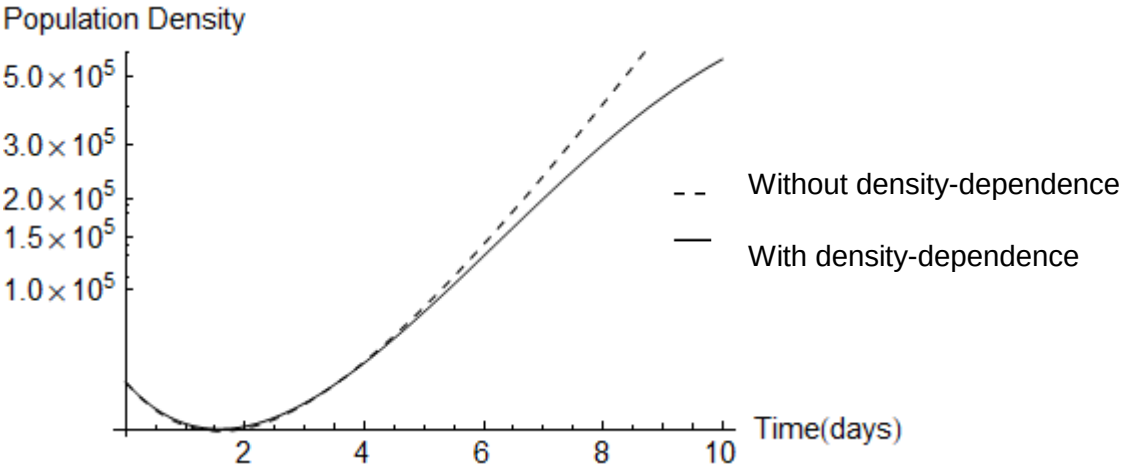

Figure S4. Simulated demographic dynamics after a salinity rise, under the hypothesis of a trade-off between environmental tolerance and reproduction. The exact analytical solution with density-dependence (eq. 24) and the simplified version assuming only the exponential growth without density-dependence (eq. 25). Parameters values: $N_0 = 5.10^4$, $\alpha = 1.10^{-6}$, $r_{max} = 0.6$, $\lambda = 1/5$, $\Delta = 1.5$.

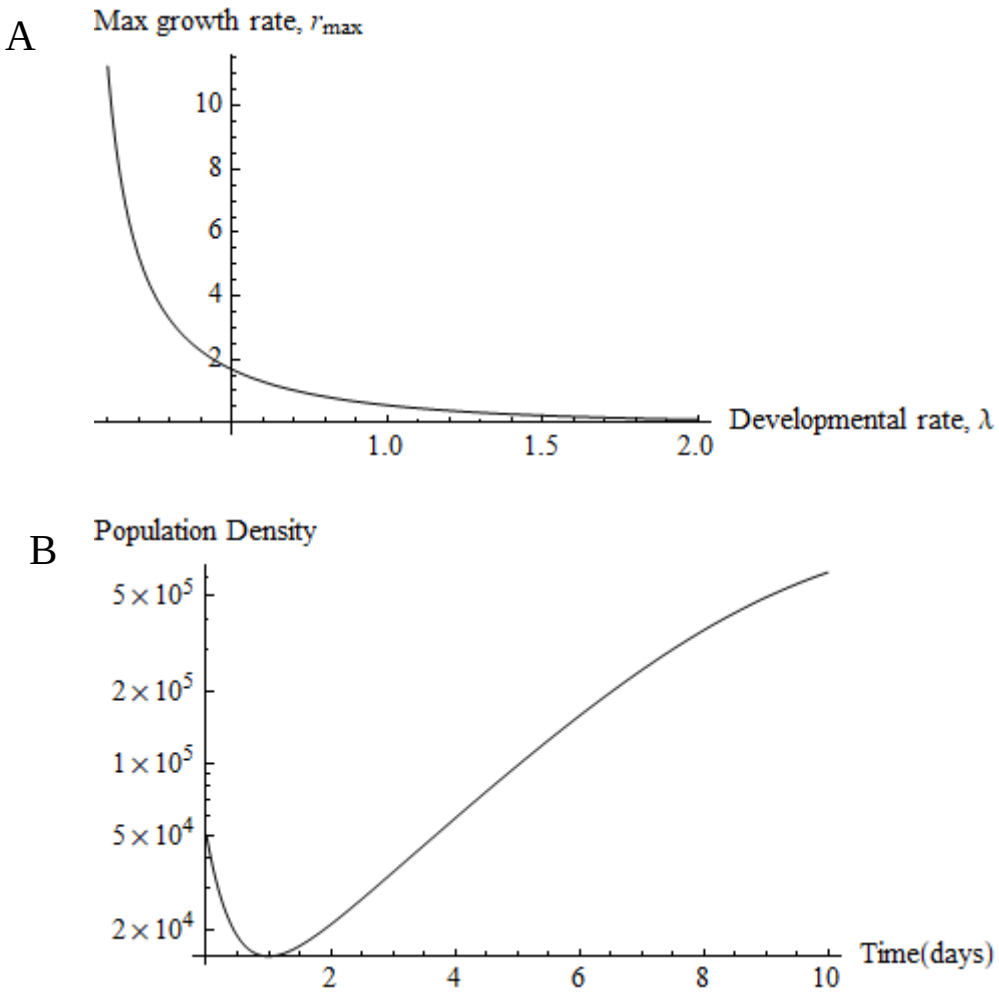

Figure S5. (A) Relation between maximum growth rate and the developmental rate under specific requirements, i.e. that population declines by a total of 70%, reached on day 1 (using eq. (27)). (B) Associated population dynamics using the eq. (24) with parameters values $\lambda = 1$, $r_{max} = 0.549$, $\Delta = 2.847$.

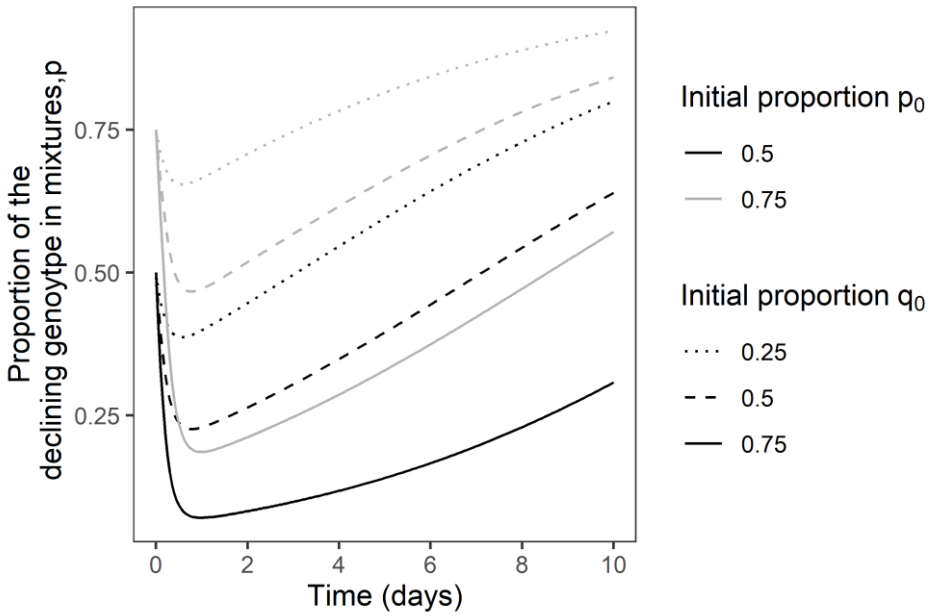

Figure S6. Frequency p of the declining genotype in mixed population in the stressful phase, under hypothesis of the cell heterogeneity (using numerical solution for eq. 10 combined to eqq. 8 and 9), with different initial proportions p_0 of the declining genotype, and q_0 of bad cells within this genotype. Parameters values: $N_0 = 5.10^4$, $r_B = -4$, $r_G = 1$, $r_C = 1$, $\alpha = 2.10^{-6}$, $\tau = 0.1$.

Additional results for cell heterogeneity model

We also determined the strain A density resolving the eq. (7) by inserting the analytical solution of proportion q (eq. 15), leading to

$$N_A = \frac{(e^{(\tau+\delta r_S)t}\,(\tau+q_0\,\delta r_S)-\delta r_S(1-q_0))\,N_{A,0}\,r_B(\tau-r_G)e^{(r_G-\tau)t}}{\begin{array}{l}(r_B^2((e^{t(r_G-\tau)}-1)(1-q_0)N_{A,0}\alpha-\tau+r_G)-(e^{tr_B}-1)N_{A,0}\alpha(\tau-r_G)(\tau-q_0 r_G)\\ +r_B(-\tau((e^{tr_B}-1)q_0 N_{A,0}\alpha+\tau)+((1-e^{t(r_G-\tau)}(1-q_0)-2q_0+e^{tr_B}q_0)N_{A,0}\alpha+2\tau-r_G)r_G))\end{array}}.$$

Since the previous equation was too complex to manage, we assumed that the degradation rate is negligible compared to the differential growth rate. We can then use eq. (18) to solve eq. (7), and we obtained the following density of strain A over time such as

$$N_A(t) = \frac{e^{r_G\,t}\,(1+(e^{\delta r_S\,t}-1)p_0)N_{A,0}r_B r_G}{r_B(r_G+(e^{r_G\,t}-1)(1-p_0)\alpha\,N_{A,0})+(e^{r_B\,t}-1)\,p_0\,N_{A,0}\,\alpha r_G}, \qquad \text{(Eq. S1)}$$

where $N_{A,0}$ is the initial density of strain A at the beginning of the period, corresponding to 1/10 of the population size of the previous period (in order to mimic the experimental setup of salinity changes with dilution). This equation allowed us to model the characteristic decline-rebound demographic pattern of strain A after a salinity rise and obtained similar results as in Fig. 1. It is worthy to note that as expected, a minimal proportion of bad cells is required to triggered the population decline. The population size at stationary phase correspond to $N_{A,eq} = \frac{r_A}{\alpha} \approx \frac{r_G}{\alpha}$, that showed that the remaining cells are essentially the in good shape cells.

Discussion générale

Ces travaux de thèse portent sur l'évolution d'un trait paradoxal qui est la mort cellulaire déclenchée activement en réponse à un stress environnemental par un organisme unicellulaire. Nous l'avons étudié chez la microalgue halotolérante *Dunaliella salina* soumise à une salinité fluctuante. Nos objectifs principaux étaient d'une part, examiner les facteurs influençant l'intensité de la mort cellulaire et les conséquences d'un tel trait sur les dynamiques démographiques et notamment sur la valeur sélective des populations, et d'autre part, explorer comment la sélection pourrait agir sur ce trait qui est létal au niveau individuel, mais qui semble bénéfique pour la population. Enfin, nous voulions modéliser les mécanismes biologiques pouvant expliquer cette dynamique complexe de déclin démographique suivi d'un rebond.

Evolution de la mort cellulaire programmée chez un unicellulaire

Déclin de population et mort cellulaire programmée

Nous avons caractérisé dans le chapitre 1 le déclin de population subi par une souche de *D. salina*, en réponse à un choc hyper-osmotique. Notre hypothèse principale pour expliquer ce déclin de population était la mort cellulaire programmée (PCD), c'est-à-dire une mort activement déclenchée en réponse à un signal environnemental. Ce mécanisme biologique nous semblait plausible car des études ont démontré son occurrence dans le genre *Dunaliella* (Segovia et al. 2003), notamment face à un choc hyper-osmotique (Jiménez et al. 2009) et chez notre espèce modèle dans l'obscurité (Orellana et al. 2013). Nous avons démontré que l'intensité du déclin démographique peut être diminuée (chap. 1), voire complètement inhibée (chap. 2), par l'ajout d'un inhibiteur d'activité de caspases, connues pour être un élément clé dans la cascade métabolique menant à la mort cellulaire programmée (Slee et al. 2001; Danial and Korsmeyer 2004; Kasuba et al. 2015; Barreto Filho et al. 2022*a*). Cette expérience d'inhibition est un argument pour établir le caractère actif de cette mort et nous conforte dans la caractérisation de ce phénomène en tant que mort cellulaire programmée. Cependant nous sommes conscients que l'activité des métacaspases n'est pas spécifique à la PCD (Barreto Filho et al. 2022*a*) car ces protéases sont aussi impliquées dans d'autres processus cellulaires (Abraham and Shaham 2004), et que l'agent à large spectre utilisé, Z-VAD-FMK, est aussi capable d'inhiber l'activité des cathepsines B (Schotte et al. 1999). A cela s'ajoute la confusion sur la classification des caspases et autres familles proches (métacaspases, paracaspases)

(Minina et al. 2020) et sur l'identification de quelle protéase exactement agit dans la mort cellulaire de l'espèce ciblée (les inhibiteurs ayant été conçus pour être spécifiques aux caspases impliquées dans la PCD chez les mammifères) (Barreto Filho et al. 2022*a*). Néanmoins, le fait que cette molécule puisse ralentir ou arrêter le déclin de population induit par le stress hyperosmotique conforte son rôle d'inhibiteur de la PCD dans notre système.

Caractère plastique de la mort cellulaire programmée

Nous avons proposé que la mort cellulaire programmée peut être considérée comme un trait plastique puisqu'elle est exprimée en réponse à un signal environnemental (obscurité, UV, choc thermique, et dans notre cas salinité…). Toutefois, nous nuançons en soulignant que dans les populations quasi-clonales utilisés dans nos expériences, uniquement une partie des cellules ayant pourtant le même génotype déclenche leur mort en réponse à un choc hyper-osmotique. Autrement dit, le trait plastique est la probabilité d'induire la mort programmée, et non sa réalisation effective chez un individu. Cette vision plastique du trait peut aussi nous donner une piste de réflexion pour expliquer la différence d'induction de PCD chez la souche A, par l'hypothèse d'une stratégie de minimisation de risques face à un stress environnemental (ou *bet-hedging* en anglais) (Libby et al. 2018). On peut faire le parallèle de probabilité d'induire la PCD chez la souche A avec l'exemple de probabilité d'éclosion des œufs chez le crustacé *Branchipodopsis wolfi* (Pinceel et al. 2021). A cause de l'imprédictibilité de la pluie, en saison désertique, une partie seulement des œufs éclosent, l'autre partie assurant la survie de la population dans le cas où l'étang se dessèche. Les communautés faisant face à des fluctuations imprévisibles auraient pu évoluer vers une telle stratégie de traits de vie lorsque le trait est plastique (Gavrilets and Scheiner 1993; De Jong 1999; Lande 2009; Libby et al. 2018).

Nous avons aussi observé une certaine plasticité dans la modulation de l'intensité du déclin en fonction des facteurs externes, avec une probabilité plus grande de déclencher sa propre mort pour les cellules cultivées en conditions plus optimales (plus de lumière, moins de compétition intraspécifique et ressources non limitées). La nature contexte-dépendance de la PCD semble primordiale pour comprendre son rôle écologique et sa nature (Reece et al. 2011; Durand and Ramsey 2019), et donc potentiellement son histoire évolutive.

Potentiel d'évolution de la mort cellulaire programmée

Pour que ce trait de mort cellulaire programmée soit sélectionné, il faut soit qu'il présente un avantage compensant l'effet négatif, soit qu'il soit associé à un autre trait sous sélection naturelle. Afin d'étudier comment la sélection peut favoriser un trait de mort cellulaire, nous

avons tout d'abord établi les conditions nécessaires pour que la sélection puisse agir : l'existence au sein d'une même espèce d'une variabilité pour un caractère associé à une différence de valeur sélective, et que ce caractère soit héritable. Nous avons confirmé dans le chapitre 1 l'existence de réponses démographiques différentes face à une hausse de salinité entre deux souches de notre espèce modèle, (comme précédemment souligné dans Leung et al. 2022), dues à des taux de mort cellulaire différents. Ce trait de mort cellulaire semble bien génétiquement déterminé puisque les populations clonales obtenues à partir de différentes cellules présentent la même réponse par souche.

Nous avons établi une forte corrélation positive entre l'intensité du déclin et le taux de croissance dans la phase exponentielle chez la souche qui décline, alors que la souche ne déclinant pas initialement présente un taux de croissance exponentielle plus faible. Le chapitre 1 nous permet de répondre au premier objectif de la thèse, en arguant que la mort cellulaire peut être associée à une meilleure valeur sélective à travers sa corrélation avec un rebond démographique.

Hypothèses adaptives sur le maintien de la PCD

Trait promouvant la croissance de la population

Une hypothèse souvent mise en avant pour expliquer le maintien de la mort cellulaire programmée chez les unicellulaires est qu'il s'agirait d'un comportement altruiste, où les cellules qui meurent relâchent lors du processus des molécules pouvant être utilisées par les cellules survivantes. Ces molécules peuvent être de nature nutritive, directement utilisables par les conspécifiques (Fröhlich and Madeo 2000; Durand et al. 2011, 2014; Brown and Kubanek 2020) ou bien reminéralisées par des archées (Orellana et al. 2013). Nos résultats expérimentaux ne vont pas dans le sens d'une telle hypothèse puisque les populations de la souche A qui ont été cultivées dans un filtrat où de la PCD a été précédemment déclenchée ('filtrat PCD' et donc devant contenir les supposées molécules relarguées) ne croissent pas mieux que lorsqu'elles sont cultivées en milieu standard, contrairement à ce qui a été observé chez l'algue verte *Chlamydomonas reinhardtii* (Durand et al. 2011). Cependant nous n'écartons pas complétement cette hypothèse, car les défis techniques de cette expérience laissent planer un doute sur la présence de ces supposées ressources nutritives en quantité suffisamment importante pour observe un effet. En effet pour récupérer le milieu de culture sans les cellules, nous avons dû centrifuger le milieu (et donc potentiellement induire une dégradation physique des cellules résultant aussi en l'excrétion de molécules dans les populations n'ayant pas subi de

PCD) puis le filtrer (on peut supposer que le diamètre du filtre était plus petit que les molécules relarguées, mais peu probable), et enfin le diluer avec du milieu sans ressource. Pour cette raison, nous avons quand même modélisé dans le chapitre 3 cette excrétion de ressources nutritives, nous permettant de mimer ce rebond démographique suivant le déclin.

Si la meilleure croissance que nous avons observée suite au déclin initial résulte d'un comportement altruiste par la production de biens communs, on s'attendrait à ce que celui-ci soit sélectionné s'il existe une structuration spatiale et génétique des apparentés (Débarre et al. 2012). Or, dans nos milieux de culture en flasque, il n'y a pas de structuration spatiale particulière des cellules, d'autant plus que les milieux sont homogénéisés avant chaque mesure (c'est-à-dire quotidiennement pendant les phases à haute salinité) mais aussi avant chaque transfert. Une alternative est qu'en absence de structure spatiale, ce trait peut évoluer si les molécules produites ('biens privés') sont un bénéfice dirigé préférentiellement vers les individus apparentés (Estrela et al. 2016).

Une autre hypothèse évolutive liée à la production de biens publics par la PCD est celle la reine noire (Morris 2015; Ndhlovu et al. 2021), selon laquelle une partie de la communauté microbienne laisse échapper des biens publics et subit le coût, tandis que les autres ont perdu cette fonction mais sont 'bénéficiaires' (Morris 2015). Cette hypothèse a été proposée pour expliquer l'absence de PCD chez certains taxons unicellulaires en supposant une origine ancestrale du trait, mais on pourrait appliquer le même cheminement pour expliquer l'absence de PCD chez certaines souches de la même espèce. La souche C aurait pu perdre cette fonction car en cohabitation avec une souche qui portait le coût (la souche A ayant été échantillonné sur le même site), ou bien après sa mise en culture en isolation car le maintien de cette fonction est trop couteux (échantillonnage en 1976). Cependant, il n'existe pas d'analyses prouvant la perte de cette fonction pour le moment, et on ne peut pas complétement écarter l'idée que la souche C soit capable d'activer la PCD en réponse à d'autres signaux non testés, puisque l'activation de la PCD est contexte-dépendent (Reece et al. 2011; Durand and Ramsey 2019).

Nos expériences ne semblent pas montrer que la souche C profite des ressources excrétées ('biens publics') par la souche A, que ce soit en tant que tricheur (contexte coopération, Estrela et al. (2019)) ou bénéficiaire (contexte reine noire Morris (2015)). En effet elle ne croit pas plus vite lorsqu'elle est cultivée dans le milieu 'filtrat PCD' (figure 4 du chp. 1) ni lorsqu'elle est en coculture avec la souche A déclenchant de la PCD vs coculture avec inhibition de PCD (figure 5 du chp. 2). De plus, si le trait sous-jacent au déclin est impliqué dans des interactions entre les deux souches (comme par ex relargage de ressources) alors la

croissance de la population totale en coculture devrait être déterminée par une forte composante de densité-dépendance inter-souches, et donc peu prévisible par les dynamiques en isolation. Or nos résultats du chapitre 2 montrent une croissance similaire pour la souche ne déclinant pas (figure 3 du chp. 2), qu'elle soit en présence ou non de la souche déclinant.

Trait altruiste empêchant la population d'induire encore de la PCD

Une autre fonction potentielle de molécules relarguées par les cellules effectuant la PCD pourrait être d'avertir les autres cellules sur les conditions environnementales, dans un mécanisme de quorum-sensing (Abisado et al. 2018; Durand 2020). L'expérience de filtrat du chapitre 1 nous a mené vers cette piste de molécules signal, car les populations de la souche A cultivées dans un filtrat PCD ont décliné moins intensément que dans les autres milieux de culture, suggérant qu'un signal empêche les cellules restantes d'induire leur propre mort. Nous avons donc modélisé cette hypothèse dans le chapitre 3, alors qu'elle n'était pas prévue initialement. Cependant une telle hypothèse n'explique pas la raison d'une croissance plus importante après le déclin. Nous pouvons faire l'hypothèse d'une combinaison de différents types de molécules activement relarguées pendant la mort, ou de l'utilisation des restes organiques des cellules mortes. Par exemple chez *Myxococcusxanthus*, face à un manque de ressources nutritives les cellules choisissant d'induire un mécanisme menant à leur mort relarguent un set de 6 acides aminés en quantité fixe, tel que la quantité totale dans le milieu est proportionnelle au nombre de cellules mourantes. Lorsque la quantité excrétée dépasse un seuil limite, les cellules restantes répriment leur mort et poursuivent leur croissance, renforcée par l'utilisation des acides aminés (Kaiser 1996). La plausibilité de cette hypothèse est renforcée par le fait que *Dunaliella salina* est capable, comme d'autres microalgues, d'induire un métabolisme hétérotrophe dans certaines conditions (Chavoshi and Shariati 2019).

Hypothèse non-adaptive sur le maintien de la PCD

Nous avons aussi envisagé l'hypothèse non-adaptative sur le maintien de la mort cellulaire programmée, en tant que trait mal-adaptatif et sans bénéfice direct. Une des suggestions proposée dans l'introduction de cette thèse était que la PCD est un mécanisme inévitable de la balance métabolique de la cellule (Bidle and Falkowski 2004). Dans ce scénario, lorsque des cellules bactériennes actives en croissance subissent un arrêt brutal de croissance dû à un stress modéré (sous-léthal), la production d'énergie (c'est-à-dire le métabolisme) continue alors que l'utilisation de l'énergie s'arrête (la croissance). Cette dissociation entraine une accumulation de radicaux libres qui est létale pour la cellule (Aldsworth et al. 1999). Cette proposition est

cohérente avec le fait que des populations en phase exponentielle sont plus enclines à déclencher activement de la mort cellulaire que des populations en phase stationnaire, comme cela a été montrée expérimentalement chez *E. coli* (Hazan et al. 2004). Ceci est compatible avec notre observation d'un déclin démographique moins prononcé pour les populations en phase stationnaire prolongée, comparé aux populations en phase plus active (exponentielle ou début de stationnaire) dans le chapitre 1 de cette thèse.

Dynamiques démographiques complexes

Lorsqu'une population subit un déclin démographique face à un stress environnemental, l'interprétation la plus commune est qu'il s'agit d'une réponse passive liée à la tolérance des nouvelles conditions environnementales, et non d'un mécanisme actif comme la PCD. Lorsque ce déclin est suivi d'un rebond démographique, on l'associe facilement à du sauvetage évolutif, où la croissance de la population est restaurée par la sélection d'un taux de croissance moyen positif, à travers la variance génétique initialement présente ou introduite par mutation au cours du déclin. Or l'utilisation dans la partie expérimentale de populations quasi-clonale chez une espèce dont le taux de reproduction est ~1/jour nous a permis d'écarter cette explication par la faible variance génétique présente et la faible probabilité d'une mutation. Nous nous sommes donc penchés sur les autres mécanismes biologiques qui pourraient expliquer ce déclin-rebond, et leur impact sur les dynamiques démographiques.

Hétérogénéité de l'état physiologique des cellules

Notre première hypothèse alternative est que le déclin est dû à l'élimination des cellules en mauvais état ou endommagées, n'étant pas capables de tolérer le stress environnemental. Le rebond résulterait du plus grand taux de croissance moyen des cellules restantes car en meilleur état physiologique, dans un processus similaire au sauvetage évolutif (Gomulkiewicz and Holt 1995), mais où la 'sélection' agit sur une variation phénotypique non-héritable. On s'attend donc à ce que le déclin soit de moins en moins important au cours de stress environnementaux successifs. Cependant la persistance du déclin au cours de deux (chap. 1), puis plusieurs cycles de salinité successifs (chap. 2), couplé avec les requis du modèle dans le chapitre 3 rendent cette hypothèse peu probable. En effet, pour observer un déclin répété et massif, une large part de la population (>50%) doit être dans cet état dégradé (le pourcentage de ces cellules représentant le pourcentage de la réduction dans la taille de la population). Ainsi le taux de dégradation doit être excessivement grand (et donc biologiquement peu plausible) afin de produire suffisamment de cellules endommagées en un court laps de temps dans la phase non stressante (dans le chap.

1 cette durée étant de deux semaines, mais dans le chp. 2 la durée est raccourci à 4 ou 7 jours). De plus, si le mécanisme est dû à une accumulation de cellules en mauvais état, on s'attend à ce que les populations 'plus âgées' présentent un déclin démographique plus prononcé, ce qui n'est pas le cas avec notre expérience dans le chapitre 1 où les populations en phase stationnaire tardive montrent un déclin plus faible que celui des populations plus jeunes. Enfin, il serait peu probable que cette hétérogénéité physiologique n'existe que dans une des deux souches de collection utilisées dans nos expériences.

Compromis entre tolérance et reproduction

Notre troisième hypothèse est un compromis entre tolérance à la salinité et reproduction (hypothèse sur vitesse de la plasticité), selon lequel la souche qui décline investit plus dans la reproduction, aux dépens de la tolérance au stress. Dans notre exemple biologique *D. salina*, un bon candidat serait le mécanisme d'halotolérance à travers le glycérol, qui est un osmoprotectant (Ben-Amotz et al. 2009) et dont la production est couteuse en termes de ressources produite par photosynthèse ou accumulée (Ben-Amotz and Avron 1973). Le contenu intracellulaire de glycérol augmente au bout de quelque(s) heures (1- à 3 h) après un choc hyper-osmotique, pour atteindre sa valeur maximale 24 heures après le stress (Zhao et al. 2013), ce qui concorderait avec le déclin maximal observé. De plus, il a été montré que certaines espèces du genre *Dunaliella* sont capables d'utiliser le glycérol excrété dans le milieu de culture (Lin et al. 2013). L'investissement dans l'halotolérance pourrait donc être une production de glycérol plus précoce ou bien l'assimilation du glycérol extra-cellulaire (pour la souche C ne déclinant pas). Un concept similaire en écologie est le compromis entre la résistance et la récupération, en rapport avec la résilience (Hodgson et al. 2015).

Si le déclin démographique est dû à un trait plastique, notre manière de le modéliser dans le chapitre 3 mènerait la population à décliner à chaque changement environnemental de manière symétrique, à moins d'avoir un taux de croissance plus important en environnement non-stressant pour compenser la mal-adaptation initiale. Or notre modèle expérimental est un exemple de l'importance de la directionnalité du changement environnemental, impliquant la directionnalité de la réponse du trait. Par exemple, l'excrétion du glycérol hors de la cellule en réponse à une baisse de la salinité est un mécanisme beaucoup plus rapide (quelques secondes/minutes) que la production de glycérol face à une hausse de salinité qui s'étale sur plusieurs heures (Chen and Jiang 2009), induisant une asymétrie démographique dans l'effet des transitions de salinité bas-haut versus haut-bas (Rescan et al 2020, 2022).

Enfin, si le trait impliqué dans la tolérance est juste physiologique, alors on s'attend à ce que la croissance de chaque génotype soit indépendante de l'autre en compétition, mais dépendante de l'environnement, de sorte que les dynamiques en monocultures prédisent bien les cocultures. Les résultats de la compétition à long-terme du chapitre 2 concordent partiellement, puisque les deux souches présentent des dynamiques de croissances plus sensibles à leur propre densité plutôt à qu'à celle de leur compétiteur.

Les deux souches peuvent exprimer différentes stratégies osmotiques (= réponses de glycérol différentes), démographiques (PCD déclenchée ou non), écologiques (cellules altérées, ou utilisation de différentes ressources donc pas de compétition inter-souche), ou un mélange des trois. En effet, ces hypothèses ne sont pas mutuellement incompatibles, par exemple la maintenance de la PCD en tant que trait altruiste serait d'autant plus bénéfique au niveau de la population si ce sont les cellules en mauvais état ou sénescentes qui déclenchent leur propre mort (Reece et al. 2011).

Sélection et démographie

Combiner approche expérimentale et théorique

Combiner données expérimentales et modèles mathématiques est une approche productive pour mieux comprendre the mécanismes biologiques sous-jacents aux observations expérimentales, et distinguer les effets de ces explications alternatives afin d'évaluer leur comptabilité avec les données. Cette stratégie s'avère d'autant plus pertinente en écologie évolutive, où les processus se déroulent sur de multiples générations, rendant l'identification des facteurs de ces dynamiques compliqué dans la plupart des systèmes naturels. Une manière de contourner cette limitation de temps expérimentalement est d'utiliser des organismes avec un temps de génération court (de quelques minutes à quelques jours), et suivre leur démographie et la sélection au cours du temps. Les observations récoltées sont ainsi dynamiques plutôt que statiques, et donc porteuses de plus d'information. Cependant, interpréter et comprendre des dynamiques démographiques d'évolution expérimentales reste complexe, il est donc parfois nécessaire de coupler ces observations aux prédictions des modèles formalisant mathématiquement les processus censés les produire. C'est d'autant plus vrai pour des dynamiques de population non triviales, reliant risque d'extinction et évolution en environnement fluctuant.

L'expérience d'évolution expérimentale du chapitre 2 nous a permis de comprendre comment ce trait létal au niveau individuel peut être maintenu chez un unicellulaire. Au bout

de 180 générations sous des conditions de salinité fluctuante, nous avons constaté une coexistence stable des deux souches, malgré les fortes fluctuations de leur fréquence au cours de chaque cycle, suite au déclin persistant de la souche A. Etonnamment, les taux de croissance de chaque souche montrent surtout une densité-dépendance à leur propre densité plutôt qu'à la densité totale ou à la densité du compétiteur. Nous avons modélisé les trois mécanismes précédemment présentés afin de vérifier la compatibilité de leur requis pour mimer la dynamique spécifique.

Modèles d'écologie

Le choix du modèle écologique pour représenter la dynamique démographique est primordial, puisqu'il implique de trouver un équilibre entre généralisation du processus biologique et spécificité à un exemple. Dans le chapitre 3, nous avons démontré que le modèle sans densité-dépendance sous l'hypothèse du compromis tolérance-reproduction est suffisant pour étudier la dynamique de déclin-rebond, car celle-ci se déroule dans une gamme de taille de population où la densité n'affecte pas la démographie (c'est-à-dire dans la phase exponentielle où les ressources ne sont pas limitantes). Cependant pour étudier les conséquences d'une telle dynamique initiale sur la croissance de deux souches en compétition, il est nécessaire de modéliser cette densité-dépendance. En effet si une souche arrive en premier à sa capacité de charge, nous pouvons penser que leur dynamique soit densité-dépendance à la densité totale, ou au contraire qu'elles incluent un fort effet compétition inter-souches. Nous avons utilisé une formulation $r - \alpha$ plutôt que $r - K$ pour la croissance logistique dans le chapitre 3, car cela permet que la taille de population à l'équilibre soit dépendante du taux de croissance plutôt qu'être arbitrairement choisi par environnement (Mallet 2012), mais aussi de simuler plus facilement l'effet de la compétition intra et inter-génotypes.

Sélection densité-dépendante ou non

Bien qu'utiliser le taux de croissance comme proxy pour prédire le résultat de la compétition est une manière simplifiée d'interpréter les processus biologiques, les résultats du chapitre 2 nous indiquent que les prédictions faites à partir des dynamiques en monocultures sont assez cohérentes avec les dynamiques de population de chaque souche lorsqu'elles sont cultivées ensemble, car les dynamiques en cocultures sont principalement guidées par la compétition intra-souche qu'inter-souche. Cependant, la sélection dans notre expérience est fortement densité-dépendante, et semble agir sur la phase stationnaire, avec peu d'influence des dynamiques complexes ayant lieu lors de la phase exponentielle. Ainsi, utiliser le taux de croissance comme proxy pour la valeur sélective afin d'estimer le coefficient net de sélection

sur un cycle de salinité ne serait pas pertinent (Chevin 2011). Au-delà de ce constat, les modèles du chapitre 3 devraient être complexifiés pour tenir compte d'une densité dépendante qui varie entre souches, puisqu'à l'heure actuelle ils supposent une densité dépendance liée à la taille totale de population, fortement rejetée par nos analyses statistiques du chapitre 2.

Limites et perspectives

Partie expérimentale

L'une des limites de mes travaux de thèse est qu'ils reposent sur l'utilisation de deux souches de collection en tant qu'exemple, qui ne me permettent pas d'établir de généralité sur plusieurs génotypes, voire sur les populations naturelles. J'ai préféré me concentrer sur l'utilisation de deux génotypes aux réponses bien contrastées plutôt que de multiplier les souches de collection utilisées, afin de bien comprendre les facteurs impactant leurs différences et d'étudier leurs conséquences évolutives. Par ailleurs, l'utilisation de ces souches bien caractérisées dans des publications antérieures constituait une sécurité pour mes encadrants, et le fait qu'elles soient génétiquement proches malgré leurs phénotypes contrastés en faisait un bon cas d'étude. Cependant, les enseignements apportés par l'étude détaillée de cet exemple sont utiles pour comprendre des mécanismes plus généraux de sélection sur la PCD, et du lien entre démographie et évolution.

Lors de ma thèse, j'ai participé à l'échantillonnage de populations naturelles de *D. salina* dans les marais salants de Gruissan et La Palme, sur des sites balayant la gamme de salinité que l'espèce est capable de supporter. Des populations clonales ont été lancées à partir de cellules uniques isolées de ces échantillons, puis ont été soumises à des transferts de salinité par l'ingénieur de l'équipe. Ces populations ont présenté une large gamme d'intensité de déclins face aux chocs hyper-osmotiques, suggérant que ce mécanisme puisse être présent dans des systèmes 'naturels'. Etudier la compétition entre ces différentes populations en les reliant à leur distance génétique pourrait nous donner d'autres éléments pour l'hypothèse adaptative du maintien de la PCD chez un unicellulaire.

Une autre limite est que nous n'avons pas pu explorer la piste de l'induction de la mort cellulaire programmée par l'infection de virus chez *D. salina*, alors qu'il s'agit un signal déclencheur bien connu chez de nombreux unicellulaires (Bidle and Falkowski 2004; Bidle 2015). En effet, la PCD peut avoir comme rôle écologique d'éviter la propagation dans la population des pathogènes infectant la cellule déclenchant de la PCD, de manière similaire à ce qui se passe chez les multicellulaires (Del Pozo & Lam, 1998). Nous pourrions séquencer nos

milieux de culture pour chercher la présence potentielle de virus. Cependant, une induction par des virus semble peu compatible avec le fort rebond démographique observé suite au déclin.

Analyses statistiques et mathématiques

Une limite de nos analyses statistiques est que les dynamiques démographiques et les fréquences de souches dans les cocultures n'ont pas été traitées comme des séries temporelles, c'est-à-dire où la valeur à un temps donné dépend explicitement de la valeur au temps précédent. De ce fait, nous n'avons pas pris suffisamment en compte la variance résiduelle, ce qui peut augmenter artificiellement la significativité des tests. Cependant, la plupart des résultats présentés sont hautement significatifs, de sorte qu'il est peu probable que cette absence de considération de l'autocorrélation temporelle des résidus ait pu avoir un fort impact sur ces résultats.

Une autre limite concernant les dynamiques démographiques et les fréquences de souches en cocultures est que nous avons peu de points de données sur les phases suivant les transferts hypo-osmotiques (plan expérimental initialement conçu de cette manière car le phénomène d'intérêt se passe après un transfert hyper-osmotique). Or la surprenante coexistence stable des deux souches sur le long-terme, malgré la forte variation de fréquence de la souche A lors de la phase à haute salinité, nous a amené à supposer que la souche C semble être favorisée lors de la phase à plus basse salinité, et compenser sa diminution de fréquence lors de la phase précédente. Dès lors, il serait intéressant d'estimer la fréquence des souches après le choc hypo-osmotique, pour vérifier si la souche C y serait avantagée. Cependant, nous devrons contourner le problème que, à plus basse salinité, les deux souches sont moins phénotypiquement différenciables à travers leur fluorescence naturelle, rendant notre méthode d'estimation moins certaine. Quoi qu'il en soit, si un tel mécanisme a lieu, la durée de chaque phase devrait influer sur le maintien et la fréquence de chaque souche à long terme, comme modélisé dans un autre contexte chez les levures (Collot et al. 2018).

Enfin du côté de la modélisation, nous avons effectué la partie conceptualisation des modèles, c'est-à-dire la traduction des processus biologiques en termes d'équations, ainsi que la partie exploratoire des paramètres clés pour chaque modèle, afin d'identifier les conditions menant au patron démographique de déclin-rebond. Cependant, par manque de temps je n'ai pas pu mener à terme la comparaison de l'ajustement de chaque modèle sur les données expérimentales, comme initialement prévu. Ce travail reflète bien l'équilibre à trouver entre le choix de spécialiser un modèle à un exemple biologique particulier et celui de le généraliser.

Ainsi, nous souhaitons d'une part spécialiser les modèles afin de les ajuster sur nos données de l'évolution expérimentale du chapitre 2, comme nous avons commencé à le faire lors du stage M1 de Sudeshna Chakraborty (résultats non présentés). Distinguer les effets de ces explications alternatives nous permettrait d'éclairer le mécanisme en œuvre dans notre système biologique, et d'apporter une approche combinant expérimental et modélisation sur la manière dont la mort cellulaire peut évoluer chez un unicellulaire en milieu changeant. Dans cette optique d'ajustement à nos données, nous intègrerons aussi une compétition intra-génotype spécifique, comme observé dans la compétition à long-terme du chp. 2. D'autre part, nous souhaitons généraliser ces modèles dans des contextes de déclin démographiques de populations en tant que réponse transitoire face à un stress (pas uniquement chez les unicellulaires) et simuler l'évolution agissant sur plusieurs générations, voire sur une série d'épisodes d'exposition au stress. Garder des modèles aussi simples que possibles sert ces deux objectifs : cela permet d'une part de trouver des résultats analytiques qui aident à interpréter et généraliser les données au-delà des valeurs spécifiques des paramètres, et d'autre part cela facilite l'ajustement de ces modèles sur les données.

Conclusion

Les travaux de cette thèse ont porté sur la mort cellulaire et son potentiel évolutif en prenant comme modèle biologique l'algue halotolérante *Dunaliella salina*. L'ensemble de mes résultats montrent que la mort cellulaire ayant lieu chez cette espèce est un trait qui peut évoluer, même à de courtes échelles de temps, qu'il s'agisse une réponse active ou passive. Ils représentent ainsi un exemple expérimental de maintien de ce trait léthal chez un unicellulaire. De plus, la dynamique de déclin et rebond permet d'étudier le lien entre sélection et démographie dans un contexte non trivial.

Annexes

Communications scientifiques

• **Zeballos N**, Grulois D, Fereol S, Rieu O, Leung C & Chevin L-M (Novembre 2022). *Acceptable loss: Fitness consequences of salinity-induced cell death?* - Conférence Internationale conjointe SFE² GfÖ EEF sur les Sciences Ecologiques, Metz (**Poster**).

• **Zeballos N**, Grulois D, Fereol S, Rieu O, Leung C & Chevin L-M (Octobre 2022). Is *Programmed Cell Death in a unicellular green alga a form of adaptive plasticity ?* – Réunion annuelle du GDR Plasticité Phénotypique, Montpellier **(Présentation orale**).

• **Zeballos N**, Grulois D, Fereol S, Rieu O, Leung C & Chevin L-M (Juin 2022). *Adaptive potential of salinity-induced cell death in a halotolerant microalga.* Evolution, Cleveland (**Présentation pré-enregistrée en ligne**).

• **Zeballos N**, Grulois D, Fereol S, Rieu O, Leung C & Chevin L-M (Mai 2022). *Adaptive potential of salinity-induced cell death in a halotolerant microalga.* Le Petit Pois Déridé, Lille **(Présentation orale**).

• Présentations orales lors des séminaires d'équipe, lors de la Journée des doctorants au CEFE (2021) ainsi que présentation expresse lors de la sortie du Département aux salines.

• Organisation de séminaires du personnel temporaire (équipe GEE, CEFE) : échanges de pratiques scientifiques, discussion sur la carrière, la gestion du stress, le bien-être au travail…

Enseignement et expériences d'encadrement

Enseigner dans le supérieur est une vraie source de motivation dans mon parcours professionnel. Pour cette raison, j'ai choisi de réaliser entre 45h et 64h/an d'enseignement à l'Université de Montpellier - Faculté des Sciences et à l'Université Paul-Valery (dont les UE sont désignées par * dans la liste ci-dessous). J'ai particulièrement apprécié de tester divers types d'enseignement et méthodes pédagogiques (TD étude de cas, TD exercices classiques, TP informatique sur R, TP en écologie, suivi de projet, jeux sérieux, introduction des notions par le TD/TP avant le CM…) ainsi que de préparer mes propres contenus (Soutien sur l'utilisation de R et rappel des notions essentielles en épidémiologie évolutive sous forme de cours). J'ai ainsi appris à m'adapter à différents publics étudiants.

Les Unités d'enseignement dans lesquelles je suis intervenue sont :

- Soutien en Statistiques sur R et en Ecologie évolutive (M1 Eco-EPI, 6h, réf : C. Moulia)
- Des organismes aux écosystèmes, TP et TD (L1 SVSE, 36h)
- Cycle de vie 1, TD (L1 SVSE, 12h)
- Introduction à l'évolution, TD (L2 SVSE-BE, 15h)
- Suivi de projet en Ecologie et Biodiversité (M1 GIEBioTE, 2.5h)
- Bases génétiques de l'évolution, TP et/ou TD – (L3 SVSE-BE, 21h/an)
- Biologie Humaine*, TD (L1 Psychologie, 24h/an)
- Ecologie comportementale*, TD (L1 Sociologie, 26h)

Cette volonté de transmission des savoirs s'est aussi concrétisée par l'encadrement de deux étudiantes M1. J'ai particulièrement apprécié ce rôle de supervision scientifique (de la conception du sujet à la correction des rendus en passant par la formation de microbiologie et de bio-informatique), mais aussi de tutorat pour leurs projets professionnels.

- Encadrement de Sudeshna Chakraborty **(**Etudiante M1 MEME - Université de Montpellier) - 3 mois : modélisation de dynamique démographiques sur données empiriques. Printemps 2022.
- Encadrement de Océane Rieu (Etudiante M1 Darwin - Université de Montpellier) - 3 mois : évolution expérimentale. Printemps 2021.

Références

Abisado, R. G., S. Benomar, J. R. Klaus, A. A. Dandekar, and J. R. Chandler. 2018. Bacterial quorum sensing and microbial community interactions. mBio 9.

Abraham, M. C., and S. Shaham. 2004. Death without caspases, caspases without death. Trends in Cell Biology 14:184–193.

Aguilera, A., A. Distéfano, C. Jauzein, N. Correa-Aragunde, D. Martinez, M. V. Martin, and D. J. Sueldo. 2022. Do photosynthetic cells communicate with each other during cell death? From cyanobacteria to vascular plants. Journal of Experimental Botany 73:7219–7242.

Aldsworth, T. G., R. L. Sharman, and C. E. R. Dodd. 1999. Bacterial suicide through stress. Cellular and Molecular Life Sciences 56:378–383.

Ambastha, V., B. C. Tripathy, and B. S. Tiwari. 2015. Programmed cell death in plants: A chloroplastic connection. Plant Signaling and Behavior 10:2.

Ameisen, J. C. 2002. On the origin, evolution, and nature of programmed cell death: a timeline of four billion years. Cell Death and Differentiation 9:367–393.

Ameisen, J. C., T. Idziorek, O. Billaut-Mulot, M. Loyens, J. P. Tissier, A. Potentier, and A. Ouaissi. 1995. Apoptosis in a unicellular eukaryote (Trypanosoma cruzi): Implications for the evolutionary origin and role of programmed cell death in the control of cell proliferation, differentiation and survival. Cell Death and Differentiation 2:285–300.

Ashander, J., L. M. Chevin, and M. L. Baskett. 2016. Predicting evolutionary rescue via evolving plasticity in stochastic environments. Proceedings of the Royal Society B: Biological Sciences 283:20161690.

Assunção, P., R. Jaén-Molina, J. Caujapé-Castells, M. Wolf, M. A. Buchheim, A. de la Jara, K. Freijanes, et al. 2013. Phylogenetic analysis of ITS2 sequences suggests the taxonomic re-structuring of Dunaliella viridis (Chlorophyceae, Dunaliellales). Phycological Research 61:81–88.

Barreto Filho, M. M., I. L. Bagatini, and P. M. Durand. 2022*a*. How shall we measure programmed cell death in eukaryotic microalgae? European Journal of Phycology 58:13–34.

Barreto Filho, M. M., P. M. Durand, N. E. Andolfato, A. Jordaan, H. Sarmento, and I. L. Bagatini. 2022*b*. Programmed cell death in the coccoid green microalga Ankistrodesmus densus

Korshikov (Sphaeropleales, Selenastraceae). European Journal of Phycology 57:196–206.

Beaman, J. E., C. R. White, and F. Seebacher. 2016. Evolution of Plasticity: Mechanistic Link between Development and Reversible Acclimation. Trends in Ecology and Evolution 31:237–249.

Bell, G. 2017. Evolutionary Rescue.

Bell, G., and A. Gonzalez. 2009. Evolutionary rescue can prevent extinction following environmental change. Ecology Letters 12:942–948.

Ben-Amotz, A., and M. Avron. 1973. The Role of Glycerol in the Osmotic Regulation of the Halophilic Alga Dunaliella parva . Plant Physiology 51:875–878.

Ben-Amotz, A., J. E. W. Polle, and D. V. Subba Rao. 2009. The Alga Dunaliella Biodiversity, Physiology , Genomics and Biotechnology.

Berges, J. A., and P. G. Falkowski. 1998. Physiological stress and cell death in marine phytoplankton: Induction of proteases in response to nitrogen or light limitation. Limnology and Oceanography 43:129–135.

Berngruber, T. W., S. Lion, and S. Gandon. 2013. Evolution of suicide as a defence strategy against pathogens in a spatially structured environment. Ecology Letters 16:446–453.

Bidle, K. D. 2015. The Molecular Ecophysiology of Programmed Cell Death in Marine Phytoplankton. Pages 341–375 *in* Carlson, CA and Giovannoni, SJ, ed. ANNUAL REVIEW OF MARINE SCIENCE, VOL 7, Annual Review of Marine Science (Vol. 7).

Bidle, K. D. 2016. Programmed Cell Death in Unicellular Phytoplankton. Current Biology 26:R594–R607.

Bidle, K. D., and S. J. Bender. 2008. Iron starvation and culture age activate metacaspases and programmed cell death in the marine diatom Thalassiosira pseudonana. Eukaryotic Cell 7:223–236.

Bidle, K. D., and P. G. Falkowski. 2004. Cell death in planktonic, photosynthetic microorganisms. Nature Reviews Microbiology 2:643–655.

Bidle, K. D., L. Haramaty, J. B. Ramos, and P. Falkowski. 2007. Viral activation and recruitment of metacaspases in the unicellular coccolithophore, Emiliania huxleyi. Proceedings of the National Academy of Sciences of the United States of America 104:6049–6054.

Bodbyl Roels, S. A., and J. K. Kelly. 2011. Rapid evolution caused by pollinator loss in Mimulus guttatus. Evolution 65:2541–2552.

Borenstein, M., L. V Hedges, J. P. T. Higgins, and H. R. Rothstein. 2021. Introduction to meta-analysis. John Wiley \& Sons.

Bradshaw, A. D. 1965. Evolutionary Significance of Phenotypic Plasticity in Plants. Advances in Genetics 13:115–155.

Brown, E. R., and J. Kubanek. 2020. Harmful alga trades off growth and toxicity in response to cues from dead phytoplankton. Limnology and Oceanography 65:1723–1733.

Burke, M. K., J. P. Dunham, P. Shahrestani, K. R. Thornton, M. R. Rose, and A. D. Long. 2010. Genome-wide analysis of a long-term evolution experiment with Drosophila. Nature 467:587–590.

Burny, C., V. Nolte, M. Dolezal, and C. Schlötterer. 2022. Genome-wide selection signatures reveal widespread synergistic effects of two different stressors in Drosophila melanogaster. Proceedings of the Royal Society B: Biological Sciences 289.

Cabon, L., A. C. Martinez-Torres, and S. A. Susin. 2013. La mort cellulaire programmée ne manque pas de vocabulaire. Medecine/Sciences 29:1117–1124.

Charles, D. 1859. On the origin of species. John Murray, London.

Chavoshi, Z. Z., and M. Shariati. 2019. Lipid production in dunaliella bardawil under autotrophic, heterotrophicand mixotrophic conditions. Biologia 74:1579–1590.

Chen, H., and J. G. Jiang. 2009. Osmotic responses of Dunaliella to the changes of salinity. Journal of Cellular Physiology 219:251–258.

Chevin, L. M. 2011. On measuring selection in experimental evolution. Biology Letters 7:210–213.

Chevin, L. M., R. Lande, and G. M. Mace. 2010. Adaptation, plasticity, and extinction in a changing environment: Towards a predictive theory. PLoS Biology 8:e1000357.

Christensen, S. T., H. Sorensen, N. H. Beyer, K. Kristiansen, L. Rasmussen, and M. I. Rasmussen. 2001. Cell death in Tetrahymena thermophila: New observations on culture conditions. Cell Biology International 25:509–519.

Christensen, S. T., D. Wheatley, M. Rasmussen, and L. Rasmussen. 1995. Mechanisms

controlling death, survival and proliferation in a model unicellular eukaryote Tetrahymena thermophila. Cell death and differentiation 2:301–308.

Collot, D., T. Nidelet, J. Ramsayer, O. C. Martin, S. Méléard, C. Dillmann, D. Sicard, et al. 2018. Feedback between environment and traits under selection in a seasonal environment: Consequences for experimental evolution. Proceedings of the Royal Society B: Biological Sciences 285.

Crow, J. F., and M. Kimura. 1970. An Introduction to Population Genetics. (M. Harper and Row, NewYork. Reprinted by Burgess International, ed.).

Danial, N. N., and S. J. Korsmeyer. 2004. Cell Death: Critical Control Points. Cell 116:205–219.

De Jong, G. 1999. Unpredictable selection in a structured population leads to local genetic differentiation in evolved reaction norms. Journal of Evolutionary Biology 12:839–851.

Débarre, F., S. Lion, M. van Baalen, and S. Gandon. 2012. Evolution of host life-history traits in a spatially structured host-parasite system. American Naturalist 179:54–63.

Delong, J. P., and D. T. Hanson. 2009. Metabolic rate links density to demography in Tetrahymena pyriformis. ISME Journal 3:1396–1401.

Deponte, M. 2008. Programmed cell death in protists. Biochimica et Biophysica Acta 1783:1396–1405.

DeWitt, T. J., A. Sih, and D. S. Wilson. 1998. Costs and limits of phenotypic plasticity. Trends in Ecology and Evolution 13:77–81.

Dey, S., S. R. Proulx, and H. Teotónio. 2016. Adaptation to Temporally Fluctuating Environments by the Evolution of Maternal Effects. PLoS Biology 14:1–29.

Droop, M. R. 1973. Some Thoughts on Nutrient Limitation in Algae. Journal of Phycology.

Dudley, S. A., and J. Schmitt. 1996. Testing the Adaptive Plasticity Hypothesis : Density-Dependent Selection on Manipulated Stem Length in Impatiens capensis 147:445–465.

Durand, P. M. 2020. The evolutionary origins of life and death. University of Chicago Press.

Durand, P. M., R. Choudhury, A. Rashidi, and R. E. Michod. 2014. Programmed death in a unicellular organism has species-specific fitness effects. Biology Letters 10:8–11.

Durand, P. M., and G. Ramsey. 2019. The Nature of Programmed Cell Death. Biological Theory 14:30–41.

Durand, P. M., A. Rashidi, and R. E. Michod. 2011. How an organism dies affects the fitness of its neighbors. American Naturalist 177:224–232.

Emami, K., E. Hack, A. Nelson, C. M. Brain, F. M. Lyne, E. Mesbahi, J. G. Day, et al. 2015. Proteomic-based biotyping reveals hidden diversity within a microalgae culture collection: An example using Dunaliella. Scientific Reports 5:1–15.

Estrela, S., E. Libby, J. Van Cleve, F. Débarre, M. Deforet, W. R. Harcombe, J. Peña, et al. 2019. Environmentally Mediated Social Dilemmas. Trends in Ecology and Evolution 34:6–18.

Estrela, S., J. J. Morris, and B. Kerr. 2016. Private benefits and metabolic conflicts shape the emergence of microbial interdependencies. Environmental Microbiology 18:1415–1427.

Fagan, W. F., and E. E. Holmes. 2006. Quantifying the extinction vortex. Ecology Letters 9:51–60.

Frade, J. M., and T. M. Michaelidis. 2005. Origin of eukaryotic programmed cell death A consequence of aerobic metabolism. BioEssays 19:745–837.

Franklin, D. J., C. P. D. Brussaard, and J. A. Berges. 2006. What is the role and nature of programmed cell death in phytoplankton ecology? European Journal of Phycology 41:1–14.

Fröhlich, K. U., and F. Madeo. 2000. Apoptosis in yeast - A monocellular organism exhibits altruistic behaviour. FEBS Letters 473:6–9.

Gallet, R., T. F. Cooper, S. F. Elena, and T. Lenormand. 2012. Measuring selection coefficients below 10-3: Method, Questions, and Prospects. Genetics 190:175–186.

Gause, G. F. 1934. Experimental analysis of Vito Volterra's mathematical theory of the struggle for existence. Science 79:16–17.

Gavrilets, S., and S. M. Scheiner. 1993. The genetics of phenotypic plasticity. V. Evolution of reaction norm shape. Journal of Evolutionary Biology 6:31–48.

Geider, R. J., E. H. Delucia, P. G. Falkowski, A. C. Finzi, J. Philip Grime, J. Grace, T. M. Kana, et al. 2001. Primary productivity of planet earth: Biological determinants and physical constraints in terrestrial and aquatic habitats. Global Change Biology 7:849–882.

Ghalambor, C. K., J. K. McKay, S. P. Carroll, and D. N. Reznick. 2007. Adaptive versus non-

adaptive phenotypic plasticity and the potential for contemporary adaptation in new environments. Functional Ecology 21:394–407.

Ginzburg, M., and B. Z. Ginzburg. 1985. Ion and glycerol concentrations in 12 isolates of Dunaliella. Journal of Experimental Botany 36:1064–1074.

Gomulkiewicz, R., and R. D. Holt. 1995. When does evolution by natural selection prevent extinction? Evolution 49:201–207.

Gould, S. J., and E. S. Vrba. 1982. Exaptation—a Missing Term in the Science of Form. Paleobiology 1:4–15.

Hamilton, W. D. 1964. The genetic evolution of social behaviour. II. Journal of theoretical biology 7:17–52.

Hartl, D. L., and A. G. Clark. 1997. Principles of Population Genetics. Biometrics. Sunderland : Sinauer Associates.

Hazan, R., B. Sat, and H. Engelberg-Kulka. 2004. Escherichia coli mazEF-mediated cell death is triggered by various stressful conditions. Journal of Bacteriology 186:3663–3669.

Henriques, G. J. B., and M. M. Osmond. 2020. Cooperation can promote rescue or lead to evolutionary suicide during environmental change. Evolution 74:1255–1273.

Hodgson, D., J. L. McDonald, and D. J. Hosken. 2015. What do you mean, “resilient”? Trends in Ecology and Evolution 30:503–506.

Jacob, S. W., & Herschler, R. 1986. Pharmacology of DMSO. Cryobiology 23(1):14–27.

Jiménez, C., J. M. Capasso, C. L. Edelstein, C. J. Rivard, S. Lucia, S. Breusegem, T. Berl, et al. 2009. Different ways to die: Cell death modes of the unicellular chlorophyte Dunaliella viridis exposed to various environmental stresses are mediated by the caspase-like activity DEVDase. Journal of Experimental Botany 60:815–828.

Jones, T. W., and R. Galloway. 1979. Effect of light quality and intensity on glycerol production content in Dunaliella tertiolecta (Chlorophycea) and the relationship to cell growth/osmoregulation. Journal of Phycology 15:101–106.

Kaiser, D. 1996. Bacteria Also Vote. Science 272:1598–1599.

Kasuba, K. C., S. L. Vavilala, and J. S. D’Souza. 2015. Apoptosis-like cell death in unicellular photosynthetic organisms - A review. Algal Research 12:126–133.

Kojic, M., and M. Milisavljevic. 2020. When disaster strikes: Reconstitution of population density by expansion of survivors. Molecular Ecology 29:4757–4764.

Kot, M. 2001. Elements of Mathematical Ecology. Cambridge University Press.

Kourtis, N., and N. Tavernarakis. 2009. Autophagy and cell death in model organisms 21–30.

Kozik, C., E. B. Young, C. D. Sandgren, and J. A. Berges. 2019. Cell death in individual freshwater phytoplankton species: relationships with population dynamics and environmental factors. European Journal of Phycology 54:369–379.

Kroemer, G. 1997. Mitochondrial implication in apoptosis . Towards an endosymbiont hypothesis of apoptosis evolution 443–456.

Kroemer, G., L. Galluzzi, P. Vandenabeele, J. Abrams, E. S. Alnemri, E. H. Baehrecke, M. V. Blagosklonny, et al. 2009. Classification of cell death: Recommendations of the Nomenclature Committee on Cell Death 2009. Cell Death and Differentiation 16:3–11.

Lande, R. 2009. Adaptation to an extraordinary environment by evolution of phenotypic plasticity and genetic assimilation. Journal of Evolutionary Biology 22:1435–1446.

———. 2014. Evolution of phenotypic plasticity and environmental tolerance of a labile quantitative character in a fluctuating environment. Journal of Evolutionary Biology 27:866–875.

Leist, M., and M. Jäättelä. 2001. Four deaths and a funeral: From caspases to alternative mechanisms. Nature Reviews Molecular Cell Biology 2:589–598.

Leroi, A. M., A. F. Bennett, and R. E. Lenski. 1994. Temperature acclimation and competitive fitness: An experimental test of the beneficial acclimation assumption. Proceedings of the National Academy of Sciences of the United States of America 91:1917–1921.

Leung, C., D. Grulois, and L.-M. Chevin. 2022. Plasticity across levels: relating epigenomic, transcriptomic, and phenotypic responses to osmotic stress in a halotolerant microalga. Molecular Ecology.

Leung, C., M. Rescan, D. Grulois, and L. M. Chevin. 2020. Reduced phenotypic plasticity evolves in less predictable environments. Ecology Letters 23:1664–1672.

Levins, R. 1963. Theory of Fitness in a Heterogeneous Environment. II. Developmental Flexibility and Niche Selection. The American Naturalist 97:75–90.

Levy, S. F., J. R. Blundell, S. Venkataram, D. A. Petrov, D. S. Fisher, and G. Sherlock. 2015. Quantitative evolutionary dynamics using high-resolution lineage tracking. Nature 519:181–186.

Libby, E., W. W. Driscoll, and W. C. Ratcliff. 2018. Programmed cell death can increase the efficacy of microbial bet-hedging. Scientific Reports 8:1–11.

Lin, H., L. Fang, C. S. Low, Y. Chow, and Y. K. Lee. 2013. Occurrence of glycerol uptake in Dunaliella tertiolecta under hyperosmotic stress. FEBS Journal 280:1064–1072.

Lindsey, H. A., J. Gallie, S. Taylor, and B. Kerr. 2013. Evolutionary rescue from extinction is contingent on a lower rate of environmental change. Nature 494:463–467.

MacArthur, R., and R. Levins. 1967. The limiting similarity, convergence, and divergence of coexisting species. The American Naturalist 101:377–385.

Mallet, J. 2012. The struggle for existence: How the notion of carrying capacity, K, obscures the links between demography, Darwinian evolution, and speciation. Evolutionary Ecology Research 14:627–665.

Marin-Martinez, F., and J. Sánchez-Meca. 2010. Weighting by inverse variance or by sample size in random-effects meta-analysis. Educational and Psychological Measurement 70:56–73.

Medlin, L. K., M. Lange, and E. M. Nothig. 2000. Genetic diversity in the marine phytoplankton: A review and a consideration of Antarctic phytoplankton. Antarctic Science 12:325–333.

Minina, E. A., J. Staal, V. E. Alvarez, J. A. Berges, I. Berman-Frank, R. Beyaert, K. D. Bidle, et al. 2020. Classification and Nomenclature of Metacaspases and Paracaspases: No More Confusion with Caspases. Molecular Cell 77:927–929.

Monod, J. 1949. The growth of bacterial cultures. Annual Reviews in M 3:371–394.

Morris, J. J. 2015. Black Queen evolution: The role of leakiness in structuring microbial communities. Trends in Genetics 31:475–482.

Murik, O., A. Elboher, and A. Kaplan. 2014. Dehydroascorbate: A possible surveillance molecule of oxidative stress and programmed cell death in the green alga Chlamydomonas reinhardtii. New Phytologist 202:471–484.

Nakagawa, S., and H. Schielzeth. 2013. A general and simple method for obtaining R2 from

generalized linear mixed-effects models. Methods in Ecology and Evolution 4:133–142.

Ndhlovu, A., P. M. Durand, and G. Ramsey. 2021. Programmed cell death as a black queen in microbial communities. Molecular Ecology 30:1110–1119.

Nedelcu, A. M., W. W. Driscoll, P. M. Durand, M. D. Herron, and A. Rashidi. 2011. On the paradigm of altruistic suicide in the unicellular world. Evolution 65:3–20.

Orellana, M. V, W. L. Pang, P. M. Durand, K. Whitehead, and N. S. Baliga. 2013. A Role for Programmed Cell Death in the Microbial Loop. PLOS ONE 8:e62595.

Oren, A. 2005. A hundred years of Dunaliella research: 1905-2005. Saline Systems 1:2.

———. 2017. Glycerol metabolism in hypersaline environments. Environmental Microbiology 19:851–863.

Pandey, S. S., S. Singh, C. Pathak, and B. S. Tiwari. 2018. " Programmed Cell Death : A Process of Death for Survival " – How Far Terminology Pertinent for Cell Death in Unicellular Organisms.

Pigliucci, M. 1996. How organisms respond to environmental changes-from phenotypes to molecules (and vice versa). Trends in Ecology & Evolution 11:168–173.

Pinceel, T., F. Buschke, A. Geerts, J. Vanoverbeke, L. Brendonck, and B. Vanschoenwinkel. 2021. An empirical confirmation of diversified bet hedging as a survival strategy in unpredictably varying environments. Ecology 102:1–12.

Polle, J. E. W., K. Barry, J. Cushman, J. Schmutz, D. Tran, L. T. Hathwaik, W. C. Yim, et al. 2017. Draft nuclear genome sequence of the halophilic and beta-carotene-accumulating green alga Dunaliella salina strain CCAP19/18 5:17–19.

Price, G. R. 1970. Selection and covariance. Nature 227:520–521.

Ramsayer, J., O. Kaltz, and M. E. Hochberg. 2013. Evolutionary rescue in populations of Pseudomonas fluorescens across an antibiotic gradient. Evolutionary Applications 6:608–616.

Reece, S. E., L. C. Pollitt, N. Colegrave, and A. Gardner. 2011. The meaning of death: Evolution and ecology of apoptosis in protozoan parasites. PLoS Pathogens 7:1–9.

Reed, T. E., S. W. Robin, D. E. Schindler, J. J. Hard, and M. T. Kinnison. 2010. Phenotypic plasticity and population viability: The importance of environmental predictability. Proceedings of the Royal Society B: Biological Sciences 277:3391–3400.

Rêgo, A., F. J. Messina, and Z. Gompert. 2019. Dynamics of genomic change during evolutionary rescue in the seed beetle Callosobruchus maculatus. Molecular Ecology 28:2136–2154.

Rescan, M., D. Grulois, E. O. Aboud, P. de Villemereuil, and L.-M. Chevin. 2021. Predicting population genetic change in an autocorrelated random environment: Insights from a large automated experiment. PLOS Genetics 17:e1009611.

Rescan, M., D. Grulois, E. Ortega-Aboud, and L. M. Chevin. 2020. Phenotypic memory drives population growth and extinction risk in a noisy environment. Nature Ecology and Evolution 4:193–201.

Rescan, M., N. Leurs, D. Grulois, and C. Luis-Miguel. 2022. Experimental evolution of environmental tolerance , acclimation , and physiological plasticity in a randomly fluctuating environment. Evolution Letters 1–15.

Ronce, O. 2007. How does it feel to be like a rolling stone? Ten questions about dispersal evolution. Annual Review of Ecology, Evolution, and Systematics 38:231–253.

Sathe, S., M. V. Orellana, N. S. Baliga, and P. M. Durand. 2019. Temporal and metabolic overlap between lipid accumulation and programmed cell death due to nitrogen starvation in the unicellular chlorophyte Chlamydomonas reinhardtii. Phycological Research 67:173–183.

Scheiner, S. M., and L. Y. Yampolsky. 1998. The evolution of Daphnia pulex in a temporally varying environment. Genetics Research 72:25–37.

Schlichting, C. D., and M. Pigliucci. 1998. Phenotypic evolution: a reaction norm perspective. Sinauer Associates Incorporated.

Schotte, P., W. Declercq, S. Van Huffel, P. Vandenabeele, and R. Beyaert. 1999. Non-specific effects of methyl ketone peptide inhibitors of caspases. FEBS Letters 442:117–121.

Segovia, M., and J. A. Berges. 2009. Inhibition of caspase-like activities prevents the appearance of reactive oxygen species and dark-induced apoptosis in the unicellular chlorophyte dunaliella tertiolecta. Journal of Phycology 45:1116–1126.

Segovia, M., L. Haramaty, J. A. Berges, and P. G. Falkowski. 2003. Cell Death in the Unicellular Chlorophyte Dunaliella tertiolecta. Plant Physiology 132:99–105.

Slee, E. A., C. Adrain, and S. J. Martin. 2001. Executioner Caspase-3, -6, and -7 Perform

Distinct, Non-redundant Roles during the Demolition Phase of Apoptosis. Journal of Biological Chemistry 276:7320–7326.

Sui, Y., and P. J. Harvey. 2021. Effect of light intensity and wavelength on biomass growth and protein and amino acid composition of dunaliella salina. Foods 10.

Sultan, S. E. 1995. Phenotypic plasticity and plant adaptation. Acta Botanica Neerlandica 44:363–383.

Sunda, W. G., K. W. Shertzer, and D. R. Hardison. 2009. Ammonium uptake and growth models in marine diatoms: Monod and Droop revisited. Marine Ecology Progress Series 386:29–41.

Thamatrakoln, K., B. Bailleul, C. M. Brown, M. Y. Gorbunov, A. B. Kustka, M. Frada, P. A. Joliot, et al. 2013. Death-specific protein in a marine diatom regulates photosynthetic responses to iron and light availability. Proceedings of the National Academy of Sciences of the United States of America 110:20123–20128.

Thornton, D. C. O. 2002. Individuals, clones or groups? phytoplankton behaviour and units of selection. Ethology Ecology and Evolution 14:165–173.

Venables, W. N., and B. D. Ripley. 2002. Modern Applied Statistics with S. Springer, New York.

Violle, C., D. R. Nemergut, Z. Pu, and L. Jiang. 2011. Phylogenetic limiting similarity and competitive exclusion. Ecology Letters 14:782–787.

Vostinar, A. E., H. J. Goldsby, and C. Ofria. 2019. Suicidal selection: Programmed cell death can evolve in unicellular organisms due solely to kin selection. Ecology and Evolution 9:9129–9136.

Wersto, R. P., F. J. Chrest, J. F. Leary, C. Morris, M. A. Stetler-Stevenson, and E. Gabrielson. 2001. Doublet discrimination in DNA cell-cycle analysis. Communications in Clinical Cytometry 46:296–306.

Wilson, R. S., C. E. Franklin, and C. E. Franklin. 2002. Testing the beneficial acclimation hypothesis 17:66–70.

Withman, D., and A. Agrawal. 2009. What is Phenotypic Plasticity and Why is it Important? Phenotypic plasticity of insects: Mechanisms and consequences 1–63.

Yamaguchi, Y., J. H. Park, and M. Inouye. 2011. Toxin-antitoxin systems in bacteria and archaea. Annual Review of Genetics 45:61–79.

Yordanova, Z. P., E. J. Woltering, V. M. Kapchina-Toteva, and E. T. Iakimova. 2013. Mastoparan-induced programmed cell death in the unicellular alga Chlamydomonas reinhardtii. Annals of Botany 111:191–205.

Zeballos, N., D. Grulois, C. Leung, and L.-M. Chevin. 2023. Acceptable loss: Fitness consequences of salinity-induced cell death in a halotolerant microalga. The American Naturalist 201.

Zhao, L. N., W. F. Gong, X. W. Chen, and D. F. Chen. 2013. Characterization of genes and enzymes in Dunaliella salina involved in glycerol metabolism in response to salt changes. Phycological Research 61:37–45.

Zidan, M. A., M. F. Hipkins, and A. D. Boney. 1987. Loss of Intracellular Glycerol from Dunaliella tertiolecta after Decreasing the External Salinity. Journal of Plant Physiology 127:461–469.

Zuppini, A., C. Andreoli, and B. Baldan. 2007. Heat stress: An inducer of programmed cell death in Chlorella saccharophila. Plant and Cell Physiology 48:1000–1009.

Zuppini, A., C. Gerotto, and B. Baldan. 2010. Programmed cell death and adaptation: Two different types of abiotic stress response in a unicellular chlorophyte. Plant and Cell Physiology 51:884–895.

Zuppini, A., C. Gerotto, R. Moscatiello, E. Bergantino, and B. Baldan. 2009. Chlorella saccharophila cytochrome f and its involvement in the heat shock response. Journal of Experimental Botany 60:4189–4200.